

Holography Inspired Stringy Hadrons

Jacob Sonnenschein

The Raymond and Beverly Sackler School of Physics and Astronomy,
Tel Aviv University, Ramat Aviv 69978, Israel

March 2, 2022

Abstract

Holography inspired stringy hadrons (HISH) is a set of models that describe hadrons: mesons, baryons and glueballs as strings in flat four dimensional space time. The models are based on a “map” from stringy hadrons of holographic confining backgrounds. In this note we review the “derivation” of the models. We start with a brief reminder of the passage from the $AdS_5 \times S^5$ string theory to certain flavored confining holographic models. We then describe the string configurations in holographic backgrounds that correspond to a Wilson line, a meson, a baryon and a glueball. The key ingredients of the four dimensional picture of hadrons are the “string endpoint mass” and the “baryonic string vertex”. We determine the classical trajectories of the HISH. We review the current understanding of the quantization of the hadronic strings. We end with a summary of the comparison of the outcome of the HISH models with the PDG data about mesons and baryons. We extract the values of the tension, masses and intercepts from best fits, write down certain predictions for higher excited hadrons and present attempts to identify glueballs.

Contents

1	Introduction	3
2	From $AdS_5 \times S^5$ to confining string backgrounds	5
2.1	Confining background	5
2.2	Introducing fundamental quarks	6
2.3	Review of the Witten-Sakai-Sugimoto model	6
3	Hadrons as strings in holographic background	10
3.1	The holographic Wilson line	10
3.1.1	't Hooft line	13
3.2	The stringy duals of mesons	15
3.2.1	The conditions on strings rotating at constant radial coordinate	15
3.2.2	The meson as a rotating string attached to flavor branes	16
3.3	Holographic stringy baryons	20
3.4	The glueball as a rotating closed string	22
3.4.1	Classical rotating folded string	22
3.4.2	The closed string in a curved Holographic background	24
4	Holography inspired hadronic strings	25
4.1	The map from holographic strings to strings in flat space-time	25
4.2	The rotating string with massive endpoints	27
4.3	The stringy baryon and its stability	28
4.4	The stringy glueball	31
5	On the quantum stringy hadrons	31
5.1	The quantum rotating closed string in holographic background	33
5.2	On the quantization of the string in non-critical dimensions	33
5.2.1	The folded closed string	34
5.2.2	The regular open string	35
5.3	The Casimir energy of a critical static string with massive endpoints	35
5.4	On the quantization of the rotating string with massive endpoints in four dimensions	38
6	Phenomenology: Comparison between the stringy models and experimental data	39
6.1	Fitting models and procedure	39
6.2	Review of meson trajectory fits	40
6.2.1	Summary of results for the mesons	40
6.2.2	Universal slope fits	41
6.2.3	Meson trajectories in the (J, M^2) plane	42
6.2.4	Meson trajectories in the (n, M^2) plane	45
6.3	Review of baryon trajectory fits	46
6.3.1	Y-shape and central mass	47
6.3.2	Symmetric vs. imbalanced string	47
6.3.3	Splitting between trajectories of even and odd angular momentum	48
6.3.4	Summary of results	48
6.3.5	Light quark baryons	49
6.3.6	Strange baryons	50
6.3.7	Charmed baryons	51
6.3.8	Structure of the baryon in the quark-diquark model	52

6.4	Strings and the search for glueballs	54
6.4.1	The glueball candidates: The f_0 and f_2 resonances	54
6.4.2	Assignment of the f_0 into trajectories	54
6.4.3	Assignment of the f_2 into trajectories	58
6.4.4	Assignments with non-linear trajectories for the glueball	60
6.4.5	Glueball Regge trajectories in lattice QCD	61

7 Summary and future directions 63

1 Introduction

The stringy description of hadrons has been thoroughly investigated since the sixties of the last century[1]. In this paper I review the research work we have been doing in the last few years on a renewed stringy description of hadrons. This naturally raises the question of what are the reasons to go back to “square one” and revisit this question? Here are several reasons for doing it.

- (i) Up to date, certain properties, like the hadronic spectrum, the decay width of hadron and their scattering cross section, are hard to derive from QCD and relatively easy from a stringy picture.
- (ii) Holography, or gauge/string duality, provides a bridge between the underlying theory of QCD (in certain limits) and a bosonic string model of hadrons .
- (iii) To establish a framework that describes the three types of hadrons mesons, baryons and glueballs in terms of the same building blocks, namely strings.
- (iv) The passage from the holographic string regime to strings in reality is still a tremendous challenge.
- (v) Up to date we lack a full exact procedure of quantizing a rotating string with massive endpoints (which will see are mandatory for the stringy hadrons).
- (vi) There is a wide range of heavy mesonic and baryonic resonances that have been discovered in recent years. Thus the challenge is to develop a framework that can accommodate hadrons with any quark content light, medium and heavy.

The holographic duality is an equivalence between certain bulk string theories and boundary field theories. Practically most of the applications of holography are based on relating bulk fields (not strings) and operators on the dual boundary field theory. This is based on the usual limit of $\alpha' \rightarrow 0$ with which we go, for instance, from a closed string theory to a theory of gravity. However, to describe realistic hadrons it seems that we need strings since after all in nature the string tension which is inversely proportional to α' is not very large. In holography this relates to the fact that one needs to describe nature $\lambda = g^2 N_c$ is of order one and not very large one.

The main theme of this review paper is that there is a wide sector of hadronic physical observables which cannot be faithfully described by bulk fields but rather require dual stringy phenomena. It is well known that this is the case for a Wilson, a 't Hooft and a Polyakov lines (for a review see for instance [2]). We argue here that in fact also the spectra, decays and other properties of hadrons: mesons, baryons and glueballs can be recast only by holographic stringy hadrons and not by fields that reside in the bulk or on flavor branes. The major argument against describing the hadron spectra in terms of fluctuations of fields like bulk fields or modes on probe flavor branes is that they generically do not admit properly the Regge behavior of the spectra. For M^2 as a function of J we get from flavor branes only $J = 0, J = 1$ mesons and there is a big gap of order λ (or certain fractional power of λ depending

on the model) in comparison to high J mesons described in terms of strings. Moreover the attempts to get the observed linearity between M^2 and n the excitation number is problematic, whereas for strings it is an obvious property.

The main ideas of this project is (i) To analyze string configurations in holographic string models that correspond to hadrons, (ii) to bypass the usual transition from the holographic regime of large N_c and large λ to the real world via a $\frac{1}{N_c}$ and $\frac{1}{\lambda}$ expansion and state a model of stringy hadrons in flat four dimensions that is inspired by the corresponding holographic strings. (iii) To confront the outcome of the models with the experimental data in [3],[4] [5].

Confining holographic models are characterized by a “wall” that truncates in one way or another the range of the radial direction (see figure 2). A common feature to all the holographic stringy hadrons is that there is a segment of the string that stretches along a constant radial coordinate in the vicinity of the “wall”. For the stringy glueball it is the whole folded closed string that rotates there and for the open string it is part of the string, the horizontal segment, that connects with vertical segments either to the boundary for a Wilson line or to flavor branes for the meson and for the baryon. This fact that the classical solutions of the flatly rotating strings reside at fixed radial direction is behind the map to rotating strings in flat four dimensional space-time. A key ingredient of the map is the m_{sep} , the “string endpoint mass” that provides in the four flat space-time description the dual of the vertical string segments. It is important to note (i) This mass parameter is neither the QCD mass parameter nor that of the constituent quark mass. (ii) As will be seen below the m_{sep} parameter is not an exact map of a vertical segment but rather only an approximation that is more accurate the longer the horizontal string is.

As we have mentioned above the stringy picture of meson has been thoroughly investigated in the past and we will not cite here this huge body of papers. It turns out that also in recent years there were several attempts to describe hadrons in terms of strings. Papers on the subject that have certain overlap with our approach are for instance [6],[7],[8],[9]. Another approach to the stringy nature of QCD is the approach of low-energy effective theory on long strings. This approach is different but shares certain features with the approach presented in this paper. A recent review of the subject can be found in [10].

The alternative description of hadrons in terms of fields in the bulk or on flavor branes is not discussed in this paper. For a review paper about this approach and reference therein see [11] The paper is organized in the following manner. After this section of an introduction there is a review section that describes the passage from the $AdS_5 \times S^5$ string background to that of various confining backgrounds. We describe in some details the prototype model of Sakai and Sugimoto and its generalization. Section (§3) is devoted to hadrons as strings in a holographic background. In this section we separately describe in (§3.1) the holographic Wilson line, in (§3.2) the stringy duals of mesons and in (§3.3) the glueball as a rotating folded closed string. We then describe in section (§4) the HISH model. We present the map between the holographic strings and strings in flat space-time in (§4.1). We classically solve the system of an open string with massive endpoints and we determine its energy and angular momentum (§4.2). We then in (§4.3) discuss the stringy baryon of HISH and in particular the stability of Y shape string configurations. Next in section (§5) we present our current understanding of the quantization of the HISH model. In §(5.1) we review the attempt to quantize the closed string in holographic background. We then describe the derivation of the Casimir energy for a static case with massive endpoints in (§5.2). The Liouville or Polchinski-Strominger terms for quantizing the string in non-critical dimension is discussed in (§5.3). Phenomenology: Comparison between the stringy models and experimental data is reviewed in section (§6). We first describe the fitting models (§6.1) and procedure and then present separately the meson trajectory fits (§6.2) and the baryon trajectory fits (§6.3) and finally we describe the search of glueballs (§6.4). We summarize and describe several future directions in (§7)

2 From $AdS_5 \times S^5$ to confining string backgrounds

The original duality equivalence is between the $\mathcal{N} = 4$ SYM theory and string theory in $AdS_5 \times S^5$. Obviously the $\mathcal{N} = 4$ is not the right framework to describe hadrons that should resemble those found in nature. Instead we need stringy dual of four dimensional gauge dynamical system which is non-supersymmetric, non-conformal and confining. The main two requirements on the desired string background is that it (i) admits confinement and (ii) that it includes matter in the fundamental representation invariant under chiral flavor symmetry and that the latter is spontaneously broken.

2.1 Confining background

There are by now several ways to get a string background which is dual to a confining boundary field theory.

- Models based on deforming the $AdS_5 \times S^5$ by a relevant or marginal operator which breaks conformal invariance and supersymmetry. This approach was pioneered in [12]. There were afterwards many followup papers. For a list of references of them see for instance in the review paper [13].
- An important class of models is achieved by compactifying higher dimensional theories to four dimensions in a way which (partially) breaks supersymmetry. A prototype model of this approach is that of a compactified D5 or NS5 brane on S^2 . In an appropriate decoupling limit this provides a dual of the $3 + 1$ dimensional $\mathcal{N} = 1$ SYM theory[14]. Another model of this class is the so called Witten's model [15] which is based on the compactification of one space coordinate of a D4 brane on a circle. The sub-manifold spanned by the compactified coordinate and the radial coordinate has geometry of a cigar. Imposing on the circle anti-periodic boundary conditions for the fermions, in particular the gauginos, render them massive and hence supersymmetry is broken. In the limit of small compactified radius one finds that the dual field theory is a contaminated low energy effective YM theory in four dimensions. This approach will be described in (§2.3)
- It was realized early in the game that one can replace the S^5 part of the string background with orbifolds of it or by the T_{11} conifold. In this way conformal invariance is maintained, however, parts of the supersymmetry can be broken. In particular the dual of the conifold model has $\mathcal{N} = 1$ instead of $\mathcal{N} = 4$. It was shown in [16] that one can move from the conformal theory to a confining one by deforming the conifold. The corresponding gauge theory is a cascading gauge theory.
- In analogy to Dp brane background solutions of the ten dimensional equations of motion [17] one can find solutions for the metric dilaton and RR forms in non-critical $d < 10$ dimensions. In particular there is a six dimensional model of $D4$ branes compactified on a S^1 [18]. This model resembles Witten's model with the difference that the dual field theory is in the large N_c limit but with 't Hooft coupling $\lambda \sim 1$.
- The AdS/QCD is a bottom-up approach, namely it not a solution of the ten dimensional equations of motion, based on an AdS_5 gravity background with additional fields residing on it. The idea is to determine the background in such a way that the corresponding dual boundary field theory has properties that resemble those of QCD. The basic model of this kind is the “hard wall” model where the five-dimensional AdS_5 space is truncated at a certain value of the radial direction $u = u_\Lambda$. The conformal invariance of the AdS_5 space corresponds to the asymptotic free UV region of the gauge theory. Confinement is achieved by the IR hard wall as will be seen (§3.1). This construction was first introduced in [19]. Since this model does not admit a Regge behaviour for the corresponding meson spectra there was a proposal [20] to improve the model by “softening”

the hard wall into a soft-wall model. It was argued that in this way one finds an excited spectrum of the form $M_n^2 \sim n$ but, as will be discussed below also, this model does not describe faithfully the spectra of mesons.

- Another AdS/QCD model is the improved holographic QCD model (IHQCD)[21] which is essentially a five-dimensional dilaton-gravity system with a non-trivial dilaton potential. By tuning the latter, it was shown that one can build a model that admits certain properties in accordance with lattice gauge theory results both at zero and finite temperature.

2.2 Introducing fundamental quarks

Since the early days of string theory it has been understood that fundamental quarks should correspond to open strings. In the modern era of closed string backgrounds this obviously calls for D branes. It is thus natural to wonder, whether one can consistently add D brane probes to supergravity backgrounds duals of confining gauge theories, which will play the role of fundamental quarks. In case that the number of D brane probes $N_f \ll N_c$ one can convincingly argue that the back reaction of the probe branes on the bulk geometry is negligible. It was also well known that open strings between parallel N_f D7 branes and N_c D3 branes play the role of flavored quarks in the $SU(N_c)$ gauge theory that resides on the D3 4d world volume. Karch and Katz [22] proposed to elevate this brane configuration into a supergravity background by introducing D7 probe branes into the $AdS_5 \times S^5$ background. Note that these types of setups are non-confining ones. This idea was further explored in [23] and in many other followup works. For a list of them see the review [11]. There have been certain attempts to go beyond the flavor probe approximation for instance [24]. The first attempt to incorporate flavor branes in a confining background was in [25] where D7 and anti-D7 branes were introduced to the Klebanov-Strassler model [16]. This project was later completed in [26]. An easier model of incorporating D8 and anti D8 branes will be discussed in the next subsection. Flavor was also introduced in the bottom-up models confining models. For instance the Veneziano limit of large N_f in addition to the large N_c was studied in [27].

2.3 Review of the Witten-Sakai-Sugimoto model

Rather than describing a general confining background, or the whole list of such models, we have chosen a prototype model, the Sakai Sugimoto model, which will be described in details in the next subsection.

Witten's model [15] describes the near-horizon limit of a configuration of large N_c number of D4-branes, compactified on a circle in the x_4 direction (see figure 1) with anti-periodic boundary conditions for the fermions[15].

This breaks supersymmetry and renders only the gauge field to remain massless whereas the gauginos and scalars become massive. To incorporate flavor this model is then elevated to the so called Sakai Sugimoto model [28] to which a stack of N_f D8-branes (located at $x_4 = 0$) and a stack of N_f anti-D8-branes (located at the asymptotic location $x_4 = L_{as}$) is added. This is dual to a 4 + 1 dimensional maximally supersymmetric $SU(N_c)$ Yang-Mills theory (with coupling constant g_5 and with a specific UV completion that will not be important for us), compactified on a circle of radius R with anti-periodic boundary conditions for the fermions, with N_f left-handed quarks located at $x_4 = 0$ and N_f right-handed quarks located at $x_4 = L$ (obviously we can assume $L_{as} \leq \pi R$).

In the limit $N_f \ll N_c$, this background can be described by N_f probe D8-branes inserted into the near-horizon limit of a set of N_c D4-branes compactified on a circle with anti-periodic boundary conditions for the fermions. This background is simply related to the (near-horizon limit of the) background of near-extremal D4-branes by exchanging the roles (and signatures) of the time direction and of one

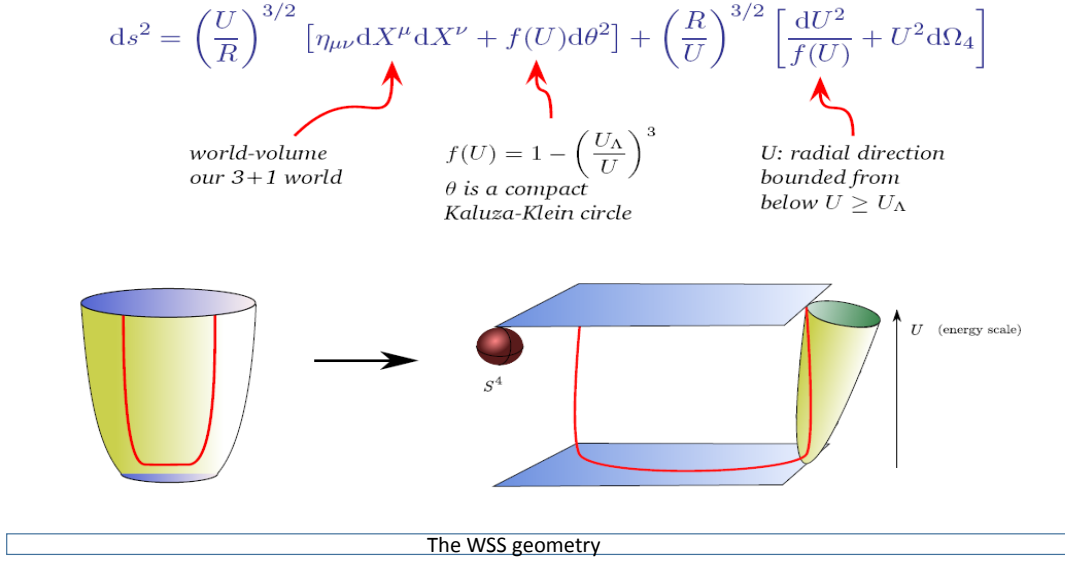


Figure 1: The WSS geometry. The compact direction of the D4 brane denoted in the figure as θ is referred to as x_4 in the text.

of the spatial directions. Let us now briefly review this model, emphasizing the manifestations of confinement and chiral symmetry breaking. The background of type IIA string theory is characterized by the metric, the RR four-form and a dilaton given by

$$\begin{aligned}
 ds^2 &= \left(\frac{u}{R_{D4}}\right)^{3/2} [-dt^2 + \delta_{ij} dx^i dx^j + f(u) dx_4^2] + \left(\frac{R_{D4}}{u}\right)^{3/2} \left[\frac{du^2}{f(u)} + u^2 d\Omega_4^2 \right], \\
 F_{(4)} &= \frac{2\pi N_c}{V_4} \epsilon_4, \quad e^\phi = g_s \left(\frac{u}{R_{D4}}\right)^{3/4}, \quad R_{D4}^3 \equiv \pi g_s N_c l_s^3, \quad f(u) \equiv 1 - \left(\frac{u_\Lambda}{u}\right)^3,
 \end{aligned} \tag{1}$$

where t is the time direction and x^i ($i = 1, 2, 3$) are the uncompactified world-volume coordinates of the D4 branes, x_4 is a compactified direction of the D4-brane world-volume which is transverse to the probe D8 branes, the volume of the unit four-sphere Ω_4 is denoted by V_4 and the corresponding volume form by ϵ_4 , l_s is the string length and finally g_s is a parameter related to the string coupling. The submanifold of the background spanned by x_4 and u has the topology of a cigar (as in both sides of figure 2 below) where the minimum value of u at the tip of the cigar is u_Λ . The tip of the cigar is non-singular if and only if the periodicity of x_4 is

$$\delta x_4 = \frac{4\pi}{3} \left(\frac{R_{D4}^3}{u_\Lambda}\right)^{1/2} = 2\pi R \tag{2}$$

and we identify this with the periodicity of the circle that the 4 + 1-dimensional gauge theory lives on.

The parameters of this gauge theory, the five-dimensional gauge coupling g_5 , the low-energy four-dimensional gauge coupling g_4 , the glueball mass scale M_{gb} , and the string tension T_{st} are determined from the background (1) in the following form :

$$g_5^2 = (2\pi)^2 g_s l_s, \quad g_4^2 = \frac{g_5^2}{2\pi R} = 3\sqrt{\pi} \left(\frac{g_s u_\Lambda}{N_c l_s}\right)^{1/2}, \quad M_{gb} = \frac{1}{R},$$

$$T_{st} = \frac{1}{2\pi l_s^2} \sqrt{g_{tt}g_{xx}}|_{u=u_\Lambda} = \frac{1}{2\pi l_s^2} \left(\frac{u_\Lambda}{R_{D4}} \right)^{3/2} = \frac{2}{27\pi} \frac{g_4^2 N_c}{R^2} = \frac{\lambda_5}{27\pi^2 R^3}, \quad (3)$$

where $\lambda_5 \equiv g_5^2 N_c$, M_{gb} is the typical scale of the glueball masses computed from the spectrum of excitations around (1), and T_{st} is the confining string tension in this model (given by the tension of a fundamental string stretched at $u = u_\Lambda$ where its energy is minimized). The gravity approximation is valid whenever $\lambda_5 \gg R$, otherwise the curvature at $u \sim u_\Lambda$ becomes large. Note that as usual in gravity approximations of confining gauge theories, the string tension is much larger than the glueball mass scale in this limit. At very large values of u the dilaton becomes large, but this happens at values which are of order $N_c^{4/3}$ (in the large N_c limit with fixed λ_5), so this will play no role in the large N_c limit that we will be interested in. The Wilson line of this gauge theory (before putting in the D8-branes) admits an area law behavior [29], which means a confining behavior, as can be easily seen using the conditions for confinement of [30].

Naively, at energies lower than the Kaluza-Klein scale $1/R$ the dual gauge theory is effectively four dimensional; however, it turns out that the theory confines and develops a mass gap of order $M_{gb} = 1/R$, so (in the regime where the gravity approximation is valid) there is no real separation between the confined four-dimensional fields and the higher Kaluza-Klein modes on the circle. As discussed in [15], in the opposite limit of $\lambda_5 \ll R$, the theory approaches the 3 + 1 dimensional pure Yang-Mills theory at energies small compared to $1/R$, since in this limit the scale of the mass gap is exponentially small compared to $1/R$. It is believed that there is no phase transition when varying λ_5/R between the gravity regime and the pure Yang-Mills regime, but it is not clear how to check this.

Next, we introduce the probe 8-branes which span the coordinates t, x^i, Ω_4 , and follow some curve $u(x_4)$ in the (x_4, u) -plane. Near the boundary at $u \rightarrow \infty$ we want to have N_f D8-branes localized at $x_4 = 0$ and N_f anti-D8-branes (or D8-branes with an opposite orientation) localized at $x_4 = L_{as}$. Naively one might think that the D8-branes and anti-D8-branes would go into the interior of the space and stay disconnected; however, these 8-branes do not have anywhere to end in the background (1), so the form of $u(x_4)$ must be such that the D8-branes smoothly connect to the anti-D8-branes (namely, u must go to infinity at $x_4 = 0$ and at $x_4 = L_{as}$, and du/dx_4 must vanish at some minimal u coordinate $u = u_0$). Such a configuration spontaneously breaks the chiral symmetry from the symmetry group which is visible at large u , $U(N_f)_L \times U(N_f)_R$, to the diagonal $U(N_f)$ symmetry. Thus, in this configuration the topology forces a breaking of the chiral symmetry; this is not too surprising since chiral symmetry breaking at large N_c follows from rather simple considerations. The most important feature of this solution is the fact that the D8 branes smoothly connect to the anti D8 branes.

In order to find the 8-brane configuration, we need the induced metric on the D8-branes, which is

$$\begin{aligned} ds_{D8}^2 &= \left(\frac{u}{R_{D4}} \right)^{3/2} [-dt^2 + \delta_{ij} dx^i dx^j] + \left(\frac{u}{R_{D4}} \right)^{3/2} \left[f(u) + \left(\frac{R_{D4}}{u} \right)^3 \frac{u'^2}{f(u)} \right] dx_4^2 \\ &+ \left(\frac{R_{D4}}{u} \right)^{3/2} u^2 d\Omega_4^2 \end{aligned} \quad (4)$$

where $u' = du/dx_4$. It is easy to check that the Chern-Simons (CS) term in the D8-brane action does not affect the solution of the equations of motion. More precisely, the equation of motion of the gauge field has a classical solution of a vanishing gauge field, since the CS term includes terms of the form $C_5 \wedge F \wedge F$ and $C_3 \wedge F \wedge F \wedge F$. So, we are left only with the Dirac-Born-Infeld (DBI) action. Substituting the determinant of the induced metric and the dilaton into the DBI action, we obtain (ignoring the factor of N_f which multiplies all the D8-brane actions that we will write) :

$$S_{DBI} = T_8 \int dt d^3x dx_4 d^4\Omega e^{-\phi} \sqrt{-\det(\hat{g})} = \frac{\hat{T}_8}{g_s} \int dx_4 u^4 \sqrt{f(u) + \left(\frac{R_{D4}}{u} \right)^3 \frac{u'^2}{f(u)}}, \quad (5)$$

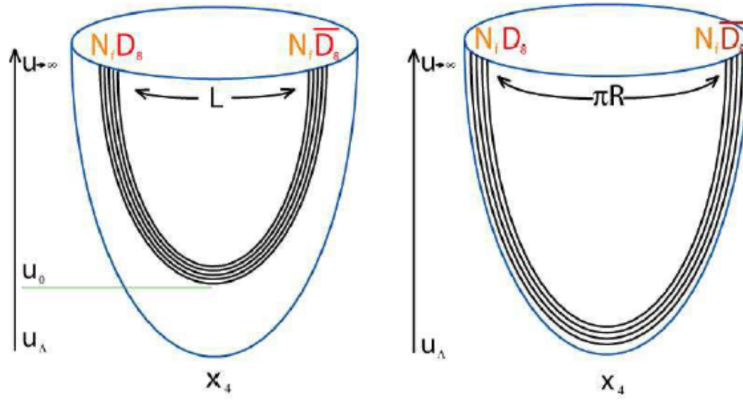


Figure 2: The dominant configurations of the D8 and anti-D8 probe branes in the Sakai-Sugimoto model at zero temperature, which break the chiral symmetry. The same configurations will turn out to be relevant also at low temperatures. On the left a generic configuration with an asymptotic separation of L_{as} , that stretches down to a minimum at $u = u_0$, is drawn. The figure on the right describes the limiting antipodal case $L_{as} = \pi R$, where the branes connect at $u_0 = u_\Lambda$.

where \hat{g} is the induced metric (4) and \hat{T}_8 includes the outcome of the integration over all the coordinates apart from dx_4 . From this action it is straightforward to determine the profile of the D8 probe branes. The form of this profile which is drawn in figure 2(a) is given by

$$\begin{aligned}
 L_{as} &= \int dx_4 = 2 \int_{u_0}^{\infty} \frac{du}{u'} = 2R_{D4}^{3/2} \int_{u_0}^{\infty} du \frac{1}{f(u)u^{3/2} \sqrt{\frac{f(u)u^8}{f(u_0)u_0^8} - 1}} \\
 &= \frac{2}{3} \left(\frac{R_{D4}^3}{u_0} \right)^{1/2} \sqrt{1 - y_\Lambda^3} \int_0^1 dz \frac{z^{1/2}}{(1 - y_\Lambda^3 z) \sqrt{1 - y_\Lambda^3 z - (1 - y_\Lambda^3) z^{8/3}}}, \quad (6)
 \end{aligned}$$

where $y_\Lambda \equiv u_\Lambda/u_0$. Small values of L_{as} correspond to large values of u_0 . In this limit we have $y_\Lambda \ll 1$ leading to $L \propto \sqrt{R_{D4}^3/u_0}$. For general values of L_{as} the dependence of u_0 on L is more complicated.

There is a simple special case of the above solutions, which occurs when $L_{as} = \pi R$, namely the D8-branes and anti-D8-branes lie at antipodal points of the circle. In this case the solution for the branes is simply $x_4(u) = 0$ and $x_4(u) = L_{as} = \pi R$, with the two branches meeting smoothly at the minimal value $u = u_0 = u_\Lambda$ to join the D8-branes and the anti-D8-branes together (see figure 1). This is the solution advocated in [28]. The generalized, not necessarily antipodal configuration that was described above was introduced in [31]. As will be discussed in section §(4, 2) the difference between the antipodal and the non-antipodal will translate to the difference between stringy meson with massless versus massive endpoints. It was also found out in [32] that, in order to have attraction between flavor instantons that mimic the baryons, the setup has to be non-antipodal. In the approach of considering the duals of the mesons as fluctuation modes of the flavor branes[28], and not as we argue here in this review as string configuration, it turned out that the difference between u_0 and u_Λ is not the dual of the QCD quark masses. One manifestation of this is the fact that the Goldstone bosons associated with the breakdown of the chiral flavor symmetry remain massless even for the non-antipodal case. This led to certain generalizations of the Sakai Sugimoto model by introducing additional adjoint “tachyonic” field into the bulk [33],[34], [35] and by introducing an open Wilson line[36]. In view of the HISH these type of

generalization are obviously not necessary.

This type of antipodal solution is drawn in figure 2(b).

It was shown in [37] that the classical configurations both the antipodal and the non-antipodal are stable. This was done by a perturbative analysis (in $g_s N_f$) of the backreaction of the localized D8 branes. The explicit expressions of the backreacted metric, dilaton and RR form were written down and it was found that the backreaction remains small up to a radial value of $u \ll l_s N_f$, and that the background functions are smooth except at the D8 sources. In this perturbative window, the original embedding remains a solution to the equations of motion. Furthermore, the fluctuations around the original embedding, do not become tachyonic due to the backreaction in the perturbative regime. This is due to a cancellation between the DBI and CS parts of the D8 brane action in the perturbed background. For further discussion of the pros and cons of the Sakai-Sugimoto model see [31].

The main results reviewed in this subsection hold also to an analogous non-critical setup [18] based on inserting D4 flavor branes into the background of compactified colored D4 branes and in particular the structure of the spontaneous breaking of the flavor chiral symmetry.

3 Hadrons as strings in holographic background

In this section we will analyze various classical string configurations in confining holographic models. In fact we will define below what is a confining string background according to the behavior of the classical static string that attaches its boundary. We will treat four types of strings:

- (i) The string dual of a Wilson line.
- (ii) A rotating open string that is attached to flavor branes. This will be the dual of a meson.
- (iii) A rotating configuration of N_c strings attached to a “baryonic vertex”, the dual of the baryon.
- (iv) A rotating folded closed string, the dual of the glueball.

3.1 The holographic Wilson line

One of the most important characteristics of non-abelian gauge theories, in particular the ones associated with the group $SU(N_c)$, is the Wilson line which is a non-local gauge invariant expectation value that takes the form

$$\langle W(C) \rangle = \frac{1}{N_c} \text{Tr} \left[P e^{\oint_C A} \right] = \frac{1}{N_c} \text{Tr} \left[P e^{\oint_C A_\mu \dot{x}^\mu(\tau) d\tau} \right] \quad (7)$$

where P denotes path ordering and C is some given contour.

For the special case where C is a strip of length L along one space direction and Δt along the time direction, one can extract from the corresponding Wilson line, in Euclidean space-time and for $\Delta t \gg L \rightarrow \infty$, the potential $E(L)$ between a quark and an anti-quark as follows

$$\langle W(\text{strip}, L, \Delta t) \rangle = A(L) e^{-\Delta t E(L)} \quad (8)$$

The holographic dual of the expectation value of the Wilson line which was determined in [38] is given by

$$\langle W(C) \rangle = e^{-S_{NG}^{ren}} \quad (9)$$

where S_{NG}^{ren} is the renormalized Nambu-Goto action of a string worldsheet whose boundary on the boundary of the bulk space-time is C . There are several methods of renormalizing the result. In particular in the one we discuss below one subtracts the infinite action of the straight strings which are duals of the masses of quark anti-quark pair.

Next we would like to apply the holographic prescription of computing the Wilson line to a particular class of holographic models. The latter are characterized by higher than five dimensional space-time with a boundary. The coordinates of these space-times include the coordinates of the boundary space-time,

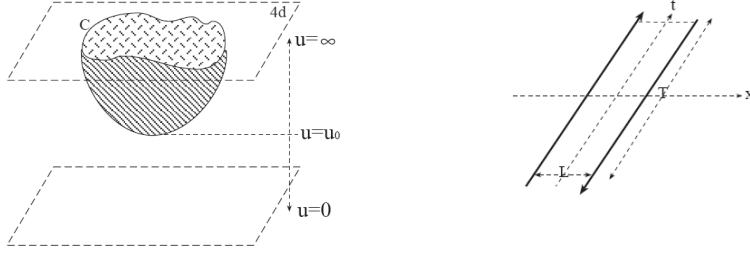


Figure 3: The geometry of the Wilson line. On the right the strip Wilson loop in real space-time that corresponds to a quark anti-quark potential and on the left the holographic description of a Wilson loop of a general contour C

a radial coordinate and additional coordinates transverse to the boundary and to the radial direction. We assume that the corresponding metric depends only on the radial coordinate such that its general form is

$$ds^2 = -g_{tt}(u) dt^2 + g_{uu}(u) du^2 + g_{x_{||}x_{||}}(u) dx_{||}^2 + g_{x_T x_T}(u) dx_T^2 \quad (10)$$

where t is the time direction, u is the radial coordinate, $x_{||}$ are the space coordinates on the boundary and x_T are the transverse coordinates. We adopt the notation in which the radial coordinate is positive defined and the boundary is located at $u = \infty$. In addition, a “horizon” may exist at $u = u_\Lambda$, such that spacetime is defined in the region $u_\Lambda < u < \infty$, instead of $0 < u < \infty$ as in the case where no horizon is present.

The construction we examine is that of the strip discussed above. This takes the form of an open string living in the bulk of the space with both its ends tied to the boundary. From the viewpoint of the field theory living on the boundary the endpoints of the string are the $q\bar{q}$ pair, so the energy of the string is related to the energy of the pair. In order to calculate the energy of this configuration on the classical level we use the notations and results of [30]. First, we define

$$\begin{aligned} f^2(u) &\equiv g_{tt}(u) g_{x_{||}x_{||}}(u) \\ g^2(u) &\equiv g_{tt}(u) g_{uu}(u) \end{aligned} \quad (11)$$

Upon choosing the worldsheet coordinates $\sigma = x$ (x is a coordinate on the boundary pointing in the direction from one endpoint of the string to the other one) and $\tau = t$. This is obviously the most natural gauge choice for the case of the strip Wilson line. If in addition we assume translation invariance along

t , the Nambu-Goto action describing the string takes the form

$$\begin{aligned}
S_{NG} &= T \int d\sigma d\tau \sqrt{\det [\partial_\alpha X^\mu \partial_\beta X^\nu g_{\mu\nu}]} \\
&= T \int dx dt \sqrt{f^2(u(x)) + g^2(u(x)) (\partial_x u)^2} \\
&= T(\Delta t) \int dx \mathcal{L}
\end{aligned} \tag{12}$$

where we assume a static configuration, Δt is the length of the strip along the time direction and T is the string tension which from here on we set to be one. Later we will bring it back again. Letting the derivative with respect to x , ∂_x , playing the role of the time derivative in standard canonical procedure, then the conjugate momentum and the Hamiltonian are

$$p = \frac{\delta \mathcal{L}}{\delta u'} = \frac{g^2(u) u'}{\sqrt{f^2(u) + g^2(u) u'^2}} \tag{13}$$

$$\mathcal{H} = p \cdot u' - \mathcal{L} = -\frac{f^2(u)}{\mathcal{L}} \tag{14}$$

As the Hamiltonian does not depend explicitly on x , its value is a constant of motion. We shall deal with the case in which $u(x)$ is an even function, and therefore there is a minimal value $u_0 = u(0)$ for which $u'(0) = 0$. At that point we see from (13) that $p = 0$. The constant of motion is therefore

$$\mathcal{H} = -f(u_0) \tag{15}$$

from which we can extract the differential equation of the geodesic line

$$\frac{du}{dx} = \pm \frac{f(u)}{g(u)} \frac{\sqrt{f^2(u) - f^2(u_0)}}{f(u_0)} \tag{16}$$

and re-express the on-shell Lagrangian (i.e. the Lagrangian on the equation of motion) as a function of $f(u)$ only

$$\mathcal{L} = \frac{f^2(u)}{f(u_0)} \tag{17}$$

Then the distance between the string's endpoints (or the distance between the “quarks”) is

$$\ell(u_0) = \int dx = \int du \left(\frac{du}{dx} \right)^{-1} = 2 \frac{1}{f(u_0)} \int_{u_0}^{u_b} du \frac{f^2(u_0)}{f^2(u)} \frac{g(u)}{\sqrt{1 - \left(\frac{f(u_0)}{f(u)} \right)^2}} \tag{18}$$

where u_0 is the minimal value in the radial direction to which the string reaches and u_b is the value of u on the boundary. The bare energy of the string is given by

$$\begin{aligned}
E_{bare}(u_0) &= \int dx \mathcal{L} = \int du \left(\frac{du}{dx} \right)^{-1} \mathcal{L} = 2 \int_{u_0}^{u_b} du \frac{g(u)}{\sqrt{1 - \left(\frac{f(u_0)}{f(u)} \right)^2}} \\
&= f(u_0) \cdot \ell(u_0) + 2 \int_{u_0}^{u_b} du g(u) \sqrt{1 - \frac{f^2(u_0)}{f^2(u)}}
\end{aligned} \tag{19}$$

Generically, the bare energy diverges and hence a renormalization procedure is needed. There are several renormalization schemes to deal with this infinity. These were summarized in [39]. Here we

follow [30] and use the mass subtraction scheme in which the bare masses of the quarks are subtracted from the bare energy. The bare external quark mass is viewed as a straight string with a constant value of x , stretching from $u = 0$ (or $u = u_\Lambda$ if there exists an horizon at u_Λ) to $u = u_b$, such that it is given by¹

$$m_{q,ext} = \int_{u_\Lambda}^{u_b} du g(u) \quad (20)$$

Then the renormalized energy would be given by

$$E(u_0) = f(u_0) \cdot \ell(u_0) - 2\mathcal{K}(u_0) \quad (21)$$

where $\mathcal{K}(u_0)$ is

$$\mathcal{K}(u_0) = \int_{u_0}^{u_b} du g(u) \left(1 - \sqrt{1 - \frac{f^2(u_0)}{f^2(u)}} \right) + \int_{u_\Lambda}^{u_0} du g(u) \quad (22)$$

It is important to emphasize that this result for the energy is only at the classical level and does not include quantum corrections.

In order to reproduce the QCD heavy quarks potential we first have to demand the holographic models to reproduce the asymptotic forms of the potential. This leads to several restrictions on the forms of the f and g functions. The condition for confining behavior at large distances was derived in [30]:

1. f has a minimum at u_{min} and $f(u_{min}) \neq 0$ or
2. g diverges at u_{div} and $f(u_{div}) \neq 0$

Then the string tension is given by $f(u_{min})$ or $f(u_{div})$, correspondingly. The second asymptotic is perturbative QCD at small distances. The conditions on the background to reproduce the leading perturbative behavior of QCD, which is Coulomb-like, were derived in [39].

The physical picture arising from this construction is as follows. The confining limit is approached as $u_0 \rightarrow u_\Lambda$, then most of the string lies at the vicinity of u_Λ which implies in the dual field theory a string-like interaction between the “quarks” with a string tension T_s (upon bringing back T that was set above to one)

$$T_s = T f(u_\Lambda) \quad (23)$$

and a linear potential

$$E = T_s \cdot \ell - 2\kappa \quad (24)$$

where $\kappa = \mathcal{K}(u_\Lambda)$ is a finite constant. On the other hand, the Coulomb-like limit is approached as $u_0/u_\Lambda \rightarrow \infty$, then the whole string is far away from u_Λ and is ruled by the geometry near the boundary. The conditions for such a behavior were analyzed in [39].

3.1.1 't Hooft line

In addition to the Wilson line one discusses also the Polyakov line and the 't Hooft line. The former is a Wilson line for which the contour C is the Euclidean time direction compactified on a circle. Correspondingly the holographic string realization of the Polyakov loop is a string whose worldsheet wraps the compactified time direction. We will not discuss it here. In YM theories the “electric-magnetic” dual of the Wilson line is the 't Hooft line. Just as one extracts the quark anti-quark potential from the former with the strip contour, the later determines for the same contour the monopole anti-monopole potential.

¹ We refer here to the dual of string that stretches to the boundary as an external quark to distinguish it from a dynamical quark whose dual is a string that ends on a flavor brane as will be explained in the next section

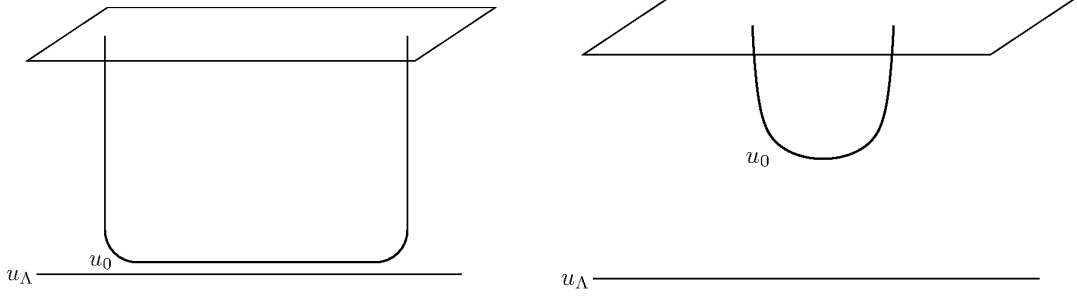


Figure 4: The physical picture arising from the present construction. Left: The confining limit is approached as the string is close to the horizon, then most of the string lies on the horizon and implies a string-like interaction between the quarks (the endpoints of the string). Right: The conformal limit is reconstructed when the string is far away from the horizon such that it is ruled by the geometry near the boundary.

We would like to address now the question of how to construct a string configuration which associates with the 't Hooft line. The answer for that question is that it should be a configuration of a $D1$ brane starting and ending on the boundary. The prototype confining background described in (§2.3) is that of a compactified D4 branes. This is a type II-A theory where the allowed D branes are only of the form $D2k$ and hence (at least in the supersymmetric case) one cannot embed a $D1$ brane. Instead we will take the stringy realization of the 't Hooft line as a $D2$ -brane ending on the $D4$ -brane. The $D2$ -brane is wrapped along the compact space direction x_4 so from the point of view of the four dimensional theory it is a point like object. The DBI action of a $D2$ -brane is

$$S = \frac{1}{(2\pi\alpha')^{3/2}} \int d\tau d\sigma_1 d\sigma_2 e^{-\phi} \sqrt{\det h}, \quad (25)$$

where h is the world-volume induced metric and ϕ is the dilaton. For the $D2$ -brane we consider, which is infinite along one direction (we denote its length by Y and winds the x_4 direction), we get

$$S = \frac{Y}{g_{YM}^2} \int dx \sqrt{\partial_x U^2 + \frac{u^3 - u_\Lambda^3}{R_4^3}}, \quad (26)$$

Note the $1/g_{YM}^2$ factor which is expected for a monopole. The distance between the monopole and the anti-monopole is

$$L = 2 \frac{R_4^{3/2}}{u_0^{1/2}} \sqrt{\epsilon} \int_1^\infty \frac{dy}{\sqrt{(y^3 - 1)(y^3 - 1 + \epsilon)}}. \quad (27)$$

where $\epsilon = 1 - (U_\Lambda/U_0)^3$. The energy (after subtracting the energy corresponding to a free monopole and anti-monopole) is

$$E = \frac{2u_0}{(2\pi)^{3/2} g_{YM}^2} \left[\int_1^\infty dy \left(\frac{\sqrt{y^3 - 1 + \epsilon}}{\sqrt{y^3 - 1}} \right) - 1 \right] + \frac{2(u_\Lambda - u_0)}{(2\pi)^{3/2}}. \quad (28)$$

For $L\Lambda \gg 1$ it is energetically favorable for the system to be in a configuration of two parallel $D2$ -branes ending on the horizon and wrapping x_0 . So in the "YM region" we find screening of the magnetic charge which is another indication to confinement of the electric charge. For further details on the holographic determination of the 't Hooft line see for instance [2].

3.2 The stringy duals of mesons

Next we want to identify among the strings that can reside in a holographic backgrounds those that correspond to mesons. Naturally a meson associates with an open string and the quark and anti-quark that it is built from with the string endpoints. As we have seen in the previous section, endpoints on the boundary of the holographic bulk correspond to infinitely heavy external quarks. Holographic backgrounds are associated with type II closed string theories. In such backgrounds open strings can start and end only on D-branes (or the boundary). Thus “dynamical quarks” should be related to string endpoints which are not on the boundary but rather they attach to D-branes. As was discussed in section §(2.2) flavored confining backgrounds include stacks of N_f D branes which are referred to as “flavor branes”. We consider only the case of $N_f \ll N_c$, where N_c is the number of branes that constitute in the near horizon limit the holographic background. Since the endpoints can freely move, then classically the strings do not shrink to zero size only if they rotate and the “centrifugal force” is balancing the string tension. Thus, to describe the stringy meson we will now discuss (i) The conditions on strings rotating at constant radial coordinate. (ii) Rotating strings attached to flavor branes.

3.2.1 The conditions on strings rotating at constant radial coordinate

Consider the background metric of (10). Setting aside the transverse coordinates, the metric reads

$$ds^2 = -g_{00}(u)dt^2 + g_{ii}(u)(dx^i)^2 + g_{uu}du^2 + \dots \quad (29)$$

where here we denote the metric along the space direction as g_{ii} , instead of $g_{||}$ as it was denoted in (10). The metric as well as any other fields of the background depend only on the radial direction u . Since we have in mind addressing spinning strings, it is convenient to describe the space part of the metric as

$$dx_i^2 = dR^2 + R^2 d\theta^2 + dx_3^2, \quad (30)$$

where x_3 is the direction perpendicular to the plane of rotation. The classical equations of motion of a bosonic string defined on this background can be formulated on equal footing in the NG formulation or the Polyakov action. Let us use now the latter. The equations of motion associated with the variation of t, θ, R and u respectively are

$$\begin{aligned} \partial_\alpha(g_{00}\partial^\alpha t) &= 0 \\ \partial_\alpha(g_{ii}R^2\partial^\alpha\theta) &= 0 \\ \partial_\alpha(g_{ii}\partial^\alpha R) - g_{ii}R\partial_\alpha\theta\partial^\alpha\theta &= 0 \\ 2\partial_\alpha(g_{uu}\partial^\alpha u) + \frac{dg_{00}}{du}\partial_\alpha t\partial^\alpha t - \frac{dg_{ii}}{du}\partial_\alpha x^i\partial^\alpha x^i - \frac{dg_{uu}}{du}\partial_\alpha u\partial^\alpha u &= 0, \end{aligned} \quad (31)$$

where α denotes the worldsheet coordinates τ and σ . In addition in the Polyakov formulation one has to add the Virasoro constraint

$$-g_{00}(\partial_\pm t)^2 + g_{ii}(\partial_\pm x^i)^2 + g_{uu}(\partial_\pm u)^2 + \dots = 0, \quad (32)$$

where $\partial_\pm = \partial_\tau \pm \partial_\sigma$, and \dots stands for the contribution to the Virasoro constraint of the rest of the background metric.

Next we would like to find solutions of the equations of motion which describe strings spinning in space-time. For that purpose we take the following ansatz

$$t = \tau \quad \theta = \omega\tau \quad R(\sigma, \tau) = R(\sigma) \quad u = \hat{u} = \text{constant}. \quad (33)$$

It is obvious that this ansatz solves the first two equations. The third equation together with the Virasoro constraint is solved (for the case that $g_{00} = g_{ii}$) by $R = A\cos(\omega\sigma) + B\sin(\omega\sigma)$ with $\omega^2(A^2 + B^2) = 1$. The boundary conditions we want to impose will select the particular combination of A and B . Let us now investigate the equation of motion associated with u and for the particular ansatz $u = \hat{u}$. This can be a solution only provided

$$\frac{dg_{00}}{du}|_{u=\hat{u}} = 0 \quad \frac{dg_{ii}}{du}|_{u=\hat{u}} = 0. \quad (34)$$

This is just the first condition for having a confining background. The condition $g_{00}g_{ii}(\hat{u}) > 0$ insures that the Virasoro constraint is obeyed in a nontrivial manner.

We would like to check the condition in the class of confining models that was discussed in §(2.3) namely those of compactified D branes and in particular the model of the near extremal $D4$ brane, compactified on an S^1 . Denoting the direction along the S^1 denoted by ψ , the corresponding component of the metric is related to that of the u direction as $g_{\psi\psi} = [g_{uu}]^{-1}$. Thus the condition for having a solution of the equation of motion with $u = \hat{u}$ includes the condition

$$\frac{dg_{\psi\psi}}{du}|_{u=\hat{u}} = -\frac{\frac{dg_{uu}}{du}}{g_{uu}^2}|_{u=\hat{u}} = 0. \quad (35)$$

This condition is obeyed if at $u = \hat{u}$ $g_{uu}(\hat{u}) \rightarrow \infty$, which is the second condition for a confining background with $\hat{u} = u_\Lambda$, and with the demand of non-vanishing $g_{00}g_{ii}(\hat{u}) > 0$ to have a non-trivial Virasoro constraint.

To summarize, we have just realized that there is a close relation between the conditions of having area law Wilson loop and of having a spinning string configuration at a constant radial coordinate.

3.2.2 The meson as a rotating string attached to flavor branes

We have seen above the conditions for having a rotating string at constant u . We would like to examine whether rotating strings with endpoints attached to flavor branes can obey these conditions. For the Wilson line in a “confining background” we found a string configuration that stretches vertically from the boundary down to the vicinity of the “wall”, then flattens along the wall and then “climbs” up vertically to a flavor brane. In a very similar manner we search for a string of the same type of profile but now not a static one. When the endpoints of the open string are not on the boundary and are not nailed down, the string does not shrink due to the tension only if it rotates and the “centrifugal force” balances the tension. Therefore we look for a solution of the string equation of motion of the form of a rotating string in a plane spanned by the x^i coordinates. Like the stringy Wilson line, the rotating string in the holographic background will include two vertical segments (region I) which connect the horizontal segment of the string (region II) to the flavor branes. Thus, the procedure to determine the holographic dual of the meson includes a solution of the equation of motion in the vertical segment (region I), a solution in the horizontal segment (region II), matching the two solutions and finally computing the corresponding energy and angular momentum as the Noether charges associated with the translation symmetry along the time and azimuthal directions. Before delving into the equations it should be useful to have a picture of the “mesonic rotating string”. It appears in figure (5).

The Nambu-Goto action associated with a rotating string in a background metric of the form (29) takes the form

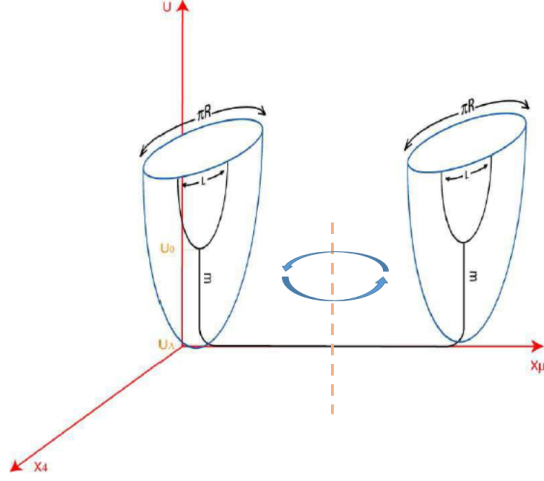


Figure 5: A meson as a rotating open string that stretches from the tip of the flavor brane at two points separated in X_i coordinates.

$$S = -T_s \int d\sigma d\tau \sqrt{((\partial_\tau X^0)^2 - R^2(\partial_\tau \theta)^2)(f^2(\partial_\sigma R)^2 + g^2(\partial_\sigma u)^2)}, \quad (36)$$

where we assume here that $g_{00} = g_{xx}$ and where f^2 and g^2 are defined in (11). Since we have in mind analysing rotating strings we do not consider the most general configuration but rather an ansatz similar to the one discussed above (33)

$$X^0 = X^0(\tau) \quad \theta = \theta(\tau) \quad R(\sigma, \tau) = R(\sigma) \quad u = u(\sigma). \quad (37)$$

The boundary conditions corresponding to this configuration are Neumann in the directions parallel to the flavor brane, and Dirichlet in the directions transverse to the brane, namely:

$$\begin{aligned} \left(\partial_\sigma X^0 = \partial_\sigma \theta = \partial_\sigma R = \partial_\sigma \lambda \right) \Big|_{\sigma=\pm\pi/2} &= 0, \\ u(\sigma) &= u_f \Big|_{\sigma=-\pi/2, \pi/2}. \end{aligned} \quad (38)$$

In fact for the rotating string we have $\theta = \omega\tau$ and since we can use the static gauge where $t = \tau$ the action in fact reads

$$\begin{aligned} S &= -T_s \int d\sigma d\tau \sqrt{(1 - R^2\omega^2)(f^2\partial_\sigma R^2 + g^2\partial_\sigma u^2)} \\ &= -T_s \int dR d\tau \sqrt{(1 - R^2\omega^2)(f^2 + g^2(u')^2)}, \end{aligned} \quad (39)$$

where here $u' = \frac{du}{dR}$

The equation of motion with respect to δu is given by

$$\frac{d}{dR} \left[\frac{1}{\gamma} \frac{g^2 u'}{\sqrt{(f^2 + g^2(u')^2)}} \right] = \frac{1}{\gamma} \frac{d\sqrt{(f^2 + g^2(u')^2)}}{du} \quad (40)$$

where $\gamma = \frac{1}{\sqrt{(1 - R^2\omega^2)}}$

Let us now examine whether this equation (40) indeed admits a solution of an horizontal part (region II) connected to flavor branes by vertical parts (region I). In regions I that are along

$$-\alpha > \sigma \geq -\pi/2 \quad \pi/2 \geq \sigma > \alpha \quad (41)$$

$$u' \rightarrow \infty, \sqrt{(f^2 + g^2(u')^2)} \rightarrow gu' \quad \gamma = \gamma(L) = \text{constant} \quad (42)$$

where along these segments $R = L$ with L is the length of the string. Thus the l.h.s of the equation turns into $\frac{dg}{dR}$ which is also the value of the r.h.s. In region II which is along

$$\alpha \geq \sigma \geq -\alpha \quad (43)$$

since we require there that $u = u_0$ is (approximately) constant we expand the equation (40) to leading order in u' . For finite $g(u_0)$ the l.h.s of the equation vanishes and thus since in this case $\sqrt{(f^2 + g^2(u')^2)} \rightarrow f$ it implies that $f(u)$ has to have an extremum at $u = u_0$. The other option that we want to examine is the case that $\lim_{u \rightarrow u_0} g^2(u) \rightarrow \infty$ which for the static case is one of the two sufficient conditions [30] to admit an confining area law behavior.

Since we took the string to stretch separately along region of the type I, region II and again region of the type I we have to reexamine the variation of the action with respect to δR .

$$\delta S = T \left(\int_{-\pi/2}^{-\alpha} + \int_{\alpha}^{\pi/2} \right) d\sigma d\tau \delta R \left[\gamma R (\dot{\theta})^2 g \partial_{\sigma} u \right] + T \int d\tau \delta R \frac{f^2 \partial_{\sigma} R}{\gamma \sqrt{f^2 + g^2(\partial_{\sigma} u)^2}} \Big|_{-\alpha}^{\alpha} \quad (44)$$

Upon substituting the solution of the bulk equations of motion and in particular that in the interval $(-\alpha, \alpha)$ $\partial_{\sigma} u = 0$, we find that the variation of the action can vanish only provided that

$$\frac{f(u_0)}{\gamma(L)} = \omega^2 L \gamma(L) \int_{u_0}^{u_f} du g(u) \quad (45)$$

Let us define now the notion of a string endpoint mass

$$m_{sep} = T \int_{u_0}^{u_f} g(u) \quad (46)$$

then the condition of the vanishing of the variation of the action takes the form

$$T_{eff} = m_{sep} \gamma^2 \omega^2 L \quad T_{eff} = T f(u_0) \quad (47)$$

As will be further discussed in section (§4.2) this is nothing but a balancing equation between the tension and the centrifugal force acting on the string endpoint, where the tension is exactly the same one that was found above for the Wilson line.

Next we determine the energy and angular momentum of the rotating string that get contributions from both the horizontal and vertical segments. The energy and angular momentum are the Noether charges associated with the invariance of the action under shifts of X^0 and θ respectively, given by

$$\begin{aligned} E &= T \int dR \gamma \sqrt{f^2 + g^2(u')^2} \\ J &= T \int dR R^2 \dot{\theta} \gamma \sqrt{f^2 + g^2(u')^2} \end{aligned} \quad (48)$$

The contribution of regions I is therefore given by

$$E_I = \frac{2m_{sep}}{\sqrt{1-\omega^2 L^2}}, \quad J_I = \frac{2m_{sep}\omega L^2}{\sqrt{1-\omega^2 L^2}} \quad (49)$$

which as will be discussed in section (§4.2) maps into the contribution to the energy and angular momentum of the massive endpoints of the string. The contribution of the string that stretches along region II is

$$\begin{aligned} E_{II} &= T_s \int_{-L}^L T \int dR \gamma \sqrt{f^2 + g^2(u')^2} \\ &= T_{eff} \frac{2}{\omega} \arcsin(\omega L) \end{aligned} \quad (50)$$

$$\begin{aligned} J_{II} &= T_s \int_{-L}^L dR R^2 \dot{\theta} \gamma \sqrt{f^2 + g^2(u')^2} \\ &= T_{eff} \left[\frac{1}{\omega^2} (\arcsin(\omega L) - \omega L \sqrt{1-\omega^2 L^2}) \right] \end{aligned} \quad (51)$$

Combining together the contributions of regions I and region II we find

$$E = T_{eff} \frac{2}{\omega} \arcsin(\omega L) + \frac{2m_{sep}}{\sqrt{1-\omega^2 L^2}} \quad (52)$$

$$J = T_g \frac{1}{\omega^2} (\arcsin(\omega L) - \omega L \sqrt{1-\omega^2 L^2}) + \frac{2m_{sep}\omega L^2}{\sqrt{1-\omega^2 L^2}}. \quad (53)$$

So far we have considered stringy holographic baryons that attach to one flavor brane. In holographic backgrounds one can introduce flavor branes at different radial locations thus corresponding to different string endpoint masses, or different quark masses. For instance, a setup that corresponds to u and d quarks of the same m_{sep} mass, a strange s quark, a charm c quark, and a bottom b quark is schematically drawn in figure (6). A B meson composed of a bottom quark and a light \bar{u}/\bar{d} anti-quark was added to the figure.

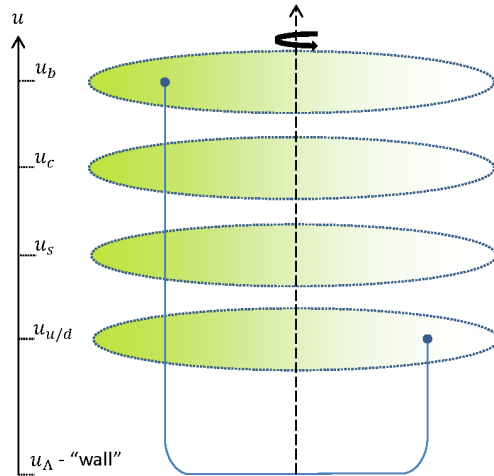


Figure 6: Holographic setup with flavor branes associated with the u, d quark, s, c and b quarks.

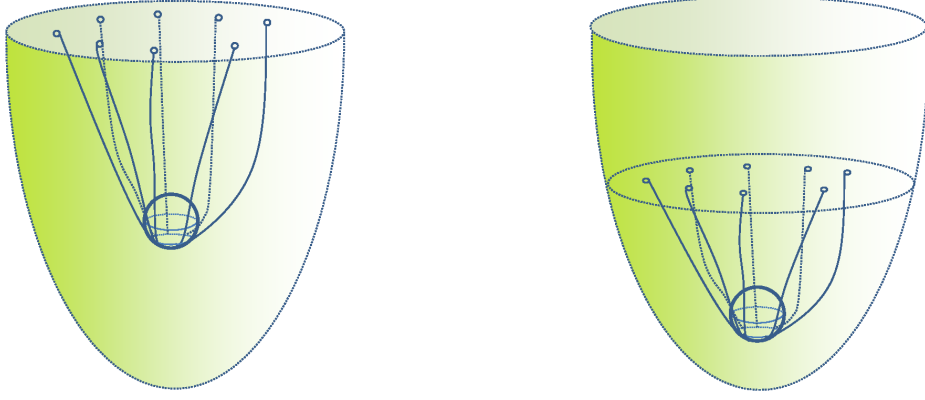


Figure 7: Schematic picture of holographic baryons. On the left is an external baryon with strings that end on the boundary, while on the right is a dynamical baryon with strings ending on a flavor brane.

3.3 Holographic stringy baryons

We have seen in the previous sections that (i) a string with its two ends on the boundary of a holographic background corresponds in the dual field theory to an external quark, and (ii) a rotating string with its ends on flavor probe branes is a dual of a meson. It is thus clear that a stringy holographic baryon has to include N_c strings that are connected together and end on flavor branes (dynamical baryon) or on the boundary (external baryon). The question is what provides the “baryonic vertex” that connects together N_c strings. In [40] it was shown that in the $AdS_5 \times S^5$ background, which is equipped with an RR flux of value N_c , a $D5$ brane that wraps the S^5 has to have N_c strings attach to it. This property can be generalized to other holographic backgrounds so that a Dp brane wrapping a non-trivial p cycle with a flux of an RR field of value N_c provides a baryonic vertex. These two possible stringy configurations are schematically depicted in figure (7). Whereas the dual of the original proposal [40] was a conformal field theory, baryons can be constructed also in holographic backgrounds that correspond to confining field theories. A prototype model of this nature is the Sakai Sugimoto model discussed in section(§ 2.3) of N_c $D4$ branes background compactified on a circle with an N_f $D8-\overline{D8}$ U-shaped flavor branes [28]. In this model the baryonic vertex is made out of a $D4$ brane that wraps an S^4 . Another model for baryons in a confining background is the deformed conifold model with $D7-\overline{D7}$ U-shaped flavor branes [41]. In this model the baryon is a $D3$ brane that wraps the three-cycle of the deformed conifold.

The argument why a Dp brane wrapping a fluxed p cycle is a baryonic vertex is in fact very simple. The world-volume action of the wrapped Dp brane has the form of $S = S_{DBI} + S_{CS}$. The CS term takes the following form

$$S_{CS} = \int_{S_p \times R_1} \sum_i c_{p_i} \wedge e^F = \int_{S_p \times R_1} c_{p-1} \wedge F = - \int_{S_p \times R_1} F_p \wedge A = -N_c \int_{R_1} A \quad (54)$$

where (i) the sum over i is over the RR p -forms that reside in the background, (ii) from the sum one particular RR form was chosen, the c_{p-1} -form that couples to the Abelian field-strength F , (iii) for simplicity we took the p cycle to be S^p , (iv) A is the Abelian connection that resides on the wrapped brane, (v) F_p is the RR p -form field strength, and (vi) in the last step we have made use of the fact that $\int_{S^p} F_p = N_c$. This implies that there is a charge N_c for the Abelian gauge field. Since in a compact space one cannot have non-balanced charges and since the endpoint of a string carries a charge one, there must be N_c strings attached to it.

It is interesting to note that a baryonic vertex, rather than being a “fractional” $D0$ brane of the form of a Dp brane wrapping a p cycle, can also be a $D0$ brane in an N_c fluxed background. This is the

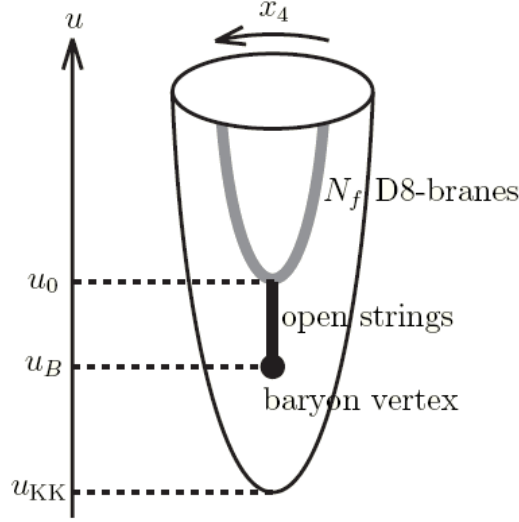


Figure 8: The location of the baryonic vertex along the radial direction of the Sakai-Sugimoto model. u_0 is the tip of the flavor branes and u_{kk} is the “confining scale” of the model.

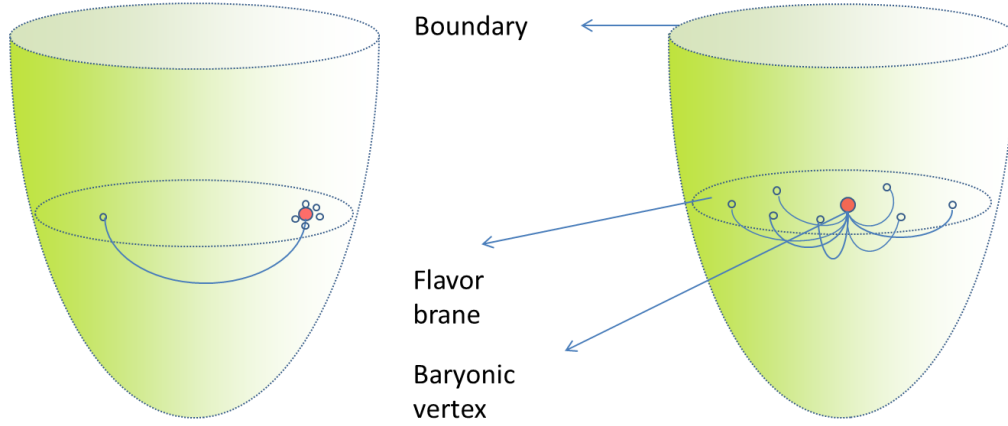


Figure 9: The location of the baryonic vertex on the flavor brane and the corresponding configuration of the baryon for some large N_c . When $N_c = 3$, the left is the analog of the quark-diquark flat space-time model, and the right the analog of the Y-shape model.

case in the non-critical string backgrounds like [18] where there is no non-trivial cycle to wrap branes over, but an “ordinary” $D0$ brane in this background there is also a CS term of the form $N_c \int_{R_1} A$.

Next we would like to determine the location of the baryonic vertex in the radial dimension. In particular the question is whether it is located on the flavor branes or below them. This is schematically depicted in figure (8) for the model of [28].

In [42] it was shown that in the model of [28] by minimizing the “mechanical energy” of the N_c strings and the wrapped brane that it is preferable for the baryonic vertex to be located on the flavor branes of the model. It was also found that for the baryonic vertex of the model of [26], if the tip of the U-shaped flavor brane is close to the lowest point of the deformed conifold the baryonic vertex is on the flavor branes, but there is also a range of parameters where it will end up below the flavor branes. It is interesting to note that for a background that corresponds to the deconfining phase of the dual gauge theory the baryonic vertex falls into the “black hole” and thus the baryon dissolves.

The locations of the baryonic vertex and the ends of the N_c strings on the flavor branes is a dynamical

issue. In figure (9) we draw two possible setups. In one the baryonic vertex is located at the center and the N_c ends of the strings are located around it in a spherically symmetric way. In the “old” stringy model of baryons for three colors this is the analog of the Y-shape configuration that we will further discuss in the sections describing the flat space-time models. Another possibility is that of a baryonic vertex is connected by $N_c - 1$ very short strings and with one long string to the flavor branes. Since the product of $N_c - 1$ fundamental representations includes the anti-fundamental one, this configuration can be viewed as a string connecting a quark with an anti-quark. For the case of $N_c = 3$ this is the analog of what will be discussed below as the quark-diquark stringy configuration. This latter string configuration (for any N_c) is similar to the stringy meson, but there is a crucial difference, which is the fact that the stringy baryon includes a baryonic vertex.

Correspondingly there are many options of holographic stringy baryons that connect to different flavor branes. This obviously relates to baryons that are composed of quarks of different flavor. In fact there are typically more than one option for a given baryon. In addition to the distinction between the central and quark-diquark configurations there are more than one option just to the latter configuration. We will demonstrate this situation in section 6.3.8, focusing on the case of the doubly strange Ξ baryon (ssd or ssu). The difference between the two holographic setups is translated to the two options of the diquark being either composed of two s quarks, whereas the other setup features a ds or us diquark. Rather than trying to determine the preferred configuration from holography we will use a comparison with experimental data to investigate this issue.

3.4 The glueball as a rotating closed string

The third type of a hadron is the glueball. The fact that the latter does not include quarks maps under the holographic duality to a string with no endpoints, namely, a closed string. Before analyzing the closed strings of holographic background we first review certain general properties of closed string. Firstly we would like to remind the reader the classical rotating string in flat space-time.

3.4.1 Classical rotating folded string

Here we use the Nambu-Goto action for the string

$$S = -\frac{1}{2\pi\alpha'} \int d\tau d\sigma \sqrt{-h}, \quad (55)$$

with

$$h = \det h_{\alpha\beta}, \quad h_{\alpha\beta} = \eta_{\mu\nu} \partial_\alpha x^\mu \partial_\beta x^\nu, \quad (56)$$

and

$$\alpha' = \frac{1}{2\pi T}. \quad (57)$$

The rotating folded string is the solution

$$x^0 = \tau \quad x^1 = \frac{1}{\omega} \sin(\omega\sigma) \cos(\omega\tau) \quad x^2 = \frac{1}{\omega} \sin(\omega\sigma) \sin(\omega\tau). \quad (58)$$

We take $\sigma \in (-\ell, \ell)$ and correspondingly ω takes the value $\omega = \pi/\ell$. The energy of this configuration is

$$E = T \int_{-\ell}^{\ell} d\sigma \partial_\tau X^0 = 2T\ell \quad (59)$$

The angular momentum we can get by going to polar coordinates ($x^1 = \rho \cos \theta$, $x^2 = \rho \sin \theta$), then

$$J = T \int_{-\ell}^{\ell} d\sigma \rho^2 \partial_\tau \theta = \frac{T}{\omega} \int_{-\ell}^{\ell} d\sigma \sin^2(\omega\sigma) = \frac{\pi T}{\omega^2} = \frac{T\ell^2}{\pi} \quad (60)$$

From the last two equations we can easily see that for the classical rotating folded string

$$J = \frac{1}{4\pi T} E^2 = \frac{1}{2} \alpha' E^2 \quad (61)$$

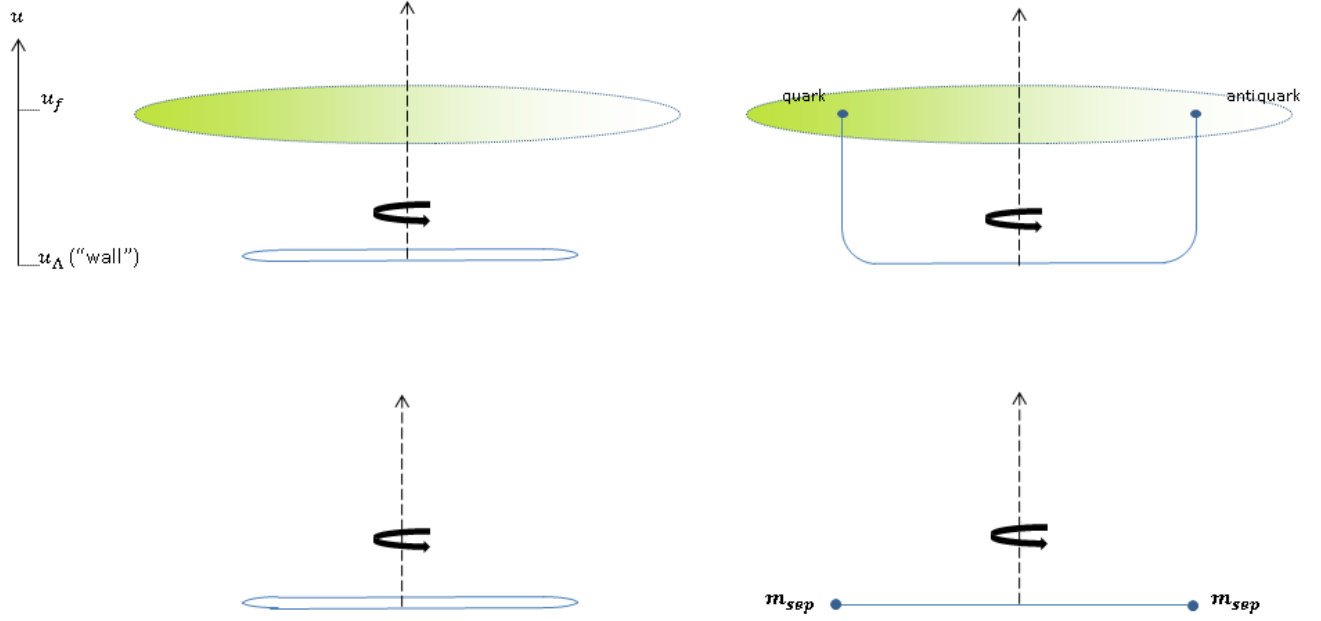


Figure 10: Closed and open strings in holographic backgrounds (above), and their mappings into flat spacetime (below). For the open string, the mapping from curved to flat background adds endpoint masses to the strings, with the vertical segments mapped to the point-like masses in flat space. For the closed string, we look at the simple folded string in both cases. Note that classically the rotating folded string has zero width, and as such would look like an open string with no endpoint masses, and not like in the drawing.

Thus we conclude that the Regge slope for the closed string is

$$\alpha'_{closed} = \frac{1}{2} \alpha'_{open} , \quad (62)$$

A simple explanation for this property is that one can regard the fully folded string as two strings and hence the tension of the system is twice the tension of a single open string and correspondingly the slope of the closed string is half of the open one. This property that holds also for the rotating folded string in curved holographic background, as will be shown in §(6.4), will be the main tool for our proposed phenomenological identification of glueballs (see §(3.42)).

It is well known that this ratio between the slopes (or tensions) follows also from gauge theory arguments. This is based on the fact that the potential between two static adjoint $SU(N)$ charges, is proportional to the quadratic Casimir operator. For small distances this group theory factor can be obtained easily from perturbation theory. Calculations in [43] show that what is referred to as the “Casimir scaling hypothesis” holds in lattice QCD for large distances as well, and this means that the effective string tension also scales like the Casimir operator (as the potential at large distances is simply $V(\ell) \approx T_{eff} \ell$). Therefore, a model of the glueball as two adjoint charges (or constituent gluons) joined by a flux tube predicts the ratio between the glueball and meson (two fundamental charges) slopes to be

$$\frac{\alpha'_{gb}}{\alpha'_{q\bar{q}}} = \frac{C_2(\text{Fundamental})}{C_2(\text{Adjoint})} = \frac{N^2 - 1}{2N^2} = \frac{4}{9} , \quad (63)$$

where for the last equation we take $N = 3$. For $N \rightarrow \infty$ we recover the ratio of $1/2$. Note, however, this type of determination of the ratio from QCD is not valid at higher orders non-perturbatively.

Other models attempt to tie the closed string to the phenomenological "pomeron". The pomeron slope is measured to be

$$\alpha'_{pom} = 0.25 \text{ GeV}^{-2} \approx 0.28 \times \alpha'_{meson} \quad (64)$$

and the pomeron trajectory commonly associated with both glueballs and closed strings. One string model that predicts a pomeron-like slope was proposed [44] and is presented in [45], or in more detail in [46]. It is simply the model of a rotating closed string, with a fixed circular shape. This string has two types of trajectories, a phononic trajectory (excitations propagating along the string) which has $\alpha'_{phonon} = \frac{1}{4}\alpha'_{open}$, and an orbital trajectory (the circular string rotating around an axis in the circle's plane), for which $\alpha'_{orbital} = \frac{3\sqrt{3}}{16}\alpha'_{open} \approx 0.32 \times \alpha'_{open}$. If the rotating circular loop were allowed to deform, it would have necessarily flowed towards the flattened folded string configuration that we have been discussing, which always maximizes the angular momentum at a given energy. There are also other possibilities of rigidly rotating closed string of other shapes, as in [47], which may give yet another prediction of the ratio between open and closed string Regge slopes.

3.4.2 The closed string in a curved Holographic background

Now that we spelled out the basic properties of the classical rotating folded string in flat space time, we want to explore the same type of configurations but now in holographic confining backgrounds. The full analysis of rotating closed string in holographic curved backgrounds was performed in [48]. We present here the key points in short form.

If we look at a curved background metric of the form

$$ds^2 = h(r)^{-1/2}(-dX^0 dX^0 + dX^i dX^i) + h(r)^{1/2} dr^2 + \dots, \quad (65)$$

, namely with $g_{00} = h(r)^{-1/2}$ with $i = 1, 2, 3$ and the ellipsis denoting additional transverse coordinates, the rotating folded string, namely the configuration,

$$X^0 = e\tau \quad X^1 = e \sin \sigma \cos \tau \quad X^2 = e \sin \sigma \sin \tau, \quad (66)$$

is still² a solution to the string equations of motion provided we take

$$r(\sigma, \tau) = r_0 = \text{Const.} \quad (67)$$

where r_0 is a point where the metric satisfies the condition

$$\partial_r g_{00}(r)|_{r=r_0} = 0, \quad g_{00}(r)|_{r=r_0} \neq 0 \quad (68)$$

This is also one of the sufficient conditions for the dual gauge theory to be confining [30]. Compared to the folded string in flat spacetime, the energy and angular momentum take each an additional factor in the form of $g_{00}(r_0)$:

$$E = \frac{1}{2\pi\alpha'} \int_{-\pi}^{\pi} g_{00}(r_0) d\sigma = g_{00}(r_0) \frac{e}{\alpha'} \quad (69)$$

$$J = T \int_{-\pi}^{\pi} g_{00}(r_0) \sin^2 \sigma d\sigma = g_{00}(r_0) \frac{e^2}{2\alpha'} \quad (70)$$

²We follow a somewhat different normalization here, taking $\omega = \pi/\ell$ from the previous section to be 1, and introducing a common prefactor e , but the solution is essentially the same as the flat space solution of section 3.4.1.

Defining an effective string tension $T_{eff} = g_{00}(r_0)T$ and slope $\alpha'_{eff} = (2\pi T_{eff})^{-1}$, we can write the relation

$$J = \frac{1}{2}\alpha'_{eff}E^2 \quad (71)$$

The same factor of $g_{00}(r_0)$ multiplies the effective tension in the open string case, and therefore the closed and open string slopes are still related by the factor of one half, although the open string trajectories have the additional modification which can be ascribed to the presence of endpoint masses [49, 3]. We draw the two types of strings in figure 10.

4 Holography inspired hadronic strings

In the previous section we have determined the classical string configurations that correspond to Wilson lines, mesons, baryons and glueballs in holographic background. Analyzing, and in particular quantizing, strings in curved holographic backgrounds is a rather complicated task. In this section we will argue that one can approximate the holographic string configurations by modified strings in flat space time. It is important to emphasize that whereas the stringy holographic configurations are supposed to be duals of gauge invariant objects of certain confining gauge theory in the large N and large λ approximation, the stringy picture that we discuss from here on is **a phenomenological model**. It is by no means a formal passage from the large N large λ region to the QCD domain of $N_c = 3$ and λ of $\mathcal{O}(1)$. In this section we first describe the “map” from the holographic models of classical hadronic strings to models of classical strings in flat space-time. We then analyze the system of rotating strings with massive endpoint which as will be shown below associate with both mesons and baryons. We discuss the stability of baryonic configurations and certain properties of closed strings. In the next section we will address the problem of quantizing these systems.

4.1 The map from holographic strings to strings in flat space-time

The map from holographic strings to strings in flat space-time includes several ingredients:

- All the stringy configurations in holographic confining background that were discussed in section (§3) are characterized by having a “flat string” that stretches close to the “wall” of the confining background. For the glueball it is a closed string, for the mesons and baryons a string connected to flavor D branes and for the Wilson line connected to the boundary.

In all these cases the strings are characterized by an effective string tension which is given by the “bare” string tension dressed in the following way

$$\begin{aligned} T_{eff} &= Tf(u*) = T\sqrt{g_{00}(u*)g_{xx}(u*)} \\ \text{either } f_{min} &= f(u*) \text{ or } \lim_{u \rightarrow u*} g(u) \rightarrow \infty \end{aligned} \quad (72)$$

Obviously for the closed strings the tension will be $T_{closed} = 2T_{open}$.

- All the holographic open strings: the Wilson line, the meson and the baryon include, as was shown in section (§3), two vertical strings that connect the horizontal string that stretches in the vicinity of the “wall” and flavor branes or the boundary of the holographic bulk. It was shown there that

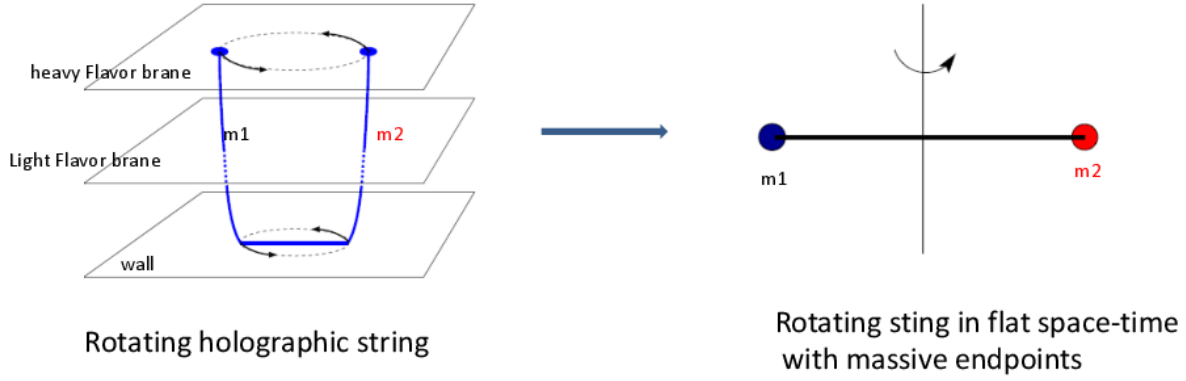


Figure 11: On the left: rotating holographic open string and on the right the corresponding open string with massive endpoints in flat space-time with $m_1 = m_2$.

the action (or energy) of these segments can be converted to the action of massive particles at the ends of the string where the mass is given by

$$m_{sep} = T \int_{u_0}^{u_f} g(u) \quad (73)$$

The role of the masses in the map is described in figure (11). In the next subsection we will classically analyze such a string with massive endpoints and in the next section we will address the issue of its quantization. It is interesting also to note the role of these masses for the stringy Wilson line in flat space time. As was discussed in section (§3.1) the holographic Wilson line diverges and has to be renormalized. This can be done in several different methods. One of them is exactly the subtraction of the action of the vertical strings, namely the mass at the endpoints. Moreover the outcome of the subtraction is that in addition to the linear term the energy of the string has also a constant term (and terms that depend on negative powers of the length). The interpretation of the constant term is that of an addition of a mass (or masses). For a detailed description see [30].

- For baryons the transition from the holographic strings to those of “Holography inspired models” there is a dramatic difference and that is that whereas in the former the number of colors N_c and hence the number of string arms is large in the latter it is taken to be $N_c = 3$. As explained above we do not claim to have a controlled method to pass from large N_c we take as an ansatz that there are three strings connected to the baryonic vertex.
- An important ingredient of the transition is the fact that whereas the original holographic models are in critical ten dimensions the model in flat space-time is taken to be non-critical in four space-time dimension. This will have a dramatic effect on the quantum action of the string due to the Liouville term.

4.2 The rotating string with massive endpoints

³ We describe the string with massive endpoints (in flat space-time) by adding to the Nambu-Goto action,

$$S_{NG} = -T \int d\tau d\sigma \sqrt{-h} \quad (74)$$

$$h_{\alpha\beta} \equiv \eta_{\mu\nu} \partial_\alpha X^\mu \partial_\beta X^\nu$$

a boundary term - the action of a massive chargeless point particle

$$S_{pp} = -m \int d\tau \sqrt{-\dot{X}^2} \quad (75)$$

$$\dot{X}^\mu \equiv \partial_\tau X^\mu$$

at both ends. There can be different masses at the ends, but here we assume, for simplicity's sake, that they are equal. We also define $\sigma = \pm l$ to be the boundaries, with l an arbitrary constant with dimensions of length.

The variation of the action gives the bulk equations of motion

$$\partial_\alpha \left(\sqrt{-h} h^{\alpha\beta} \partial_\beta X^\mu \right) = 0 \quad (76)$$

and at the two boundaries the condition

$$T \sqrt{-h} \partial^\sigma X^\mu \pm m \partial_\tau \left(\frac{\dot{X}^\mu}{\sqrt{-\dot{X}^2}} \right) = 0 \quad (77)$$

It can be shown that the rotating configuration

$$X^0 = \tau, X^1 = R(\sigma) \cos(\omega\tau), X^2 = R(\sigma) \sin(\omega\tau) \quad (78)$$

solves the bulk equations (76) for any choice of $R(\sigma)$. We will use the simplest choice, $R(\sigma) = \sigma$, from here on.⁴ Eq. (77) reduces then to the condition that at the boundary,

$$\frac{T}{\gamma} = \gamma m \omega^2 l \quad (79)$$

with $\gamma^{-1} \equiv \sqrt{1 - \omega^2 l^2}$.⁵ We then derive the Noether charges associated with the Poincaré invariance of the action, which include contributions both from the string and from the point particles at the boundaries. Calculating them for the rotating solution, we arrive at the expressions for the energy and angular momentum associated with this configuration:

$$E = -p_0 = 2\gamma m + T \int_{-l}^l \frac{d\sigma}{\sqrt{1 - \omega^2 \sigma^2}} \quad (80)$$

$$J = J^{12} = 2\gamma m \omega l^2 + T \omega \int_{-l}^l \frac{\sigma^2 d\sigma}{\sqrt{1 - \omega^2 \sigma^2}} \quad (81)$$

³The theory of a bosonic string with massive endpoints has been already addressed in the original application of string theory to hadron physics. For instance see[95]. It is worth mentioning though that up to date the quantization of this system has not been fully solved.

⁴Another common choice is $X^0 = \tau, x^1 = \sin(\sigma) \cos(\omega\tau), X^2 = \sin(\sigma) \sin(\omega\tau)$.

⁵Notice that in addition to the usual term γm for the mass, the tension that balances the “centrifugal force” is $\frac{T}{\gamma}$.

Solving the integrals, and defining $q \equiv \omega l$ - physically, the endpoint velocity - we write the expressions in the form

$$E = \frac{2m}{\sqrt{1-q^2}} + 2Tl \frac{\arcsin(q)}{q} \quad (82)$$

$$J = 2ml \frac{q}{\sqrt{1-q^2}} + Tl^2 \left(\frac{\arcsin(q) - q\sqrt{1-q^2}}{q^2} \right) \quad (83)$$

The terms proportional to m are the contributions from the endpoint masses and the term proportional to T is the string's contribution. These expressions are supplemented by condition (79), which we rewrite as

$$Tl = \frac{mq^2}{1-q^2} \quad (84)$$

This last equation can be used to eliminate one of the parameters l, m, T , and q from J and E . Eliminating the string length from the equations we arrive at the final form

$$E = 2m \left(\frac{q \arcsin(q) + \sqrt{1-q^2}}{1-q^2} \right) \quad (85)$$

$$J = \frac{m^2}{T} \frac{q^2}{(1-q^2)^2} \left(\arcsin(q) + q\sqrt{1-q^2} \right) \quad (86)$$

These two equations are what define the Regge trajectories of the string with massive endpoints. They determine the functional dependence of J on E , where they are related through the parameter $0 \leq q < 1$ ($q = 1$ when $m = 0$). Since the expressions are hard to make sense of in their current form, we turn to two opposing limits - the low mass and the high mass approximations. In the low mass limit where the endpoints move at a speed close to the speed of light, so $q \rightarrow 1$, we have an expansion in (m/E) :

$$J = \alpha' E^2 \left(1 - \frac{8\sqrt{\pi}}{3} \left(\frac{m}{E} \right)^{3/2} + \frac{2\sqrt{\pi^3}}{5} \left(\frac{m}{E} \right)^{5/2} + \dots \right) \quad (87)$$

from which we can easily see that the linear Regge behavior is restored in the limit $m \rightarrow 0$, and that the first correction is proportional to \sqrt{E} . The Regge slope α' is related to the string tension by $\alpha' = (2\pi T)^{-1}$. The high mass limit, $q \rightarrow 0$, holds when $(E - 2m)/2m \ll 1$. Then the expansion is

$$J = \frac{4\pi}{3\sqrt{3}} \alpha' m^{1/2} (E - 2m)^{3/2} + \frac{7\pi}{54\sqrt{3}} \alpha' m^{-1/2} (E - 2m)^{5/2} + \dots \quad (88)$$

4.3 The stringy baryon and its stability

Next we discuss the stringy baryon. For the case of $N_c = 3$, the asymmetric configuration depicted in figure 7. is the analog of what will be discussed below as the quark-diquark stringy configuration. This latter string configuration (for any N_c) is similar to the stringy meson, but there is a crucial difference, which is the fact that the stringy baryon includes a baryonic vertex which carries the baryon number.

It was shown in [49] that the classical rotating holographic stringy configuration of the meson can be mapped into that of a classical rotating bosonic string in flat space-time with massive endpoints. A similar map applies also to holographic stringy baryons that can be transformed into stringy baryons in flat space time with massive endpoints. We will proceed now to discuss this map for the central and asymmetric layouts of figure (9). The asymmetric holographic configuration of a quark and $N_c - 1$ quarks on the two ends of the holographic string depicted in figure (12) is mapped into a similar stringy configuration in flat space-time where the vertical segments of the string are transferred into massive

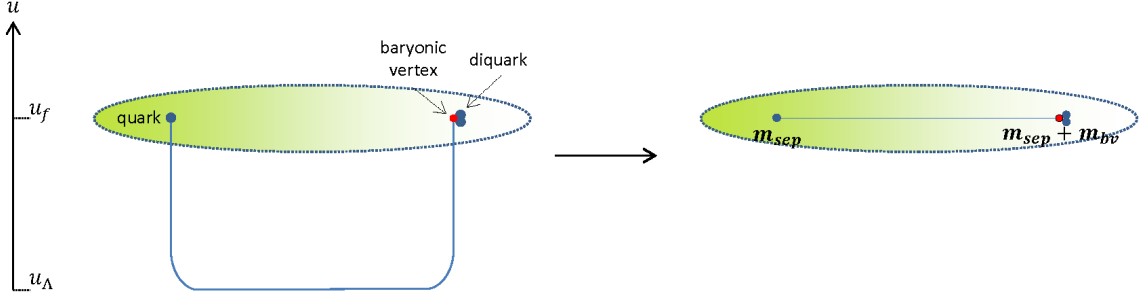


Figure 12: The holographic setup downlifted to $N_c = 3$ of a quark and a diquark is mapped to a similar configuration in flat space-time. The vertical segments of the holographic string are mapped into masses of the endpoints.

endpoints of the string. On the left hand side of the string in flat space-time there is an endpoint with mass m_{sep} given by

$$m_{sep} = T \int_{u_\Lambda}^{u_f} du \sqrt{g_{00}g_{uu}} \quad (89)$$

where u_λ is the location of the “wall”, u_f is the location of the flavor brane, and g_{00} and g_{uu} are the 00 and uu components of the metric of the background. On the right hand side the mass of the endpoint is a sum of $m_{sep} + m_{bv}$. This is the sum of the energy associated with the vertical segment of the string, just like that of the right hand side, and the mass of the baryonic vertex. Note that even though on the right endpoint of the string there are in fact two endpoints or “two quarks” the mass is that of a single quark since there is a single vertical string. This string setup is obviously very similar to that of the meson. The only difference is the baryonic vertex that resides at the diquark endpoint. Since we do not know how to evaluate the mass of the baryonic vertex, it will be left as a free parameter to determine by the comparison with data. Our basic task in this case will be to distinguish between two options: (i) the mass of the baryonic vertex is much lighter than the endpoint mass, $m_{bv} \ll m_{sep}$, in which case the masses at the two endpoints will be roughly the same, and (ii) an asymmetric setup with two different masses if the mass of the baryonic vertex cannot be neglected.

The configuration with a central baryonic vertex can be mapped into the analog of a Y-shaped object with N_c massive endpoints and with a central baryonic vertex of mass $m_c = m_{bv} + N_c m_{sep}$. The factor of N_c is due to the fact that there are N_c strings that stretch from it vertically from the flavor brane to the “Wall”, as can be seen in figure (13) for the case of $N_c = 3$. In this case, regardless of the ratio between the mass of the baryonic vertex and that of the string endpoint, there is a massive center which is at least as heavy as three sting endpoints.

So far we have considered stringy holographic baryons that attach to one flavor brane. In holographic backgrounds one can introduce flavor branes at different radial locations thus corresponding to different string endpoint masses, or different quark masses. For instance, a setup that corresponds to u and d quarks of the same m_{sep} mass, a strange s quark, a charm c quark, and a bottom b quark is schematically drawn in figure (6). A B meson composed of a bottom quark and a light \bar{u}/\bar{d} antiquark was added to the figure.

Correspondingly there are many options of holographic stringy baryons that connect to different flavor branes. This obviously relates to baryons that are composed of quarks of different flavor. In fact there are typically more than one option for a given baryon. In addition to the distinction between the central and quark-diquark configurations there are more than one option just to the latter configuration. We will demonstrate this situation in section 6.3.8, focussing on the case of the doubly strange Ξ baryon (ssd or ssu). The difference between the the two holographic setups is translated to the two options of the diquark being either composed of two s quarks, whereas the other setup it is a ds/us diquark.

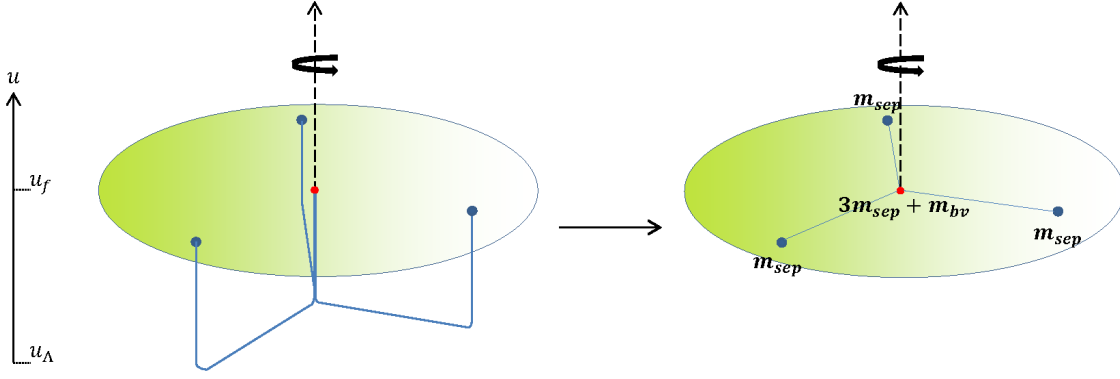


Figure 13: The map between the holographic central configuration (for $N_c = 3$) and the Y-shaped string in flat space-time.

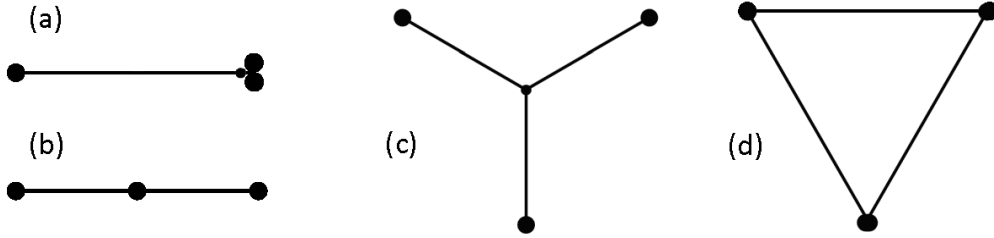


Figure 14: Four different stringy models for the baryon in flat space-time. (a) is the quark-diquark model, (b) the two-string model, (c) the three-string Y-shape, and (d) the closed Δ -shape. (a) and (c) are the models discussed in the preceding discussion of holographic strings and their mappings to flat space-time.

Rather than trying to determine the preferred configuration from holography we will use the comparison with the observational spectra to investigate this issue.

There are some words to be said about the models emerging when mapping the holographic rotating strings to flat space-time. In this section, we briefly discuss another matter: the stability of the rotating solution. Specifically, we claim that the Y-shape model of the baryon is (classically) unstable. In our analysis of the spectrum we will disregard this potential instability of the model and use the expressions for the energy and angular momentum of the unperturbed rotating solution of the Y-shape model as one of our fitting models, but it is important to remember that there is this theoretical argument against it as a universal setup for baryons before we test it out as a phenomenological model.

Other than the Y-shape and quark-diquark configurations which we analyze, there are two more possible stringy models for the baryon when considering a purely flat space-time point of view. These are drawn, together with the quark-diquark and Y-shape models, in figure (14). The additional models are the two-string model where one of the quarks is located at the center of the baryon, and the other two are attached to it by a string. The second is the Δ -shape model, in which each quark is connected to the other two. It can also be looked at as a closed string with three points along it that carry finite momentum (which can be either massive or massless). While the two-string model may have its analog in holography, with the baryonic vertex lying with the quark at the center of mass, the Δ -shaped string cannot be built if we impose the constraint that the three quarks should all be connected to a baryonic vertex.

Two independent analyses of the three-string model[50][51] concluded that the rotating solution of the Y-shape configuration is unstable, even before taking quantum effects into account. In another

work, it was found that the instability does not show itself in first order perturbation theory[52], but the claim of the unstable nature of the Y-shape model has been verified using numerical methods in [53], where the instability was observed in simulations and its dependence on endpoint masses was examined. To summarize the result, in the three-string Y-shape model, a perturbation to one of the three arms would cause it to shorten until eventually the Y-shape collapses to a form like that of the straight two-string model. From this model in turn a different kind of instability is expected[50][51]. The quark in the center of the baryon will move away from the center of mass given a small perturbation and as it approaches one of the quarks at the endpoints quantum effects will induce a collapse to the single string quark-diquark model, it being energetically favorable for two of the quarks to form an diquark bound state in the anti-fundamental color representation. It would seem that all other models have an instability that would cause them to eventually collapse to the quark-diquark configuration as two quarks get close enough to each other.⁶

From a phenomenological point of view the models differ in their prediction of the slope of the Regge trajectory. Assuming the strings in baryons have the same tension as those in mesons, we can see which of the models offers the best match. We will see that it is the configuration we know to be stable, that of a single string with a quark and a diquark at its endpoints.⁷

4.4 The stringy glueball

The map of the classical folded rotating closed string in holographic background to a similar string in flat four dimensions is simple. Unlike the case of the open string here there are no vertical segments involved and correspondingly no m_{sep} . It is just the string tension dependence on the holographic background that makes it different from an ordinary rotating folded closed string in flat space-time. However, as will be seen in (§6.1), the form of the quantum string yields another significant difference from the ordinary closed string. According to [48] we find that the relation between the energy and angular momentum is modified from the linear Regge trajectory form and looks like

$$J = \alpha'_{closed}(E - m_0)^2 + \tilde{a}. \quad (90)$$

Thus one may interpret the result as described by an action that includes a closed string plus a massive particle in the center of the closed string thought an interpretation of a quantum fluctuation as a classical particle may be suspicious. As will be mention above for the case of Witten's model m_0 is positive and hence it indeed fits the picture of a massive particle in the center whereas for the models discussed in [48] the mass is negative and thus the interpretation is less clear. The addition of the massive particle at the center maybe related to the observation made in [56] about the presence of a massive pseudoscalar axion on the worldsheet of confining flux tubes.

5 On the quantum stringy hadrons

So far we have described the model of holography inspired stringy hadrons classically. Though the basic property of the spectrum, the relation between the mass and the angular momentum, follows from the classical configuration, the quantum corrections of the classical spectrum are also quite important. It is well known that the basic classical linear Regge trajectory in the critical dimension is shifted

$$J = \alpha' M^2 \quad \rightarrow \quad J = \alpha' M^2 + a \quad (91)$$

⁶More discussion and detailed analyses of the different stringy models of the baryon and their stability are found in the work of G.S. Sharov, most recently in [54].

⁷The quark-diquark model was also used to analyze the baryon spectrum in [55].

where a is the quantum intercept and furthermore there are quantum excitations denoted by n that relate to the mass as $n = \alpha' M^2 + a$ so that altogether the linear quantum trajectories is given by

$$n + J = \alpha' M^2 + a \quad (92)$$

This form of the linear trajectory follows from the quantization of the open string. In [57] the quantization of the Nambu Goto action of the open string with Dirichlet boundary conditions was performed and yielded the following expression for the energy of the string

$$E_{stat} = \sqrt{(TL)^2 + 2\pi T \left(n - \frac{D-2}{24} \right)} \quad (93)$$

If instead of the static string we take the rotating one, we are instructed from the classical solution to replace $TL \rightarrow \sqrt{2\pi T J}$ so that we find for the rotating case

$$E_{rot} = \sqrt{2\pi T \left(J + n - \frac{D-2}{24} \right)} \quad (94)$$

which is exactly (92) when the intercept is taken to be $a = \frac{D-2}{24}$. It is indeed well known that the intercept is given in terms of the Casimir energy which is the sum of the eigenvalues of the worldsheet Hamiltonian w_n , namely

$$E_{Casimir} \equiv \frac{1}{2} \sum_{n=1}^{n=\infty} w_n = \frac{\pi(D-2)}{2L} \sum_{n=1}^{n=\infty} n = -\frac{(D-2)}{24} \frac{\pi}{L} = a \frac{\pi}{L} \quad (95)$$

where we have taken that $w_n = n$ and we have performed a zeta function regularization.

We have seen above that even at the classical level the stringy meson and baryon differ from the string associated with the linear Regge trajectory. The question at this point is to what extent is the quantum stringy hadrons different from that of the linear Regge trajectories on top of the classical difference. As will be shown the quantum picture of the HISH is much more complicated. Elevating the classical picture to the quantum one can be done in principle in two different ways: (i) Quantizing the strings in the holographic curved background, or (ii) Quantizing the strings of the HISH model, namely after mapping to flat four dimensional space-time including the impact of the Liouville mode. In principle the two paths should yield the same result. This was demonstrated in [58] where the effective action up to six-derivative order for the special case of certain confining string background was computed and found out to be the Nambu Goto action in four dimensions. However, in our prescription it is not obvious that the two procedures commute, that is if we follow (i) and then use a map to flat-space time we get the same picture as in (ii). In fact this for the closed string system this is not the case. The map of the holographic folded rotating closed string at the classical level yields a folded rotating closed string in flat space time where the only memory of the holographic background is the effective tension that depends on the background. Obviously the quantization of this string is the same as an ordinary closed string in four dimensions. However, performing the quantization in certain holographic backgrounds as was done in [48], yielded a result which is quite different from the one found following (ii).

We started this section with basic properties of the quantization of the closed and open bosonic string in flat 26 dimensions. We then review the quantization to one loop of closed string in a holographic background. Next we discuss the quantization of the string in non-critical dimensions. The case of a static string with massive endpoints in the critical dimensions is then described and finally we briefly review certain issues about the quantization of the rotating string with massive endpoints in four dimensions and in particular in the limits of small and large string endpoint masses.

5.1 The quantum rotating closed string in holographic background

In section (§3.4.2) we have described the classical configuration of the folded rotating string in a holographic confining background. The result is summarize in

$$J = \frac{1}{2} \alpha'_{eff} E^2 \quad (96)$$

where $\alpha'_{eff} = (2\pi T_{eff})^{-1}$ and $T_{eff} = g_{00}(r_0)T$. Now we will review the semi-classical quantization of this string. The calculations of the quantum corrected trajectory of the folded closed string in a curved background in different holographic backgrounds were performed in [48] and [59] using semiclassical methods. This was done in the analog of the static gauge, namely with $\tau = x^0$ and $\sigma = \rho = \sqrt{x_1^2 + x_2^2}$ by computing the spectrum of quadratic fluctuations, bosonic and fermionic, around the classical configuration of the folded string. It was shown in [48] that the Noether charges of the energy E and angular momentum J that incorporate the quantum fluctuations, are related to the expectation value of the world-sheet Hamiltonian in the following manner[60]

$$LE - J = \int d\sigma \langle \mathcal{H}_{ws} \rangle. \quad (97)$$

The contributions to the expectation value of the world-sheet Hamiltonian are from several massless bosonic modes, “massive” bosonic modes and massive fermionic modes. For the “massive” bosonic fluctuations around the rotating solution one gets a σ -dependent mass term, with equations of motion of the form

$$(\partial_\tau^2 - \partial_\sigma^2 + 2m_0^2 L^2 \cos^2 \sigma) \delta x^i = 0 \quad (98)$$

appearing in both analyses, m_0 being a mass parameter which depends on the particular geometry. A similar mass term, also with $\cos \sigma$, appears in the equations of motion for some fermionic fluctuations as well, the factor of $\cos^2 \sigma$ in the mass squared coming in both cases from the induced metric calculated for the rotating string, which is $h_{\alpha\beta} \sim \eta_{\alpha\beta} \cos^2 \sigma$. Finally summing up all the quadratic quantum fluctuation it was found in both [48] and [59] that the Regge trajectories are of the form

$$J = \alpha'_{closed} (E^2 - 2m_0 E) + a. \quad (99)$$

where m_0 is a mass parameter that characterizes the holographic model and a is the intercept which generically takes the form $a = \frac{\pi}{24} (\# \text{bosonic massless modes} - \# \text{fermionic massless modes})$. The two papers [48] and [59] use different holographic models (Klebanov-Strassler and Maldacena-Núñez backgrounds in the former and Witten background in the latter) and predict different signs for m_0 , which is given as a combination of the parameters specific to the background. In [48] m_0 is positive, while in [59] it is negative. According to [48] the slope of the closed string trajectory is left unchanged from the classical case

$$\alpha'_{closed} = \frac{1}{2} \alpha'_{open}, \quad (100)$$

5.2 On the quantization of the string in non-critical dimensions

The HISH models are by definition in four dimensional, namely in non-critical dimension. The question of quantizing the classical string not in the critical dimensions was addressed in the seminal work of Polyakov. It was later addressed again by Polchinski and Strominger in the context of an effective string theory theory [61]. Recently, it was discussed again in [8] in the context Nambu-Goto formulation and in [62] in terms of a Liouville mode. The basic observation is that for the quantum effective string action in D dimensions, to be 2d conformal invariant one has to add a Liouville term of the form

$$S_L = \frac{26 - D}{24\pi} \int d^2\sigma \sqrt{|g|} [g^{ab} \partial_a \varphi \partial_b \varphi - \mathcal{R}_2 \varphi] \quad (101)$$

where the Liouville field can be taken to be a composite field of the form

$$\varphi = -\frac{1}{2} \text{Log}(g^{ab} \partial_a x^\mu \partial_b x_\mu) \quad (102)$$

For a classical rotating string of the form

$$X \equiv (x^0, x^1, x^2) = l(\tau, \cos(\theta) \sin(\sigma), \sin(\theta) \sin(\sigma)) \quad (103)$$

one find that

$$\varphi = -\text{Log}(\sqrt{2}l \cos(\sigma)). \quad (104)$$

Thus the Liouville term reads

$$S_L = \frac{26-D}{24\pi} \int d\tau \int_{-\delta}^{\delta} d\sigma \tan^2(\sigma) = \frac{26-D}{12\pi} [\tan(\delta) - \delta] \quad (105)$$

where the span of the world sheet coordinate σ is taken to be $-\delta \leq \sigma \leq \delta$

An alternative formulation for the non-critical term was proposed by Polchinski-Strominger in ([61]). In the orthogonal gauge

$$\dot{X}^\mu \dot{X}_\mu + X'^\mu X'_\mu = 0 \quad \dot{X}^\mu X'_\mu = 0 \quad (106)$$

which can be expressed also as

$$h_{++} = \partial_+ X^\mu \partial_+ X_\mu = 0 \quad h_{--} = \partial_- X^\mu \partial_- X_\mu = 0 \quad (107)$$

it reads

$$\mathcal{S}_{ps} = \frac{26-D}{24\pi} \int d\theta \int_{-\delta}^{\delta} d\sigma \frac{(\partial_+^2 X \cdot \partial_- X)(\partial_-^2 X \cdot \partial_+ X)}{(\partial_+ X \cdot \partial_- X)^2} = \quad (108)$$

Substituting the classical solution (103) we get obviously the same result as in (103).

This term has to be added to all the HISH models to the closed string one as well as to the open string both with massless or massive endpoints.

5.2.1 The folded closed string

Let us start first with the closed string case. In this case $\delta = \frac{\pi}{2}$ and thus the non-critical term diverges. This follows from the fact that the denominator in the non-critical PS term is simply $(\dot{X}^2)^2$, so the problem emerges because the endpoints move at the speed of light. This divergence was discussed also in [8] where the quantum correction to the linear Regge trajectory was analyzed for a general dimension D . In dimensions larger than four the string rotates in two planes and the angular momentum is characterized by two quantum numbers J_1 and J_2 . The result obtained there for the Regge trajectory of the closed string is

$$\frac{\alpha'}{2} M^2 = (J_1 + J_2) - \frac{D-2}{12} + \frac{26-D}{24} \left(\left(\frac{J_1}{J_2} \right)^{\frac{1}{4}} - \left(\frac{J_2}{J_1} \right)^{\frac{1}{4}} \right)^2. \quad (109)$$

This expression is singular when $J_2 = 0$, which is necessarily the case when $D = 4$, since in four dimensions the rotation is in a single plane. Therefore the expression is not usable precisely in the context in which we would like to use it. One potential way to regularize it is to add two masses at the two endpoints of the folded string. The resulting system looks like two open strings connected at their boundaries by these masses, but not interacting in any other way. In the rotating solution the two strings lie on top of one another. The boundary condition, which is the equation of motion of the massive endpoint is modified: it is the same as for the open string, but with an effective double tension $T \rightarrow 2T$, in accordance with the ratio of the slopes of the open and closed strings discussed above. If this process of adding masses on the closed string and taking then the limit of zero mass is a legitimate way to regularize, then it is probable that the result is also simply double that of the open string, as it is for the critical dimension.

5.2.2 The regular open string

For the regular open string, namely, with no massive endpoints and for which $\delta = \frac{\pi}{2}$ the PS term diverges and correspondingly the intercept. Even for small masses $\delta \sim \frac{\pi}{2}$ where the contribution to the intercept due to this term will be very large is un-physical. Thus there is a question of how to regularize and renormalize this expression. In [8] a procedure to do it was proposed. Here we would like to mention an approach that seems natural for the case of a string with massive endpoints. One option is to add a term in the world-line action analogous to the PS or Liouville term can cancel the $\tan(\delta)$ term. One can try to introduce a Liouville term also on the world line but since $h_{\tau\tau} = l^2 \cos^2(\sigma)$ it is clear that a term of the form $\partial_\tau \varphi$ vanishes. Another option is to introduce a “counter-term” of the form

$$S_{ct} = \int d\tau \mathcal{L}_{ct} = \delta_m \int d\tau \sqrt{\dot{X}^\mu \dot{X}_\mu} = \delta_m l \cos(\delta) \quad (110)$$

It is thus clear that if we take $\delta_m = \frac{26-D}{24\pi} \frac{T}{m}$ we get $S_{ct} = \frac{26-D}{24\pi} \tan(\delta)$. This counter-term cancels the divergent term of the Polchinski Strominger or Liouville term. If we combine the finite term with the usual intercept we get [8]

$$a = \frac{D-2}{24} + \frac{26-D}{24} = 1 \quad (111)$$

This result that the intercept is D independent may look counter-intuitive

5.3 The Casimir energy of a critical static string with massive endpoints

We have seen that the stringy hadrons both mesons and baryons are described in the HISH approach as strings with massive endpoints rotating in four dimensions. Classically they were treated in section §(4.2). Before analyzing the quantum corrections to this system we first start with a static string in the critical dimension, namely without considering the Liouville term. In the next subsection will use discuss the non-critical rotating string with massive endpoints.

Consider the case of a string of length L with massive endpoints which is static (i.e. non-rotating). The endpoints can move in directions perpendicular to the direction along which the string is stretched and the string can fluctuate along those directions. The solutions for the fluctuations in the transverse directions are

$$\delta x^\mu = \frac{1}{\sqrt{2T}} \sum_{n \neq 0} e^{-i w_n t} \frac{\alpha_n^\mu}{w_n} u_n(\rho) \quad (112)$$

This solution is in the static gauge where $\tau = x^0$ and $\sigma = \rho$ where ρ is the coordinate along the string and where $\mu = 1, 2, \dots, D-2$. The orthogonality of the transverse modes is given by

$$\int_0^L d\rho u_n(\rho) u_m(\rho) \epsilon(\rho) = \delta_{nm} \quad \int_0^L d\rho u'_n(\rho) u'_m(\rho) = w_n^2 \delta_{nm} \quad (113)$$

where $\epsilon(\rho) = 1 + \frac{m}{T} [\delta(\rho + L/2) + \delta(\rho - L/2)]$.

The eigenfrequencies w_n are the roots of the following equation

$$\tan(w_n L) = \frac{2mT w_n}{m^2 w_n^2 - T^2} \quad (114)$$

where we have used the gauge $\sigma = \rho$ and hence $\delta = L$. Defining the dimensionless eigenfrequencies $\hat{w}_n = w_n L$ and $q = \frac{m}{TL}$ we get the equation

$$\tan(\hat{w}_n) = \frac{2q \hat{w}_n}{q^2 \hat{w}_n^2 - 1} \quad (115)$$

On the w axis the roots are placed symmetrically around $w = 0$ and hence it is enough to consider only the positive roots.

Upon quantization the creation and annihilation operators α_n obey the algebra

$$[\alpha_n^\mu, \alpha_m^\nu] = w_n \delta^{\mu\nu} \delta_{n+m,0} \quad (116)$$

The energy due to the fluctuations is given by

$$E = \frac{T}{2} \int_{-L/2}^{L/2} d\rho (\delta \dot{X}^i)^2 \epsilon(\rho) + (\delta X^{i'})^2 \quad (117)$$

Substituting the creation and annihilation operators

$$\begin{aligned} E &= \frac{1}{L} \sum_{n=1}^{\infty} \sum_{i=1}^{D-2} (\alpha_n^i \alpha_n^{i\dagger} + \alpha_n^{i\dagger} \alpha_n^i) \\ &= \sum_{n=1}^{\infty} \sum_{i=1}^{D-2} \alpha_n^{i\dagger} \alpha_n^i + \frac{D-2}{2} \frac{1}{L} \sum_{n=1}^{\infty} w_n \end{aligned} \quad (118)$$

The Casimir energy of this static string reads

$$E_C(m) = \frac{1}{2} \sum_{n=1}^{\infty} w_n \quad (119)$$

For the special cases of $m = 0$ and $m = \infty$ one gets using the zeta function regularization

$$E_C(m = \infty) = E_C(m = 0) = \frac{\pi}{2L} \sum_{n=1}^{\infty} n = -\frac{\pi}{24L} \quad (120)$$

For non-trivial and finite m the eigenfrequencies take the form of $w_n = n + f(L)\frac{1}{n}$. The second term cannot be regularized using zeta function regularization. Instead following [63] we use Cauchy's theorem to regularize the sum and then we perform a renormalization procedure that yields a finite result which for the massless case coincides with the zeta function regularization.

The main idea [63] is to express the sum of the eigenfrequencies using the following relation for an analytic function $f(w)$

$$\frac{1}{2\pi i} \oint_C dw w \frac{f'(w)}{f(w)} = \frac{1}{2\pi i} \oint_C dw w [Log f(w)]' = \sum_k n_k w_k - \sum_l p_l \tilde{w}_l \quad (121)$$

where w_k denotes a zero of order k , n_k the number of them and \tilde{w}_l denotes a pole of order l and p_l the number of them. The analytic function $f(w)$ for our case is the eigenfrequencies equation (114) taken to avoid having poles in the form

$$f(w) = 2mTw \cos(wL) - (m^2 w^2 - T^2) \sin(wL) = 0 \quad (122)$$

Substituting this expression in (119) we get

$$E_C(m) = \frac{1}{4\pi i} \oint_C dw w [Log f(w)]' \quad (123)$$

where the contour C includes the real positive semiaxis where the roots of $f(w)$ occur. Since $f(w)$ does not have poles we deform the contour to be a semi-circle with radius Λ and the segment along the

imaginary axis $(-i\Lambda, i\Lambda)$. The integral along the deformed contour is finite for finite Λ and hence this can be taken as $E_C^{(reg)}(m, L)$ the regularized Casimir energy.

$$\begin{aligned} E_C^{(reg)}(m, L) &= \frac{1}{2\pi} \int_0^\Lambda dy \text{Log} [2mTy \cosh(yL) + (m^2y^2 + T^2) \sinh(yL)] \\ &+ \frac{1}{4\pi} [w \text{Log}[f(w)]]_{-\Lambda}^\Lambda + I_{sc}(\Lambda) \end{aligned} \quad (124)$$

where the second term is the surface term that follows from the integration by parts and the third term is the semi-circular integral at radius Λ . For large Λ the surface term becomes $2\Lambda^2L + \Lambda \text{Log}[-\frac{1}{4}(m\Lambda + T)^4]$. However, if one integrate by parts also the integral along the semi-circle then the surface terms drop out.

To perform the renormalization we subtract $E_C^{(reg)}(m, L \rightarrow \infty)$. In this method the renormalized Casimir energy reads

$$E_C^{(ren)}(m, L) = \lim_{\Lambda \rightarrow \infty} [E_C^{(reg)}(m, L) - E_C^{(reg)}(m, L \rightarrow \infty)] \quad (125)$$

The subtracted Casimir energy is the asymptotic value of the regularized Casimir energy when $L \rightarrow \infty$. It also has three contributions. However, it easy to see that the surface term takes the same value as the one in (124) for large Λ . Moreover, the difference between the integrals along the semi-circle radius vanishes. Thus the subtracted energy takes finally the form

$$E_C^{(reg)}(m, L \rightarrow \infty) = \frac{1}{2\pi} \int_0^\Lambda dy \text{Log} \left[e^{(yL)} \frac{(my + T)^2}{2} \right] \quad (126)$$

and hence the renormalized Casimir energy is given by

$$E_C^{(ren)}(m, L) = \frac{1}{2\pi L} \int_0^\infty dx \text{Log} \left[1 - e^{-2x} \left(\frac{(x-a)}{x+a} \right)^2 \right] \quad (127)$$

where a is the dimensionless quantity $a = \frac{TL}{m}$. For the special case of massless endpoints one finds

$$E_C^{(ren)}(m=0, L) = E_C^{(ren)}(m=\infty, L) = \frac{1}{2\pi} \int_0^\infty dx \text{Log} [1 - e^{-2x}] = -\frac{\pi}{24L} \quad (128)$$

Note that one cannot get rid of the divergences by computing the difference of the integral for two different finite length L or two different tensions T or two different masses. The difference in these cases is still divergent.

Defining the ratio of the Casimir energy of a finite and infinite string endpoint mass one gets

$$\eta(q) = \frac{E_c^{(ren)}(m, L)}{E_c^{(ren)}(m=\infty, L)} = -\frac{12}{\pi^2} \int_0^\infty dz \text{Log} \left[1 - e^{-2z} \left(\frac{1-az}{1+az} \right)^2 \right] \quad (129)$$

The dependence of η on $\text{Log}_{10}(q)$ is drawn in figure(15). In both limits of $q \rightarrow 0$ and $q \rightarrow \infty$, $\eta \rightarrow 1$ and its extremum is around $q = \frac{m}{TL} \sim 2$.

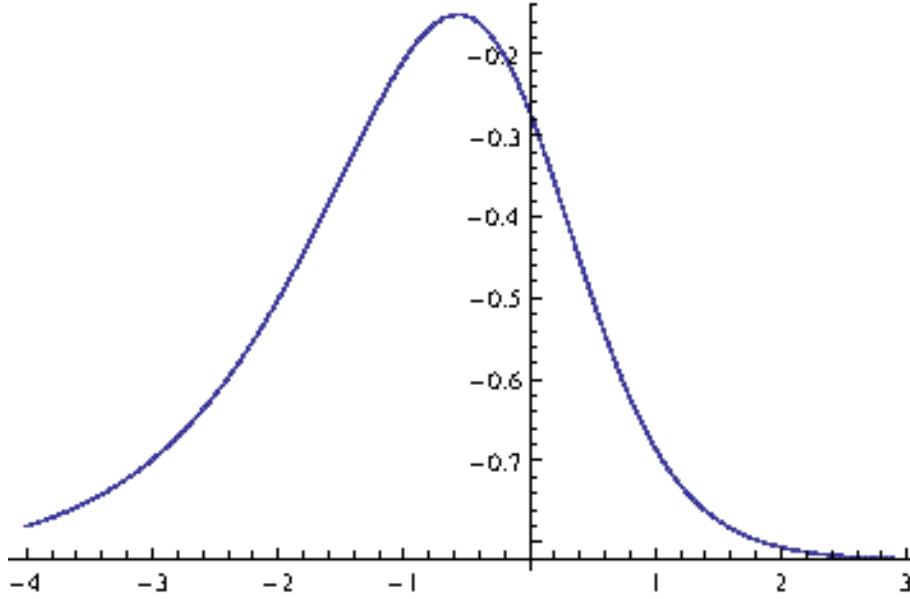


Figure 15: η as a function of $\text{Log}_{10}(a)$

5.4 On the quantization of the rotating string with massive endpoints in four dimensions

We have determined the classical trajectories of the strings with massive endpoints, we have described the quantization of the regular open string in non-critical dimension and the quantization of the static string with massive endpoints. Now we would like to combine all these ingredients to determine the semi-classical stringy meson (and baryon). This task is under current investigation[64]. Here we briefly mention several of its features.

- In section §(4.2) we were using the Nambu Goto action for the string and the length of the endpoints worldline as the particle action. For the string one can use also the Polyakov formulation and for the particle an action with an auxiliary field so that in fact there are four possible formulation of the action of the combined system.
- The source of the difficulty of quantizing this system is the fact that in the Polyakov formulation of the string there are only the two diffeomorphism and no scale symmetry. One can gauge fix the local symmetries in various ways in particular the orthogonal gauge and the analog of the static gauge mentioned above and a gauge where the fluctuations are perpendicular to the classical configuration [65], [9].
- The non-linear nature of the system shows up in the boundary equation that in the formulation without worldsheet and worldline metrics read

$$T\partial_\sigma X^\mu \pm m\partial_\tau \left(\frac{\dot{X}^\mu}{\sqrt{-(\dot{X})^2}} \right) = 0 \quad (130)$$

- The quantum fluctuations transverse to the plane of rotation, transverse to the rotation in the plane of rotation and those along the direction of the string (which exists only for the string with massive endpoints), obey different equations of motion and have to be treated separately.

- Even without deriving a full semi-classical quantization it seems plausible that the transition from the classical trajectory given in (80) to the quantum one will be following

$$\alpha' E_{cl}^2 \rightarrow \alpha' E_{qm}^2 = \alpha' E_{cl}^2 + a = \alpha' E_{cl}^2 + (a_{Cas} + a_{PS}) \quad (131)$$

and the leftover challenge is to compute or at least estimate the contributions to the intercept a_{Cas} and a_{PS}

- Needless to say that eigenvalues of the excited string states with massive endpoints is not anymore just the integers $w_n = n$ but rather the eigenvalues discussed above in the previous section. Some low lying states were determined in [9]

6 Phenomenology: Comparison between the stringy models and experimental data

Now that we have completed the development of the theoretical model starting from stringy configurations in holographic models and then mapping them into strings in four dimensional flat space-time, we would like to perform a detailed set of fits between the models and the corresponding hadrons. We will first describe the fitting procedure and then present separately the fits of mesons (section 6.2)[3][4], the fits of baryons (section 6.3), and the fits of glueballs (section 6.4[5]).

6.1 Fitting models and procedure

We define the *linear* fit by

$$J + n = \alpha' E^2 + a \quad (132)$$

where the fitting parameters are the *slope* α' and the *intercept*, a .

For the *massive* fit, we use the general expressions for the mass and angular momentum of the rotating string with massive endpoints (of eqs. 85 and 86), generalized for the case of two different masses, and we add to them, by hand, an intercept and an extrapolated n dependence, assuming the same replacement of $J \rightarrow J + n - a$ when moving from the classical result to the real, quantum world.

$$E = \sum_{i=1,2} m_i \left(\frac{q_i \arcsin(q_i) + \sqrt{1 - q_i^2}}{1 - q_i^2} \right) \quad (133)$$

$$J + n = a + \sum_{i=1,2} \pi \alpha' m_i^2 \frac{q_i^2}{(1 - q_i^2)^2} \left(\arcsin(q_i) + q_i \sqrt{1 - q_i^2} \right) \quad (134)$$

With the relation between q_1 and q_2 as in eq. 79:

$$\frac{T}{\omega} = m_1 \frac{q_1}{1 - q_1^2} = m_2 \frac{q_2}{1 - q_2^2} \quad (135)$$

With the two additions of n and a , the two equations reduce to that of the linear fit in (132) in the limit where both masses are zero.

Now the fitting parameters are a and α' as before, as well as the two endpoint masses m_1 and m_2 . In many cases we assume $m_1 = m_2$ and retain only one free mass parameter, m .

Fitting procedure: For the *meson and baryon fits* of sections 6.2 and 6.3, the fits are made to minimize χ^2 , defined here as

$$\chi^2 = \frac{1}{N-1} \sum_i \left(\frac{M_i^2 - E_i^2}{M_i^2} \right)^2 \quad (136)$$

M_i and E_i are, respectively, the measured and calculated value of the mass of the i -th particle, and N the number of points in the trajectory. We will also use the subscripts l (for linear fit) or m (for massive fit) to denote to which fitting model a given value of χ^2 belongs. We put M_i^2 in the denominator instead of the experimental uncertainty ΔM_i^2 , because our models cannot replicate the high accuracy with which some hadron masses are measured. In the above definition χ^2 is normalized in such a way that $\sqrt{\chi^2}$ gives the percentage of deviation in M^2 .

For the *glueballs and lattice fits* of section 6.4, we work with the definition of χ^2 with experimental (or computational on the lattice) uncertainty in the denominator

$$\chi^2 = \frac{1}{N-1} \sum_i \left(\frac{M_i^2 - E_i^2}{\Delta(M_i^2)} \right)^2. \quad (137)$$

6.2 Review of meson trajectory fits

We begin with a summary of the main results of the meson fits. Following that we present a “universal” fit for the (J, M^2) trajectories of mesons composed of u , d , s , and c quarks. The latter parts of this section are more detailed discussion of the different meson fits.

6.2.1 Summary of results for the mesons

Traj.	N	m	α'	a
π/b	4	$m_{u/d} = 90 - 185$	$0.808 - 0.863$	$(-0.23) - 0.00$
ρ/a	6	$m_{u/d} = 0 - 180$	$0.883 - 0.933$	$0.47 - 0.66$
η/h	5	$m_{u/d} = 0 - 70$	$0.839 - 0.854$	$(-0.25) - (-0.21)$
ω	6	$m_{u/d} = 0 - 60$	$0.910 - 0.918$	$0.45 - 0.50$
K^*	5	$m_{u/d} = 0 - 240$ $m_s = 0 - 390$	$0.848 - 0.927$	$0.32 - 0.62$
ϕ	3	$m_s = 400$	1.078	0.82
D	3	$m_{u/d} = 80$ $m_c = 1640$	1.073	-0.07
D_s^*	3	$m_s = 400$ $m_c = 1580$	1.093	0.89
Ψ	3	$m_c = 1500$	0.979	-0.09
Υ	3	$m_b = 4730$	0.635	1.00

Table 1: The results of the meson fits in the (J, M^2) plane. For the uneven K^* fit the higher values of m_s require $m_{u/d}$ to take a correspondingly low value. $m_{u/d} + m_s$ never exceeds 480 MeV, and the highest masses quoted for the s are obtained when $m_{u/d} = 0$. The ranges listed are those where χ^2 is within 10% of its optimal value. N is the number of data points in the trajectory. m is given in MeV and α' in GeV^{-2} .

Tables 1 and 2 summarize the results of the fits for the mesons in the (J, M^2) plane and (n, M^2) plane respectively.

The higher values of α' and a always correspond to higher values of the endpoint masses, and the ranges listed are those where χ^2 is within 10% of its optimal value.

We list in the tables the optimal ranges for each fit done individually, but we want to consider the results as a whole. In the (J, M^2) plane we see that the trajectories fitted, which are all the leading

Traj.	N	m	α'	a
π/π_2	$4 + 3$	$m_{u/d} = 110 - 250$	$0.788 - 0.852$	$a_0 = (-0.22) - 0.00$ $a_2 = (-0.00) - 0.26$
a_1	4	$m_{u/d} = 0 - 390$	$0.783 - 0.849$	$(-0.18) - 0.21$
h_1	4	$m_{u/d} = 0 - 235$	$0.833 - 0.850$	$(-0.14) - (-0.02)$
ω/ω_3	$5 + 3$	$m_{u/d} = 255 - 390$	$0.988 - 1.18$	$a_1 = 0.81 - 1.00$ $a_3 = 0.95 - 1.15$
ϕ	3	$m_s = 510 - 520$	$1.072 - 1.112$	1.00
Ψ	4	$m_c = 1380 - 1460$	$0.494 - 0.547$	$0.71 - 0.88$
Υ	6	$m_b = 4725 - 4740$	$0.455 - 0.471$	1.00
χ_b	3	$m_b = 4800$	0.499	0.58

Table 2: The results of the meson fits in the (n, M^2) plane. The ranges listed are those where χ^2 is within 10% of its optimal value. N is the number of data points in the trajectory.

trajectories for mesons of various masses, are quite consistent in terms of the slopes and masses obtained from each trajectory. With the sole exception of the $b\bar{b}$ trajectory, which gives a much lower slope than the rest, all the trajectories can be fitted well (if not always optimally) using a slope of $\approx 0.9 \text{ GeV}^{-2}$. The masses of the light quarks (u and d) are not determined. The results are consistent with zero, but do not rule out masses up to 100 MeV. The fits for mesons containing s , c , and b quarks are always improved when adding masses, in terms of both quality and consistency of the slope obtained. The mass of the s quark is found around 300–400 MeV, while the c and b quarks are at their constituent masses of 1500 MeV and 4730 MeV respectively.

The intercepts appear to be scattered over different values, positive and negative. If we change our x -axis to the orbital angular momentum L instead of J (which is either L or $L + 1$), we get only negative values: around -0.2 for the light pseudoscalar trajectories (π , η), and -0.4 for the lighter vector trajectories (ρ , ω , and also K^*). As the endpoint masses get heavier (ϕ , D , D_s , Ψ , Υ) the intercept moves to zero.

In the (n, M^2) plane we have less consistency between the different trajectories. This might be expected since we base our fits on the conjecture that we can extrapolate the dependence of M^2 on n directly from its dependence on J . However, we still see that the light mesons can be fitted on linear or close-to-linear trajectories with a slope of some $0.80 - 0.85 \text{ GeV}^{-2}$. The trajectory of the $s\bar{s}$ has a higher slope. The fits of the c and b have much lower slopes than the light mesons, but work surprisingly well when fitted separately.

6.2.2 Universal slope fits

Based on the combined results of the individual fits for the (J, M^2) trajectories of the u , d , s , and c quark mesons, we assumed the values

$$m_{u/d} = 60, m_s = 220, m_c = 1500 \quad (138)$$

for the endpoint masses and attempted to find a fit in which the slope is the same for all trajectories. This wish to use a universal slope forces us to exclude the $b\bar{b}$ trajectory from this fit, but we can include the three trajectories involving a c quark. For these, with added endpoint masses (and only with added masses), the slope is very similar to that of the light quark trajectories.

The only thing that was allowed to change between different trajectories was the intercept. With the values of the masses fixed, we searched for the value of α' and the intercepts that would give the best overall fit to the nine trajectories of the π/b , ρ/a , η/h , ω/f , K^* , ϕ , D , D_s^* , and Ψ mesons. The best fit of this sort, with the masses fixed to the above values, was

$$\alpha' = 0.884 \quad (139)$$

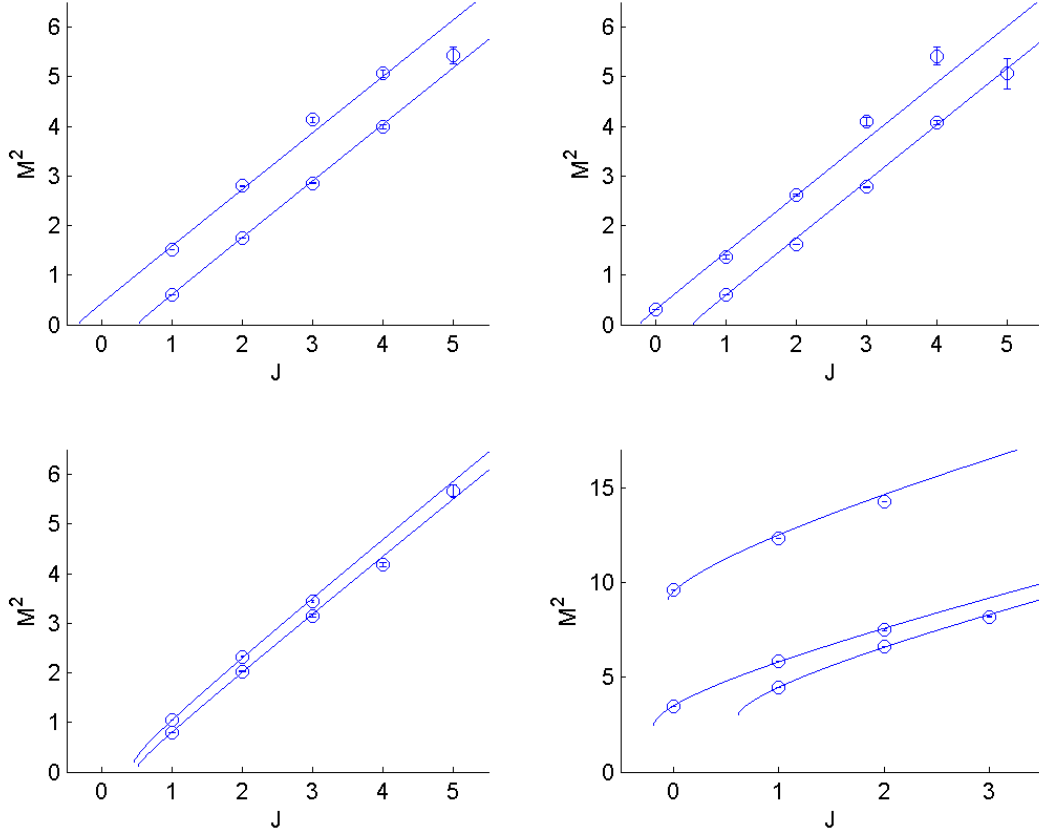


Figure 16: Nine (J, M^2) trajectories fitted using universal quark masses and slope ($m_{u/d} = 60$, $m_s = 220$, $m_c = 1500$, and $\alpha' = 0.884$). Top left: π and ρ , top right: η and ω , bottom left: K^* and ϕ , bottom right: D , D_s^* , and Ψ .

$$\begin{aligned}
 a_\pi &= -0.33 & a_\rho &= 0.52 & a_\eta &= -0.22 & a_\omega &= 0.53 \\
 a_{K^*} &= 0.50 & a_\phi &= 0.46 & a_D &= -0.19 & a_{D_s^*} &= -0.39 & a_\Psi &= -0.06
 \end{aligned}$$

and it is quite a good fit with $\chi^2 = 13.13 \times 10^{-4}$. The trajectories and their fits are shown in figure 16.

6.2.3 Meson trajectories in the (J, M^2) plane

We now present in more detail the fits to the different trajectories, beginning with the orbital trajectories, i.e. trajectories in the (J, M^2) plane.

Light quark mesons We begin by looking at mesons consisting only of light quarks - u and d . We assume for our analysis that the u and d quarks are equal in mass, as any difference between them would be too small to reveal itself in our fits. This sector is where we have the most data, but it is also where our fits are the least conclusive. The trajectories we have analyzed are those of the π/b , ρ/a , η/h , and ω/f .

Of the four (J, M^2) trajectories, the two $I = 1$ trajectories, of the ρ and the π , show a weak dependence of χ^2 on m . Endpoint masses anywhere between 0 and 160 MeV are nearly equal in terms of χ^2 , and no clear optimum can be observed. For the two $I = 0$ trajectories, of the η and ω , the linear fit is optimal. If we allow an increase of up to 10% in χ^2 , we can add masses of only 60 MeV or less.

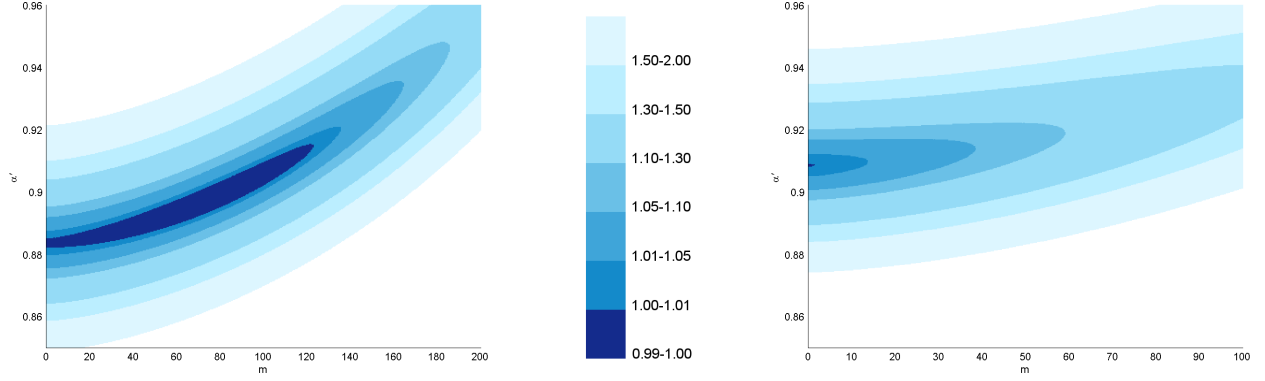


Figure 17: χ^2 as a function of α' and m for the (J, M^2) trajectory of the ρ (left) and ω (right) mesons. The intercept a is optimized to get a best fit for each point in the (α', m) plane. χ^2 in these plots is normalized so that the value of the optimal linear fit ($m = 0$) is $\chi^2 = 1$.

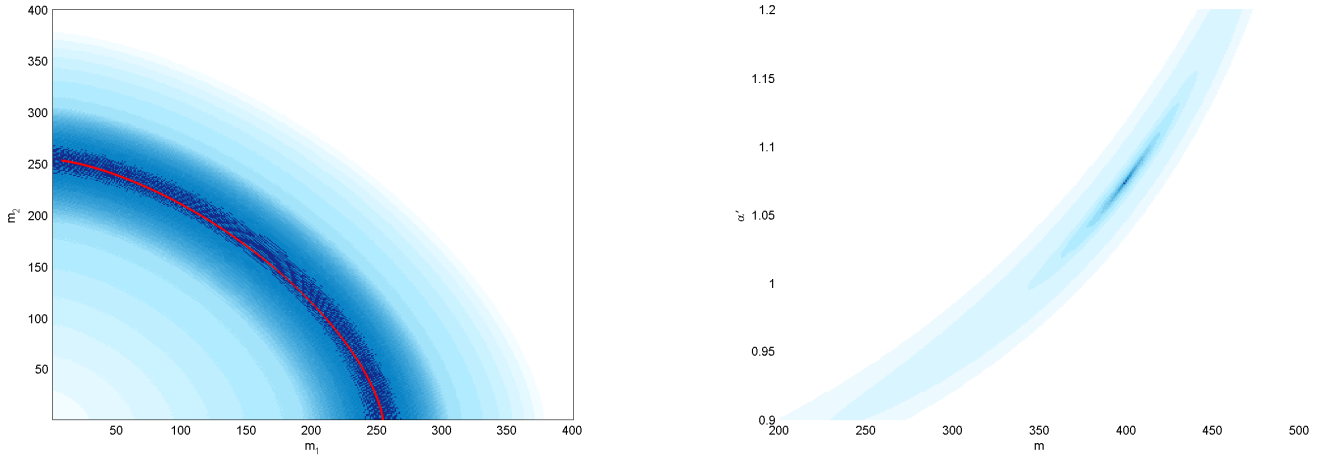


Figure 18: Left: χ^2 as a function of two masses for the K^* trajectory. a and α' are optimized for each point. The red line is the curve $m_1^{3/2} + m_2^{3/2} = 2 \times (160)^{3/2}$ along which the minimum (approximately) resides. The minimum is $\chi_m^2/\chi_l^2 = 0.925$ and the entire colored area has $\chi_m^2/\chi_l^2 < 1$. On the right is χ^2 as a function of α' and m for the (J, M^2) trajectory of the ϕ . The intercept a is optimized. The minimum is at $\alpha' = 1.07, m = 400$ with $\chi_m^2/\chi_l^2 < 10^{-4}$ at the darkest spot. The lightest colored zone still has $\chi_m^2/\chi_l^2 < 1$, and the coloring is based on a logarithmic scale.

Figure 17 presents the plots of χ^2 vs. α' and m for the trajectories of the ω and ρ and shows the difference in the allowed masses between them.

The slope for these trajectories is between $\alpha' = 0.81 - 0.86$ for the two trajectories starting with a pseudo-scalar (η and π), and $\alpha' = 0.88 - 0.93$ for the trajectories beginning with a vector meson (ρ and ω). The higher values for the slopes are obtained when we add masses, as increasing the mass generally requires an increase in α' to retain a good fit to a given trajectory. This can also be seen in figure 17, in the plot for the ρ trajectory fit.

Strange and $s\bar{s}$ mesons We analyze three trajectories in the (J, M^2) involving the strange quark. One is for mesons composed of one s quark and one light quark - the K^* , the second is for $s\bar{s}$ mesons - the trajectory of the ϕ , and the last is for the charmed and strange D_s^* , which is presented in the next subsection with the other charmed mesons.

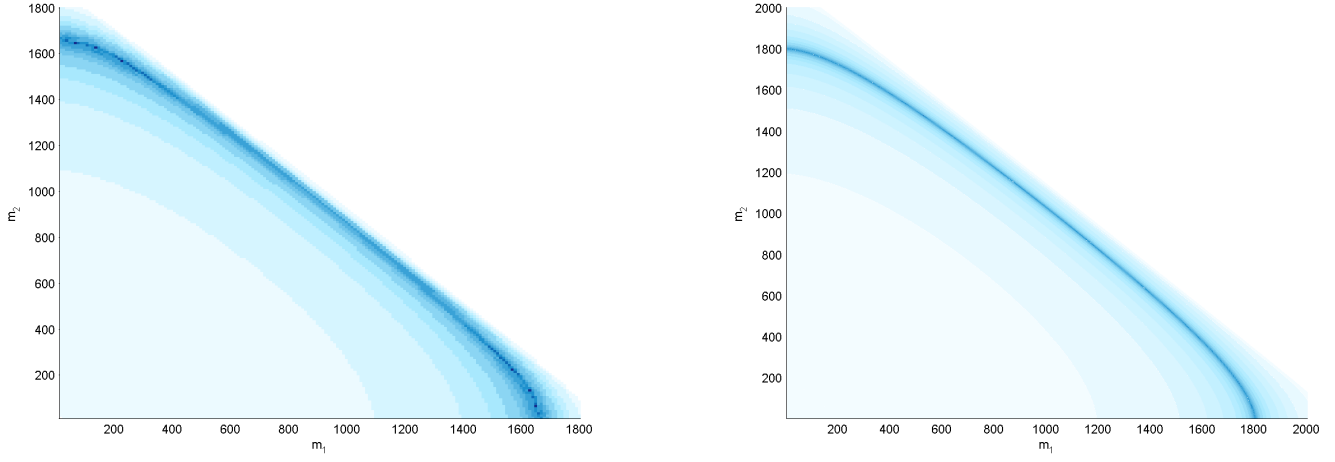


Figure 19: Top: χ^2 as a function of two masses for the D (left) and D_s^* (right) trajectories. The coloring is based on a logarithmic scale, with the entire colored area having $\chi_m^2/\chi_l^2 < 1$. The minimum is $\chi_m^2/\chi_l^2 = 5 \times 10^{-4}$ for the D , and $\chi_m^2/\chi_l^2 = 2 \times 10^{-6}$ for the D_s^* . In both plots, a and α' are optimized for each choice of the endpoint masses.

The K^* trajectory alone cannot be used to determine both the mass of the u/d quark and the mass of the s . The first correction to the linear Regge trajectory in the low mass range is proportional to $\alpha' (m_1^{3/2} + m_2^{3/2}) \sqrt{E}$. This is the result when eq. (87) is generalized to the case where there are two different (and small) masses. The plot on the left side of figure 18 shows χ^2 as a function of the two masses.

The minimum for the K^* trajectory resides along the curve $m_{u/d}^{3/2} + m_s^{3/2} = 2 \times (160)^{3/2}$. If we take a value of around 60 MeV for the u/d quark, that means the preferred value for the m_s is around 220 MeV. The higher mass fits which are still better than the linear fit point to values for the s quark mass as high as 350 MeV, again when $m_{u/d}$ is taken to be 60 MeV. The slope for the K^* fits goes from $\alpha' = 0.85$ in the linear fit to 0.89 near the optimum to 0.93 for the higher mass fits.

The trajectory of the $s\bar{s}$ mesons includes only three states, and as a result the optimum is much more pronounced than it was in previous trajectories. It is found at the point $m_s = 400$, $\alpha' = 1.07$. The value of χ^2 near that point approaches zero. The range in which the massive fits offer an improvement over the linear fit is much larger than that, as can be seen in the right side plot of figure 18. Masses starting from around $m_s = 250$ MeV still have $\chi_m^2/\chi_l^2 = 0.50$ or less, and the slope then has a value close to that of the other fits, around 0.9 GeV^{-2} .

Charmed and $c\bar{c}$ mesons There are three trajectories we analyze involving a charm quark. The first is of the D , comprised of a light quark and a c quark, the second is the D_s^* with a c and an s , and the third is $c\bar{c}$ - the Ψ . All trajectories have only three data points.

For the D meson, the optimal fit has $m_c = 1640$, $m_{u/d} = 80$ and $\alpha' = 1.07$. In this case, unlike the result for the K^* trajectory, there is a preference for an imbalanced choice of the masses, although with four fitting parameters and three data points we can't claim this with certainty. The fit for the D_s^* has a good fit consistent with the previous s and c fits at $m_c = 1580$, $m_s = 400$, and $\alpha' = 1.09$. The plots of χ^2 vs. the two masses (m_c and $m_{u/d}/m_s$) can be seen in figure 19.

In the same figure, we have χ^2 as a function of the single mass m_c for the $c\bar{c}$ Ψ trajectory. The minimum there is obtained at $m_c = 1500$ MeV, where the slope is $\alpha' = 0.98 \text{ GeV}^{-2}$.

It is worth noting that while the linear fit results in values for α' that are very far from the one obtained for the u , d , and s quark trajectories - 0.42, 0.48, and 0.52 for the Ψ , D , and D^* respectively

- the massive fits point to a slope that is very similar to the one obtained for the previous trajectories. This is also true, to a lesser extent, of the values of the intercept a .

$b\bar{b}$ mesons The last of the (J, M^2) trajectories is that of the $b\bar{b}$ Υ meson, again a trajectory with only three data points. The fits point to an optimal value of $m_b = 4730$, exactly half the mass of the lowest particle in the trajectory. The slope is significantly lower than that obtained for other mesons, $\alpha' = 0.64$ at the optimum.

6.2.4 Meson trajectories in the (n, M^2) plane

Light quark mesons In the light quark sector we fit the trajectories of the π and π_2 , the h_1 , the a_1 , and the ω and ω_3 .

The h_1 has a very good linear fit with $\alpha' = 0.83 \text{ GeV}^{-2}$, that can be improved upon slightly by adding a mass of 100 MeV, with the whole range 0 – 130 MeV being nearly equal in χ^2 .

The a_1 offers a similar picture, but with a higher χ^2 and a wider range of available masses. Masses between 0 and 225 are all nearly equivalent, with the slope rising with the added mass from 0.78 to 0.80 GeV^{-2} .

The π and π_2 trajectories were fitted simultaneously, with a shared slope and mass between them and different intercepts. Again we have the range 0 to 130 MeV, $\alpha' = 0.78 - 0.81 \text{ GeV}^{-2}$, with $m_{u/d} = 100$ MeV being the optimum. The preference for the mass arises from non-linearities in the π trajectory, as the π_2 when fitted alone results in the linear fit with $\alpha' = 0.84 \text{ GeV}^{-2}$ being optimal.

The ω and ω_3 trajectories were also fitted simultaneously. Here again the higher spin trajectory alone resulted in an optimal linear fit, with $\alpha' = 0.86 \text{ GeV}^{-2}$. The two fitted simultaneously are best fitted with a high mass, $m_{u/d} = 340$, and high slope, $\alpha' = 1.09 \text{ GeV}^{-2}$. Excluding the ground state $\omega(782)$ from the fits eliminates the need for a mass and the linear fit with $\alpha' = 0.97 \text{ GeV}^{-2}$ is then optimal. The mass of the ground state from the resulting fit is 950 MeV. This is odd, since we have no reason to expect the $\omega(782)$ to have an abnormally low mass, especially since it fits in perfectly with its trajectory in the (J, M^2) plane.

$s\bar{s}$ mesons For the $s\bar{s}$ we have only one trajectory of three states, that of the ϕ . There are two ways to use these states. The first is to assign them the values $n = 0, 1, 2$. Then, the linear fit with the slope $\alpha' = 0.54 \text{ GeV}^{-2}$ is optimal.

Since this result is inconsistent both in terms of the low value of the slope, and the absence of a mass for the strange quark, we tried a different assignment. We assumed the values $n = 0, 1$, and 3 for the highest state and obtained the values $\alpha' = 1.10, m_s = 515$ for the optimal fit. These are much closer to the values obtained in previous fits.

The missing $n = 2$ state is predicted to have a mass of around 1960 MeV. Interestingly, there is a state with all the appropriate quantum numbers at exactly that mass - the $\omega(1960)$, and that state lies somewhat below the line formed by the linear fit to the radial trajectory of the ω . Even if the $\omega(1960)$ is not the missing $s\bar{s}$ (or predominantly $s\bar{s}$) state itself, this could indicate the presence of a ϕ state near that mass.

$c\bar{c}$ mesons Here we have the radial trajectory of the J/Ψ , consisting of four states.

The massive fits now point to the range 1350–1475 MeV for the c quark mass. The biggest difference between the fits obtained here and the fits obtained before, in the (J, M^2) plane is not in the mass, but in the slope, which now is in the range 0.48 – 0.56 GeV^{-2} , around half the value obtained in the angular momentum trajectories involving a c quark - 0.9 – 1.1.

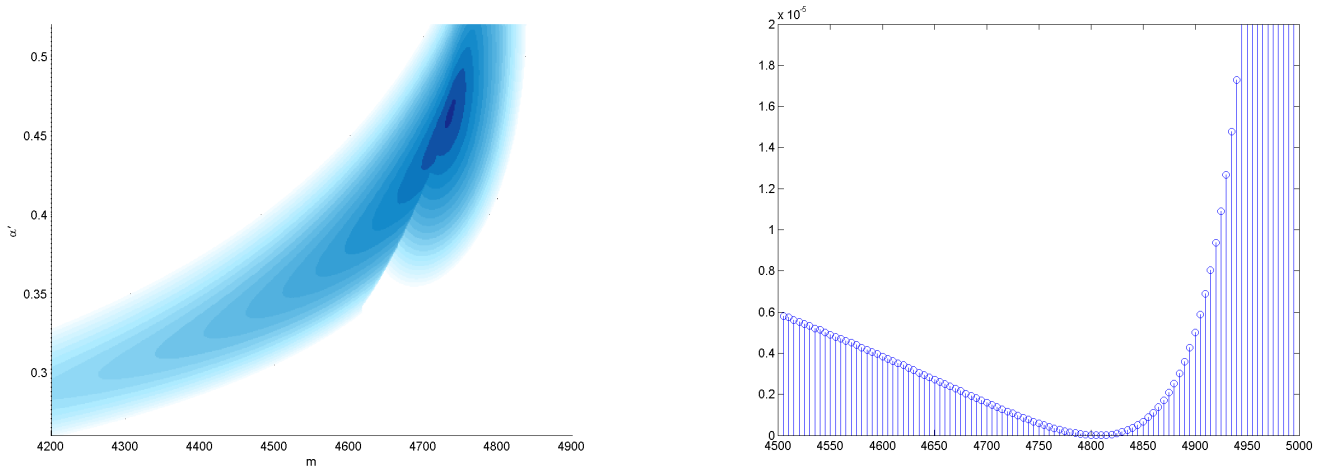


Figure 20: Left: χ^2 as a function of α' and m_b for the Υ radial trajectory. The discontinuity in the plot arises from the condition that the intercept $a \leq 1$, otherwise the mass of the ground state is undefined. The two areas in the plot are then where a is still allowed to change (left) and where a is blocked from increasing further and is fixed at $a = 1$ (oval shape on the right). Right: χ^2 as a function of m_b for the χ_b trajectory.

It is also considerably lower than the slopes obtained in the (n, M^2) trajectories of the light quark mesons, which would make it difficult to repeat the achievement of having a fit with a universal slope in the (n, M^2) plane like the one we had in the (J, M^2) plane.

$b\bar{b}$ mesons There are two trajectories we use for the $b\bar{b}$ mesons.

The first is that of the Υ meson, with six states in total, all with $J^{PC} = 1^{--}$. For this trajectory we have an excellent fit with $m_b = 4730$ MeV and the slope $\alpha' = 0.46$ GeV^{-2} . It is notable for having a relatively large number of states and still pointing clearly to a single value for the mass.

The second $b\bar{b}$ trajectory is that of the χ_b - $J^{PC} = 1^{++}$. Here we have only three states and the best fit has a slightly higher mass for the b quark - $m_b = 4800$ MeV - and a higher value for the slope $\alpha' = 0.50$ GeV^{-2} . Plots for χ^2 as a function of the b mass are shown in figure 20.

6.3 Review of baryon trajectory fits

This section offers a discussion of the fit results for the baryon Regge trajectories.

As the baryons are more complex objects than mesons, there are some issues we need to clarify before turning to the results of the fits.

We start by briefly discussing the results using the Y-shaped string model for the baryon, and the effects of including a massive baryonic vertex at the center of mass, via the replacement $M \rightarrow M - m_{bv}$. The results prove to be against these options, so the rest of the section discusses the results when using the quark-diquark model for the baryons. This means we describe the baryons simply as a single string with two masses at its endpoints.

The slope tells us that there is a quark on one end of the string and a diquark on the other. The masses can tell us more on the structure of the baryon, for example it can say something about the composition of the diquark. However, as we explain later, the data used in the Regge trajectory fits is not enough to provide us that information.

One final note we make before the fit results is on the “even-odd” effect exhibited by the light baryons: the trajectories of light baryons are split into two parallel trajectories, one for states with even

orbital angular momentum (or even parity), and another for the odd states.

We separate the results into three sections, one for the light quark baryons, the next for strange baryons, and the third for charmed baryons. In the light baryon section we also examine the radial trajectories of the N and Δ baryons. The rest of the sections have trajectories only in the angular momentum plane (J, M^2).

6.3.1 Y-shape and central mass

The Y-shaped string model is equivalent in terms of the Regge trajectories to a single string model with a higher effective string tension. In the picture we have before adding endpoint masses, we may assume (as a phenomenological model) linear trajectories for both the meson and baryon trajectories, with different slopes, α'_m and α'_b respectively. Now, the assumption that the baryons are Y-shaped strings while the mesons are straight single strings, and that there is a single universal string tension, would lead us to expect the relation

$$\alpha'_b = \frac{2}{3}\alpha'_m \quad (140)$$

between the baryon and meson Regge slopes. When we fit the data we see no such relation. What we see in our results is that in fact, the meson and baryon slopes are very similar - $\alpha'_b \approx \alpha'_m$ - supporting the same single string model for the baryons that was used for the mesons. This also excludes the triangle-shaped closed string baryon, which we have not analyzed in detail but predicts an effective slope α'_b of between $\frac{3}{8}\alpha'_m$ and $\frac{1}{2}\alpha'_m$, depending on the type of solution [66].

Our addition of endpoint masses does not change this picture, as we would still need to see a similar relation between the baryon and meson slopes, with the baryon slope being consistently lower.

As for the baryonic vertex mass, the assumption that there is a central mass that contributes to the total mass of a state but not to the angular momentum was also found to be unsupported by the data. This does not rule out the presence of a mass due to a holographic baryonic vertex, but means it is either very small or located at the string endpoint, near the diquark, and not at its center.

With these results in mind, we continue to present our fits using only the single string model with two masses at its endpoints, which is the same fitting model as the model used for the mesons.

6.3.2 Symmetric vs. imbalanced string

Now we turn to the different mass configurations in the single string model. As mentioned in the last subsection, there is no evidence to support any substantial mass located at the center of the string. To understand the structure of the baryon we would like to be able to tell how the mass is distributed between the two endpoints, but this is information we cannot gather from the Regge trajectory fits alone. In the low mass approximation for the single string, the leading order correction is proportional to $\alpha' (m_1^{3/2} + m_2^{3/2})\sqrt{E}$. Therefore, for small masses we cannot distinguish from the Regge trajectory fits alone between different configurations with equal $m_1^{3/2} + m_2^{3/2}$. There are higher order corrections, but our fits are not sensitive to them, and in practice, we see that fits with $m_1^{3/2} + m_2^{3/2} = \text{Const.}$ are nearly equivalent even for masses of a few hundred MeV.

When expanding J in E for two heavy masses, the combination in the leading term would be $m_1 + m_2$. In the mid range that cannot be described accurately by either expansion there is a transition between the two different type of curves. In both cases the symmetric fit where $m_1 = m_2 = m$ gives an indication of the total mass we can add to the endpoints for a good fit of a given trajectory. The best fitting masses are on a curve in the (m_1, m_2) plane. The choice $m_1 = m_2$ maximizes the total mass $m_1 + m_2$, whether the masses are light or heavy.

It should also be noted that for the trajectories we analyze we either have fits with low masses, where the $m^{3/2}$ approximation is valid, or trajectories with only 3 data points where we would by

default expect the optimum to be located on a curve in the (m_1, m_2) plane, seeing how there are four fitting parameters in total.

While the presentation in the following sections of the results is for the symmetric fit, this does not mean that we have found it is actually preferred by the data. The symmetric fit tells us whether there is a preference for non-zero endpoint masses or not, and allows us to obtain the values of the slope for a given total endpoints mass.

6.3.3 Splitting between trajectories of even and odd angular momentum

One of the interesting features of the baryon Regge trajectories is the splitting of the trajectories of even and odd orbital angular momentum states, which is seen in the trajectories of the light baryons, N and Δ . The states with even and odd orbital angular momentum do not lie on one single trajectory, but on two parallel linear trajectories, the odd L states being higher in mass and lying above the trajectory formed by the even states. The plot in figure 21 shows this effect for the (J, M^2) trajectory of the N . The same effect is stronger for the Δ trajectory.

For the strange Λ baryon we do not see this effect. We assume that this effect is only manifest in the trajectories of the N and Δ , and is similarly suppressed for all subsequent trajectories of heavier baryons, which do not have enough data points to confirm this assumption directly.

In our analysis, we fit the even and odd trajectories together, with the same endpoint masses and slope, and allow the intercept to carry the difference between the even and odd states.

6.3.4 Summary of results

Traj.	N	m	α'	a
N	7	$2m = 0 - 170$	$0.944 - 0.959$	$a_e = (-0.32) - (-0.23)$ $a_o = (-0.75) - (-0.65)$
$N^{[a]}$	15	$2m = 0 - 425$	$0.815 - 0.878$	$a_{1/2+} = (-0.22) - 0.07$ $a_{3/2-} = (-0.36) - (-0.06)$
Δ	7	$2m = 0 - 450$	$0.898 - 0.969$	$a_e = 0.14 - 0.54$ $a_o = (-0.84) - (-0.42)$
$\Delta^{[b]}$	3	$2m = 0 - 175$	$0.920 - 0.936$	$a = 0.11 - 0.21$
Λ	5	$2m = 0 - 125$	$0.946 - 0.955$	$a = (-0.68) - (-0.61)$
Σ	3	$2m = 1190$	1.502	$a = (-0.15)$
$\Sigma^{[c]}$	3	$2m = 1255$	1.459	$a = 1.37$
Ξ	3	$2m = 1320$	1.455	$a = 0.50$
Λ_c	3	$2m = 2010$	1.130	$a = 0.09$

Table 3: Summary table for the baryon fits. The ranges listed have χ^2 within 10% of its optimal value. N is the number of points in the trajectory. [a] is a fit to radial trajectories of the N . The fifteen states used are four states with $J^P = 1/2^+$, three with $3/2^-$, and four pairs with other values of J^P . [b] is the radial trajectory of the Δ ($3/2^+$). [c] is a trajectory beginning with the state $\Sigma(1385)$ $3/2^+$, as opposed to the $1/2^+$ Σ ground state. The rest of the trajectories are all leading trajectories in the (J, M^2) plane, and do not exclude any states.

We present here the two summary tables: in table 3 we list the results of the general fits, where we find the optimal slope and masses for each trajectory separately, while in table 4 are the results of fits done with a fixed slope, $\alpha' = 0.95 \text{ GeV}^{-2}$.

As explained in previous sections, we assume the model of a single string connecting two endpoint masses (a quark and a diquark). We present our results in terms of the total mass of the endpoints, as we cannot determine the distribution of the mass between them from the Regge trajectory fits alone.

Our massive fits for the baryons are not always consistent. For the light quark trajectories, of the N and the Δ , we have seen there is no evidence for a string endpoint mass of the light quarks. These

Traj.	N	m	a
N	7	$2m = 0 - 180$	$a_e = (-0.33) - (-0.22)$ $a_o = (-0.77) - (-0.65)$
Δ	7	$2m = 300 - 530$	$a_e = 0.31 - 0.66$ $a_o = (-0.71) - (-0.26)$
Λ	5	$2m = 0 - 10$	$a = (-0.68) - (-0.61)$
Σ	3	$2m = 530 - 690$	$a = (-0.29) - (-0.04)$
Σ^*	3	$2m = 435 - 570$	$a = 0.15 - 0.38$
Ξ	3	$2m = 750 - 930$	$a = (-0.22) - 0.10$
Λ_c	3	$2m = 1760$	$a = (-0.36)$
Ξ_c	2	$2m = 2060$	$a = (-1.13)$

Table 4: (J, M^2) fits done with the slope fixed at $\alpha' = 0.950 \text{ GeV}^{-2}$. Fits with $m_1 = m_2$ generally maximize $m_1 + m_2$. In this table we may also include a fit for two Ξ_c states. The ranges listed have χ^2 within 10% of its optimal value. N is the number of points in the trajectory.

states are best fitted by linear trajectories with a slope similar to that of the light mesons - around 0.95 GeV^{-2} for the N and 0.90 GeV^{-2} for the Δ . The (J, M^2) trajectories also exhibit a splitting between the trajectories of states with even and odd orbital angular momentum. In our fits we incorporate this difference into the intercept.

For the strange baryon trajectories there is a significant discrepancy between the Λ , which is best (and very well) fitted by a linear, massless, trajectory, and the Σ baryons which are optimally fitted with a high total mass, of around 1200 MeV and an unusually high slope, 1.5 GeV^{-2} . The fits when fixing the slope at the value obtained from the lighter baryon fits give a total mass in the more reasonable range (for the mass of an s quark) of $500 - 600 \text{ MeV}$. We have also looked into the doubly strange Ξ baryon, where we have a similar picture. We can fix the slope of the Ξ to $\alpha' = 0.95 \text{ GeV}^{-2}$ and a total mass of around 800 MeV. This choice is not only more consistent with the slopes obtained from the lighter baryons, but also with the mass obtained for the s quark in the meson fits, $m_s \approx 400 \text{ MeV}$.

The last results are those of the charmed baryons, the heaviest baryons for which we have a trajectory. The charmed Λ_c is again best fitted by a high slope, 1.2 GeV^{-2} and a total mass of a little over 1800 MeV. Once more we can bring down the mass by fixing α' at 0.95 GeV^{-2} and get $2m = 1760 \text{ MeV}$ as the best fit. For the charmed-strange Ξ_c trajectory, including only two data points and therefore fitted only with the fixed slope of 0.95 GeV^{-2} , we find a fit with $2m = 2060 \text{ MeV}$, a value consistent with the presence of both charmed and strange quarks.

6.3.5 Light quark baryons

In the light baryon sector, we look at the N and Δ resonances.

Trajectories in the (J, M^2) plane One of the most interesting features of the baryon Regge trajectories is the splitting of the trajectories of even and odd L states. The states with even and odd orbital angular momentum do not lie on one single trajectory, but on two parallel linear trajectories, the odd L states being higher in mass and lying above the trajectory formed by the even states. The plot in figure 21 shows this effect for the (J, M^2) trajectory of the N . In our analysis, we fit the even and odd trajectories together, with the same endpoint masses and slope, and allow the intercept to carry the difference between the even and odd states.

In this way, we get that the N trajectory is best fitted with a slope of around 0.95 GeV^{-2} , and that the linear fit is optimal. Only small masses, up to a total mass of $2m = 170 \text{ MeV}$, are allowed.⁸ Trying a fit using only the four highest J states (two even and two odd), we achieve a weaker χ^2 dependence

⁸Masses in what we call the “allowed” range give a value of χ^2 that is within 10% of its optimal value for that specific trajectory.

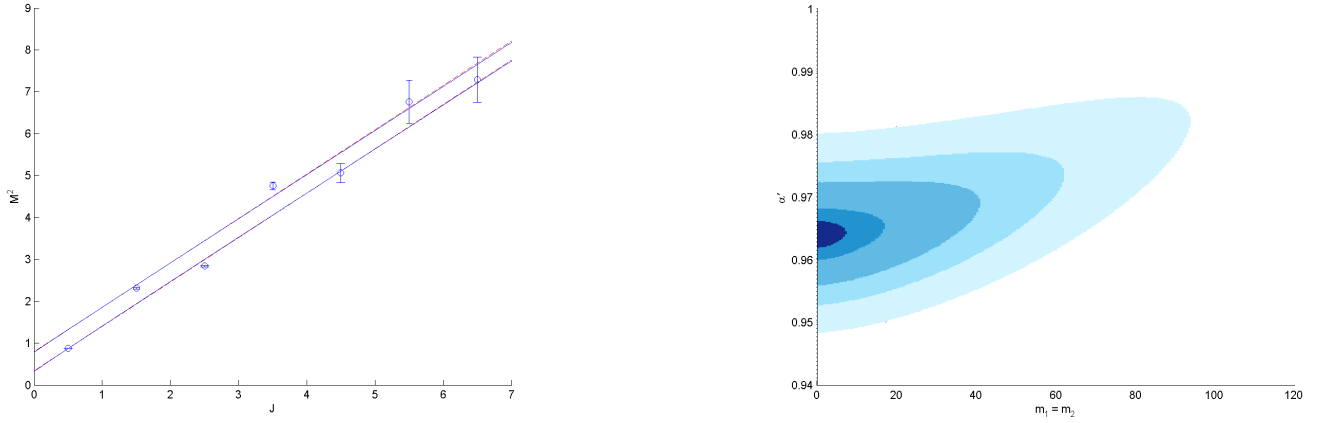


Figure 21: The light baryon trajectory fits. **Left:** The N trajectory and fits, showing the even/odd effect. **Right:** χ^2 vs. $(\alpha', 2m)$ for the N . The χ^2 plots are for fits to the (J, M^2) trajectories, and use only the even L states (results somewhat differ from those quoted for the fit to even and odd states together). The darkest areas in the χ^2 plots have $\chi_m^2/\chi_l^2 < 1$, lightest areas are $\chi_m^2/\chi_l^2 < 1.1$.

on the mass, and we can add a total mass of up to 640 MeV, with the slope being near 1 GeV^{-2} for the highest masses.

The Δ is also best fitted by the linear, massless, trajectory, but it allows for higher masses. The maximum for it is 450 MeV. The slope, for a given mass, is lower than that of the N . It is between 0.9 GeV^{-2} for the linear fit, and 0.97 GeV^{-2} for the maximal massive fits.

As for the even-odd effect, we quantify it by looking at the difference between the intercept obtained for the even L trajectory and the one obtained for the odd L trajectory. The magnitude of the even-odd splitting is higher for the Δ than it is for the N baryons. For the Δ , the difference in the intercept is of almost one unit - $a_e - a_o \approx 1$, while for the N it is less than half that: $a_e - a_o \approx 0.45$. The difference in M^2 is obtained by dividing by α' , so it is 0.5 GeV^{-2} for the N and 1.1 GeV^2 for the Δ .

Trajectories in the (n, M^2) plane The radial trajectories we analyze are also best fitted with small, or even zero, endpoint masses.

For the Δ we have three states with $J^P = 3/2^+$. The slope is between 0.92 and 0.94 GeV^{-2} and the maximal allowed total mass is less than 200 MeV.

For the N we use a total of fifteen states: four with $J^P = 1/2^+$ (the neutron/proton and higher resonances), three with $3/2^-$, and four pairs with other J^P assignments. They are all fitted with the same slope and mass. The results show a lower slope here, from 0.82 GeV^{-2} for the linear fit to 0.85 GeV^{-2} for the highest mass fit, this time with $2m = 425 \text{ MeV}$.

6.3.6 Strange baryons

In the strange section there are several trajectories we analyze.

The first is that of the Λ . There are five states in this trajectory, enough for us to see that the even-odd effect is not present - or too weak to be noticeable. The linear fit, with $\alpha' = 0.95 \text{ GeV}^{-2}$, is the optimal fit, and only small masses of the order of 60 MeV are allowed at each endpoint. Even if one of the masses is zero, the mass at the other end could not exceed 100 MeV. This is a puzzling result because the results of the meson fits, which will be compared in detail to the baryon fits in a later section, point toward a mass of 200 – 400 MeV for the s quark. We show the plot of χ^2 in figure 22.

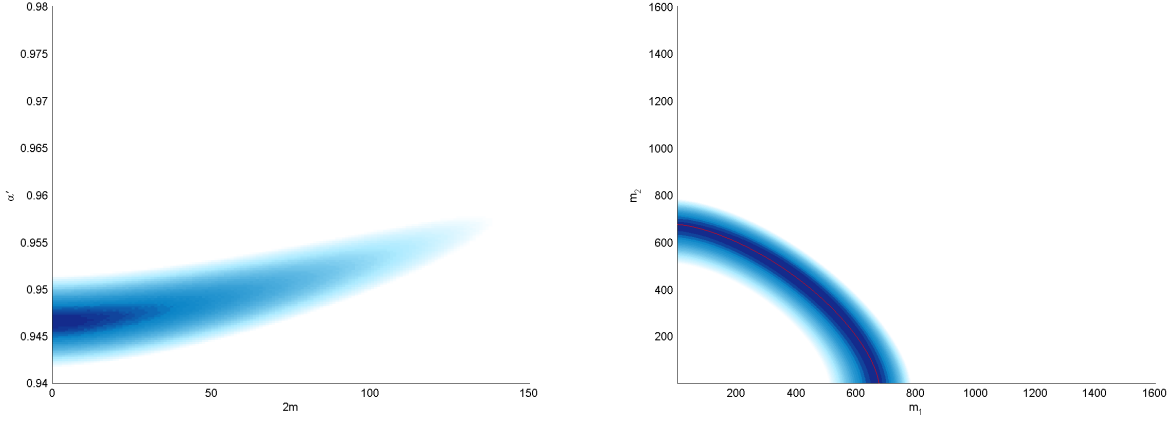


Figure 22: The strange baryon trajectory fits. **Left:** χ^2 vs. $(\alpha', 2m)$ for the Λ trajectory. **Right:** χ^2 vs. (m_1, m_2) for the Ξ trajectory, for $\alpha' = 0.950$. The red curve is $m_1^{3/2} + m_2^{3/2} = 2 \times (425)^{3/2}$.

On the other hand, the other strange baryon trajectories we examine point to very high masses, with correspondingly high values of the slope. These are the results of the two trajectories of the Σ baryon we examine. The first has three states with $J^P = 1/2^+, 3/2^-$, and $5/2^+$. The second has the parity reversed (for a given value of J): $J^P = 3/2^+, 5/2^-$, and $7/2^+$.

Since there are only three states per trajectory we cannot determine from the data alone whether or not there is an even-odd splitting effect present here (and this is the case with all following trajectories). Assuming that there is no even-odd splitting, the best fits have $2m \approx 1200$ MeV and a slope of about $1.4 - 1.5$ GeV^{-2} . Assuming splitting, we find in the case of the Σ that the linear fit connecting the two even states has $\alpha' \approx 0.9$ GeV^{-2} .

A third option, is fixing the slope at a more reasonable low value - we chose $\alpha' = 0.95$ GeV^{-2} - and redoing the massive fits (with the assumption that there is no splitting). The best fits then for the Σ are at around $2m = 500$ MeV, with the mass being somewhat higher in the trajectory beginning with of the $1/2^+$ state. This is certainly the choice that is most consistent with previous results, as we can distribute the total mass so there is a mass of $m_s \approx 400$ MeV at one end and up to 100 MeV at the other. The cost in χ^2 is fairly high: for the first trajectory χ^2 is approximately 10^{-4} for the higher slope and ten times larger for $\alpha' = 0.95$, while for the second χ^2 is almost zero for the high slope fit⁹ and about 5×10^{-4} for the fixed slope fit. In any case, the fits with $\alpha' = 0.95$ GeV^{-2} and with the added masses have a better χ^2 than the linear massless fits.

There is one more possible trajectory we examine, of the doubly strange Ξ baryon. The best fit overall is again with $\alpha' \approx 1.5$ GeV^{-2} , and at a somewhat higher mass of $2m = 1320$. Fixing the slope at 0.95 GeV^{-2} results in $2m = 850$ being optimal. This is again the best choice in terms of consistency - the total mass is exactly in the range we would expect to see where there are two s quarks present. In χ^2 , the fit with the high slope has $\chi^2 \approx 10^{-4}$ while the latter has $\chi^2 \approx 4 \times 10^{-4}$. We plot the masses in the fixed slope fit in figure 22.

6.3.7 Charmed baryons

In the charmed baryon section we have only one trajectory we can use, comprised of three states, that of the Λ_c baryon. The best fits are again at a relatively high slope, 1.1 GeV^{-2} , with the mass $2m = 2010$ MeV. This fit's χ^2 tends to zero. The fit with the slope fixed at 0.95 GeV^{-2} takes the mass down to

⁹This is often the case with three point trajectories, where we may find a choice of the parameters for which the trajectory passes through all three data points. This makes the error in the measurement hard to quantify.

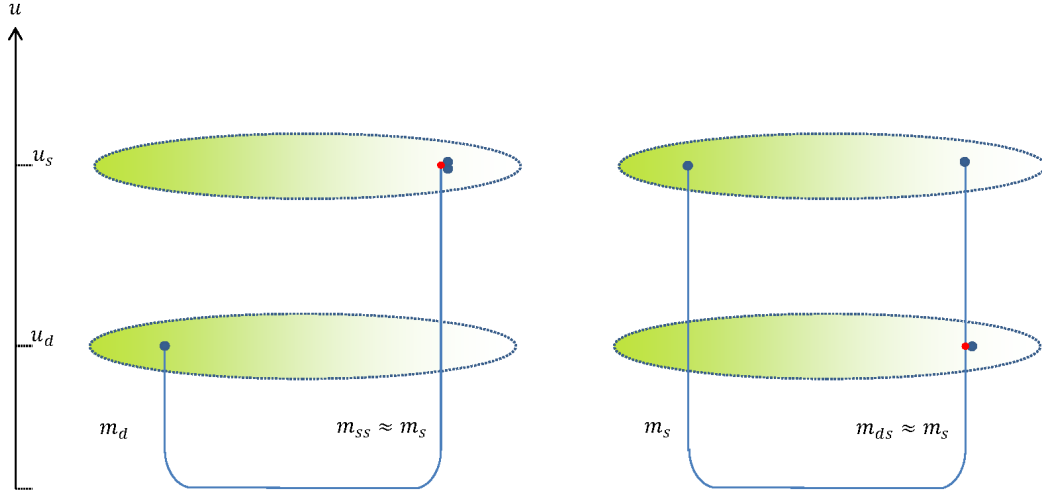


Figure 23: The two holographic setups for the Ξ^- baryon, with different compositions of the diquarks. The vertical segments of the strings contribute the measured endpoint masses.

$2m = 1760$ MeV with $\chi^2 = 3 \times 10^{-5}$. The high slope fit is equivalent to a fit with $m_1 = 1720$ MeV and $m_2 = 90$, while a the fit with $m_1 = 1400$ and $m_2 = 90$ is roughly equal to the latter fixed slope fit.

We can also do a fit using two Ξ_c states. These states are charmed and strange and are composed of dsc (Ξ_c^0) or usc (Ξ_c^+). Since we only have two states, we do only a fit with the fixed slope, $\alpha' = 0.95$ GeV $^{-2}$. The best massive fit then has $2m = 2060$ MeV.

6.3.8 Structure of the baryon in the quark-diquark model

For the light baryons our analysis of the spectrum cannot offer much new insight regarding the different baryons' structure,¹⁰ in particular because we have no way to distinguish between the two light quarks, given their small - possibly zero - masses, but also because we cannot in general make any comments regarding the mass distribution within the different baryons (both light and heavy). In spite of this, there is one interesting implication when interpreting our results in light of the underlying holographic models and the way they map the diquarks into flat space-time.

In our analysis of the meson spectrum, we argued that the mass parameter relevant to the analysis is the mass of the quark as a string endpoint, which generically was found to be between the usual QCD and constituent masses attributed to the respective quark. For the diquark the identification between string length and mass can have another implication, as illustrated in figure 23. If the relevant mass parameter is the length of the vertical segment of the string connected to the flavor brane, and if the two quarks forming the diquark and the baryonic vertex to which they are both connected all lie close to each other on the flavor brane, then we would expect the mass of the diquark - in the holographic picture, as a string endpoint - to be approximately equal to the mass of a single quark:

$$m_{qq} \approx m_q \quad (141)$$

¹⁰[55] offers a discussion of the composition of the light baryons in a model of a quark and diquark joined by a flux tube. In the analysis of the spectrum done there, the light baryons are assigned different configurations of the diquark based on the energetics of the ud diquarks.

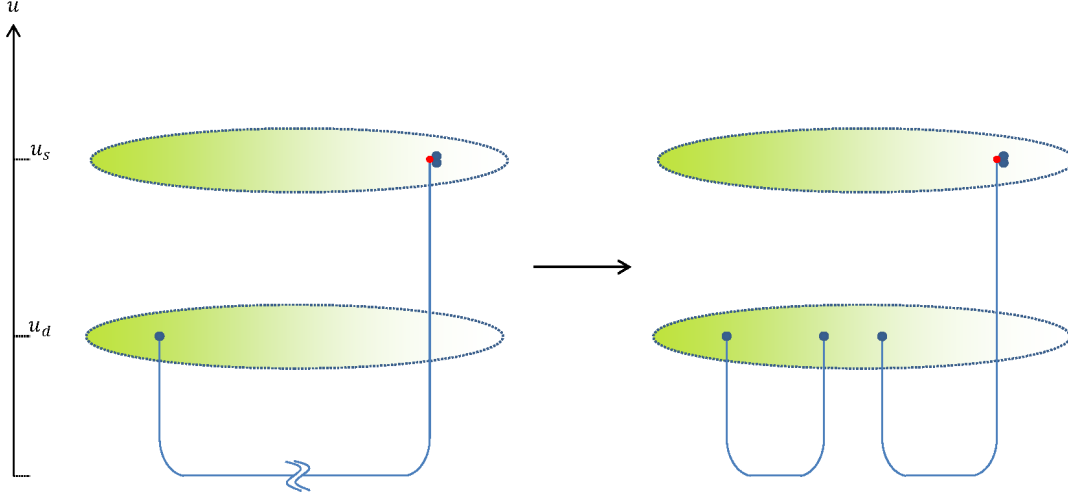


Figure 24: A doubly strange baryon with an ss diquark decaying into a doubly strange baryon and a non-strange meson. First the string tears, and then the endpoints reconnect to the flavor brane, forming a quark-anti-quark pair.

This is because we have only one contribution to the mass from the string connecting the lone quark outside the diquark and the baryonic vertex. This is a prediction that can serve as a test of the holographic interpretation of the string endpoint masses. Since we do not have an accurate figure for the mass of the light u and d quarks, and since we lack data for charmed and heavier baryons, our best avenue for verifying this experimentally is by examining the doubly strange Ξ baryon.

The two options for the Ξ quark are one where the diquark is composed of an s and a light quark, and another where the diquark is composed of two s quarks. For the first option, our holographic interpretation would lead us to expect there to be two masses at the endpoints approximately equal to the s quark mass, leading to a total mass of $2m \approx 2m_s$ at the endpoints. In the second option, the two s quarks in the diquark would contribute only once to the total mass we measure in the Regge trajectory fits, so the result for the total mass $2m$ should be around, possibly a little higher than, the mass of a single s quark.

The result from the fixed slope fit of the Ξ trajectory, $2m = 750 - 930$ MeV, is consistent, from the holographic point of view, with a ds or us diquark, as opposed to ss . This is because we expect the mass of the s to be somewhere near 400 MeV. Of course, from a purely flat space-time perspective, an ss diquark with a mass of roughly $2m_s$ is not excluded.

If we look at the decay modes of the states used in the Ξ fits we might learn something about their structure [67]. We look at a baryon's strong decays into a baryon and a meson, and our assumption is that in these decays the diquark and baryonic vertex go into the outgoing baryon while the third lone quark ends up in the meson. An illustration of this type of decay is in figure 24.

The lightest doubly strange state does not have the phase space for strong decays. If we look at the two next states in the trajectory, the $\Xi(1820)$ and the $\Xi(2030)$, we see that they decay mainly into ΛK or ΣK . The fact that they decay into a strange meson and strange baryon is against the ss diquark configuration. The leading modes of decay should leave the diquark intact, so if the diquark were ss the leading mode of decay would be $\Xi\pi$ (as it is for some of the other observed doubly strange baryons,

for which we do not have a trajectory).

For the baryons with a single strange quark, the Λ and the Σ , we have seen an odd discrepancy between the obtained mass values. The mass in the Λ baryon was less than 100 MeV, while in the Σ we have seen masses of above 400 MeV. We cannot explain this discrepancy in terms of different configurations of the diquarks, as we expect the s to contribute to the mass whether it is in the diquark or not. The decay modes do not give a straightforward answer regarding the compositions of the Λ and Σ , as the states decay both to NK and $\Sigma\pi/\Lambda\pi$. We do not see a systematic preference for decays where the s remains in the baryon (implying it is near the baryonic vertex in the diquark) or vice versa in either of the trajectories.

For the charmed-strange Ξ_c we see a mass compatible with $m_1 + m_2 = m_s + m_c$. This implies to us that the possibility of a cs diquark is excluded, since we see both quarks' masses (from the holographic point of view we expect the diquark mass to be $m_{cs} \approx m_c$). Unfortunately we cannot test this based on the decay modes. If we look at the decays of the Ξ_c baryons, we find that the Ξ_c^0/Ξ_c^- does not have the phase space to decay strongly, and the next state we take in the trajectory, $\Xi_c(2815)$, is also too light to provide information that would be useful to us. The $\Xi_c(2815)$ cannot decay to a charmed meson and a strange baryon (which is the decay mode we will naively expect if the Ξ_c is a us/ds diquark joined to a c quark), simply because the lightest of these, D^\pm/D^0 and Λ respectively, are still heavy enough so that the sum of their masses exceeds the mass of the $\Xi_c(2815)$.

For the charmed Λ_c baryon, with one c and two light u/d quarks, we have no prediction based on the masses, because in any case we expect to see a total mass of approximately $m_c = 1500$ MeV. The first state in the trajectory heavy enough to decay into a charmed meson and a baryon, the $\Lambda_c(2800)^+$, was observed to decay both to pD^0 and $\Sigma_c\pi$, but there is no quantitative data to indicate which of these modes (if any) is dominant.

6.4 Strings and the search for glueballs

6.4.1 The glueball candidates: The f_0 and f_2 resonances

The search for the glueballs is centered on the lightest states, the scalar ground state of $J^{PC} = 0^{++}$, and the lightest tensor of 2^{++} . There is an abundance of isoscalar states with the quantum numbers $J^{PC} = 0^{++}$ (the f_0 resonances) or $J^{PC} = 2^{++}$ (f_2). The Particle Data Group's (PDG) latest Review of Particle Physics [68], which we use as the source of experimental data throughout this section, lists 9 f_0 states and 12 f_2 states, with an additional 3 f_0 's and 5 f_2 's listed as unconfirmed "further states". These are all listed in table 5. In the following we make a naive attempt to organize the known f_0 and f_2 states into trajectories, first in the plane of orbital excitations (J, M^2), then in the radial excitations plane (n, M^2).

The states classified as "further states" are generally not used unless they prove to be necessary to complete the trajectories formed by the other states. The "further states" will be denoted with an asterisk below.¹¹ For a more complete picture regarding the spectrum and specifically the interpretation of the different resonances as glueballs, the reader is referred to the relevant reviews [69, 70, 71, 72] and citations therein.

6.4.2 Assignment of the f_0 into trajectories

In a given assignment, we generally attempt to include all the f_0 states listed in table 5, sorting them into meson and, if possible, glueball trajectories.

¹¹Note that the asterisk is not standard notation nor a part of the PDG given name of a state, we only use it to make clear the status of given states throughout the text.

State	Decay modes	State	Decay modes
$f_0(500)/\sigma$	$\pi\pi$ dominant	$f_2(1270)$	$\pi\pi$ [85%], 4π [10%], KK , $\eta\eta$, $\gamma\gamma$
$f_0(980)$	$\pi\pi$ dominant, $K\bar{K}$ seen	$f_2(1430)$	KK , $\pi\pi$
$f_0(1370)$	$\pi\pi$, 4π , $\eta\eta$, $K\bar{K}$	$f_2'(1525)$	KK [89%], $\eta\eta$ [10%], $\gamma\gamma$ [seen]
$f_0(1500)$	$\pi\pi$ [35%], 4π [50%], $\eta\eta/\eta\eta'$ [7%], $K\bar{K}$ [9%]	$f_2(1565)$	$\pi\pi$, $\rho\rho$, 4π , $\eta\eta$
$f_0(1710)$	$K\bar{K}$, $\eta\eta$, $\pi\pi$	$f_2(1640)$	$\omega\omega$, 4π , KK
$f_0(2020)$	$\rho\pi\pi$, $\pi\pi$, $\rho\rho$, $\omega\omega$, $\eta\eta$	$f_2(1810)$	$\pi\pi$, $\eta\eta$, 4π , KK , $\gamma\gamma$ [seen]
$f_0(2100)$		$f_2(1910)$	$\pi\pi$, KK , $\eta\eta$, $\omega\omega$
$f_0(2200)$		$f_2(1950)$	K^*K^* , $\pi\pi$, 4π , $\eta\eta$, KK , $\gamma\gamma$, pp
$f_0(2330)$		$f_2(2010)$	KK , $\phi\phi$
* $f_0(1200\text{--}1600)$		$f_2(2150)$	$\pi\pi$, $\eta\eta$, KK , $f_2(1270)\eta$, $a_2\pi$, pp
* $f_0(1800)$		$f_J(2220)$	$\pi\pi$, KK , pp , $\eta\eta'$
* $f_0(2060)$		$f_2(2300)$	$\phi\phi$, KK , $\gamma\gamma$ [seen]
		$f_2(2340)$	$\phi\phi$, $\eta\eta$
		* $f_2(1750)$	KK , $\gamma\gamma$, $\pi\pi$, $\eta\eta$
		* $f_2(2000)$	
		* $f_2(2140)$	
		* $f_2(2240)$	
		* $f_2(2295)$	

Table 5: All the f_0 and f_2 states, with their observed decay modes, as listed by the PDG. The states marked by an asterisk are classified as “further states”, i.e. in need of further experimental confirmation.

We make an exception of the $f_0(500)/\sigma$ resonance, which we do not use in any of the following sections. Its very large width (400–700 MeV) and low mass are enough to make it stand out among the other f_0 states listed in the table. We find that it does not belong on a meson Regge trajectory, nor does it particularly suggest itself as a glueball candidate.¹² Therefore, we simply “ignore” the $f_0(500)$ in the following sections.

Assignment of all states as mesons Sorting the f_0 states into trajectories with a meson-like slope leads to an assignment of the f_0 ’s into two groups of four:

$$\text{Light :} \quad 980, 1500, 2020, 2200,$$

$$s\bar{s} : \quad 1370, 1710, 2100, 2330.$$

While this simple assignment includes all the confirmed f_0 states (except the $f_0(500)$) on two parallel trajectories, it remains unsatisfactory. If there are no glueballs we expect the states in the lower trajectory to be (predominantly) composed of light quarks, while the higher states should be $s\bar{s}$. This does not match what we know about the decay modes of the different states. For example, the $f_0(1370)$ does not decay nearly as often to $K\bar{K}$ as one would expect from an $s\bar{s}$ state. In fact, this assignment of the f_0 ’s into meson trajectories was proposed in some other works [74, 75, 76], and the mismatch with the decay modes was already addressed in greater detail in [77]. This suggests that the simple picture where all resonances belong on linear trajectories is wrong.

In the following assignments we pick and single out a state as the glueball ground state and try to build the meson trajectories without it.

¹²The authors of [73] state that the interpretation of the $f_0(500)/\sigma$ as a glueball is “strongly disfavored”, from what they consider a model independent viewpoint. We found no references that suggest the opposite.

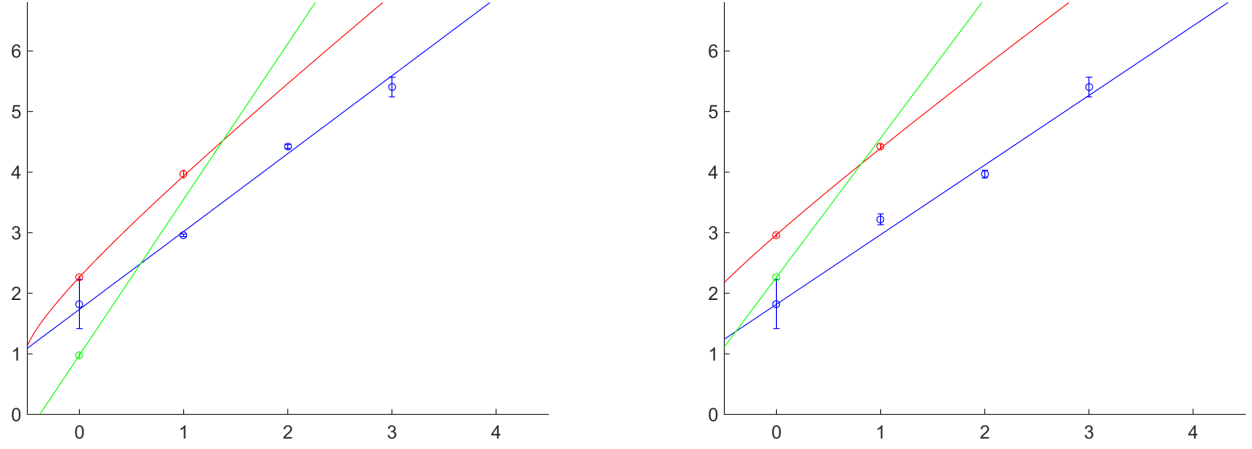


Figure 25: Two examples of an assignment with glueball trajectories. In the **left** plot $f_0(980)$ is the glueball ground state (green), $f_0(1370)$ is the light quark meson (blue), and $f_0(1505)$ is $s\bar{s}$ (red). On the **right** we have $f_0(1505)$ as glueball, $f_0(1370)$ as light meson, and $f_0(1710)$ as $s\bar{s}$.

Assignment with the $f_0(980)$ as glueball: First is the the $f_0(980)$. Assuming it is the glueball then the $f_0(2330)$ is at the right mass to be its first excited ($n = 2$) partner. However, we find that the two meson trajectories given this assignment,

$$\text{Light :} \quad 1370, 1710, 2100,$$

$$s\bar{s}: \quad 1500, 2020,$$

also predict a state very near the mass of the $f_0(2330)$, and according to this assignment, there should be two more f_0 states near the $f_0(2330)$, for a total of three. The $f_0(2200)$ has to be excluded.

We again have to put some states on trajectories that are not quite right for them: the $f_0(1710)$ has a significant branching ratio for its decay into $K\bar{K}$, while the $f_0(1500)$, which is taken as the head of the $s\bar{s}$ trajectory, decays to $K\bar{K}$ less than 10% of the time.

Note that the assignment above is the same as the one we would make if we excluded the $f_0(980)$ on the grounds of it being an exotic (but non-glueball) state and assumed all the other states are mesons. The $f_0(980)$ is commonly believed to be a multiquark state or a $K\bar{K}$ bound state,¹³ and in fact, we will find in following sections that even it is not a glueball, it is better to exclude it from the meson trajectories.

Assignment with $f_0(1370)$ as glueball From here onwards the states singled out as glueballs are too high in mass for their excited states to be in the range of the measured f_0 states listed in table 5, that is beneath 2.4 GeV.

Excluding the $f_0(1370)$, we have:

$$\text{Light :} \quad [980], 1500, *1800, 2100, 2330$$

$$s\bar{s}: \quad 1710, 2200.$$

The $f_0(980)$ is put here in brackets to emphasize that it is optional. Including or excluding it can affect some of the fitting parameters but the trajectory is certainly not incomplete if we treat $f_0(980)$ as a non-meson resonance and take $f_0(1500)$ as the head of the trajectory.

¹³See the PDG's "Note on scalar mesons below 2 GeV" (in [68]) and references therein.

The main issue here is that we have to use the state $*f_0(1800)$ to fill in a hole in the meson trajectory, a state that is still considered unconfirmed by the PDG and whose nature is not entirely known. Its observers at BESIII [78] suggest it is an exotic state - a tetraquark, a hybrid, or itself a glueball. More experimental data is needed here.

Other than that we have $f_0(2100)$ as a light meson and $f_0(2200)$ as $s\bar{s}$. This is the option that is more consistent with the decays, as $f_0(2200)$ is the one state of the two which is known to decay into $K\bar{K}$ (we again refer to the comments in [77] and references therein). However, in terms of the fit, we might do better to exchange them. It is possible that their proximity to each other affects their masses in such a way that our simple model does not predict, and this affects badly the goodness of our fit.

Assignment with $f_0(1500)$ as glueball Taking the $f_0(1500)$ to be the glueball, then the light meson trajectory will start with $f_0(1370)$, giving:

$$\text{Light :} \quad 1370, *1800, 2020, 2330,$$

$$s\bar{s}: \quad 1710, 2100.$$

With $f_0(1500)$ identified as the glueball, this assignment includes all the states except $f_0(2200)$. We could also use $f_0(2200)$ as the $s\bar{s}$ state and leave out $f_0(2100)$ instead.

There is no glaring inconsistency in this assignment with the decay modes, but we are again confronted with the state $*f_0(1800)$, which we need to complete the light meson trajectory. The $f_0(2020)$ is wider than other states in its trajectory. In particular, it is much wider than the following and last state in the trajectory, $f_0(2330)$. We can assign the $f_0(2330)$ to the $s\bar{s}$ trajectory instead, but there is no other argument for that state being $s\bar{s}$, considering it was observed only in its decays to $\pi\pi$ and $\eta\eta$. Perhaps the fact that $f_0(1370)$ and $f_0(2020)$ are both quite wide means that there should be two additional states, with masses comparable to those of $*f_0(1800)$ and $f_0(2330)$, that are also wide themselves, and those states will better complete this assignment.

Assignment with $f_0(1710)$ as glueball Excluding the $f_0(1710)$ from the meson trajectories we can make an assignment that includes all states except the $f_0(500)$ and $f_0(980)$:

$$\text{Light :} \quad 1370, *1800, 2100, 2330$$

$$s\bar{s}: \quad 1500, 2020, 2200$$

$$\text{Glue :} \quad 1710$$

The disadvantage here is that we again have to use $f_0(1500)$ as the head of the $s\bar{s}$ trajectory despite knowing that its main decay modes are to 4π and $\pi\pi$, as well as the fact the we - once again - need the $*f_0(1800)$ resonance to fill in a hole for $n = 1$ in the resulting light meson trajectory.

Conclusions from the f_0 fits It is not hard to see that the f_0 resonances listed in the PDG's Review of Particle Physics all fit in quite neatly on two parallel trajectories with a slope similar to that of other mesons. However, upon closer inspection, these trajectories - one for light quark mesons and one for $s\bar{s}$ - are not consistent with experimental data, as detailed above. For us the naive assignment is also inconsistent with what we have observed for the other $s\bar{s}$ trajectories when fitting the mesons, namely that the $s\bar{s}$ trajectories are not purely linear, and have to be corrected by adding a string endpoint mass for the s quark of at least 200 MeV.

The other novelty that we hoped to introduce, the half slope trajectories of the glueball, proved to be impractical - given the current experimental data which only goes up to less than 2.4 GeV for the relevant resonances.

There is no one assignment that seems the correct one, although the two assignments singling out either $f_0(1370)$ or $f_0(1500)$ as the glueball ground states seem more consistent than the other possibilities. The best way to determine which is better is, as always, by finding more experimental data. We list our predictions for higher resonances based on these assignments in table 6.

Ground state	Next state mass	Next state width
$f_0(980)$	2385 ± 70	405 ± 175
$f_0(1370)$	2555 ± 110	1255 ± 615
$f_0(1500)$	2640 ± 80	335 ± 30
$f_0(1710)$	2770 ± 85	350 ± 30

Table 6: Predictions for the first excited glueball based on half slope Regge trajectories. The mass could correspond to either the 0^{++} excited state with $n = 2$, or to the first orbital excitation, a 2^{++} state with $n = 0$. The width is calculated based on $\Gamma \propto L^2 \propto M^2$ (the closed string has to tear twice, with the probability for each tear proportional to the string length). The errors take into account both the uncertainty in the experimental masses and widths, and the uncertainty in the slope.

6.4.3 Assignment of the f_2 into trajectories

We now turn to the f_2 tensor resonances. We will first examine trajectories in the (J, M^2) plane, then move on to the attempt to assign all the f_2 states to trajectories in the (n, M^2) plane.

Trajectories in the (J, M^2) plane The only way to get a linear trajectory connecting a 0^{++} and a 2^{++} state with the slope $\alpha'_{gb} = \frac{1}{2}\alpha'_{meson}$ is to take the lightest f_0 glueball candidate and the heaviest known f_2 . Then we have the pair $f_0(980)$ and $f_2(2340)$, and the straight line between them has a slope of 0.45 GeV^{-2} . There is no $J = 1$ resonance near the line stretched between them. However, this example mostly serves to demonstrate once again the difficulty of forming the glueball trajectories in practice.

It is a more sound strategy to look again for the meson trajectories, see what states are excepted from them, and check for overall consistency of the results. In forming the meson trajectories, we know that we can expect the ω mesons with $J^{PC} = 1^{--}$ to be part of the trajectories, in addition to some states at higher spin ($3^{--}, 4^{++}, \dots$), which will allow us to form trajectories with more points.

We can several meson trajectories in the (J, M^2) plane of at least three states, illustrated in figure 26. The f_2 states classified in this assignment as mesons are $f_2(1270)$, $f'_2(1525)$, $f_2(1810)$, $f_2(1950)$, and $f_2(2010)$. These can perhaps be partnered to existing f_0 states as members of triplets of states with $J = 0, 1, 2$ and $PC = ++$ split by spin-orbit interactions. We do not know the exact magnitude of the splitting. There are some f_0 states close (within 20–100 MeV) to the f_2 states mentioned above, and the PDG lists some $f_1(1^{++})$ resonances that may be useful, but we do not find any such trio of states with similar properties and masses that could be said to belong to such a spin-orbit triplet. Therefore, we limit our conclusions from these Regge trajectories to the f_2 which we found we could directly place on them.

Trajectories in the (n, M^2) plane Sorting the f_2 resonances into trajectories, the situation is somewhat simpler than with the f_0 scalars, as here we have two states that belong on meson trajectories in the (J, M^2) plane, as we found in previous sections. In particular, the $f_2(1270)$ belongs to the trajectory of the ω meson, and the $f'_2(1525)$ is an $s\bar{s}$ and sits on the ϕ trajectory. Their decay modes and other properties are also well known and there is no real doubt about their nature.

The linear trajectory beginning with the $f_2(1270)$ meson includes the states $f_2(1640)$ and $f_2(1950)$. We can include one of the further states $*f_2(2240)$ as the fourth point in the trajectory. We can also

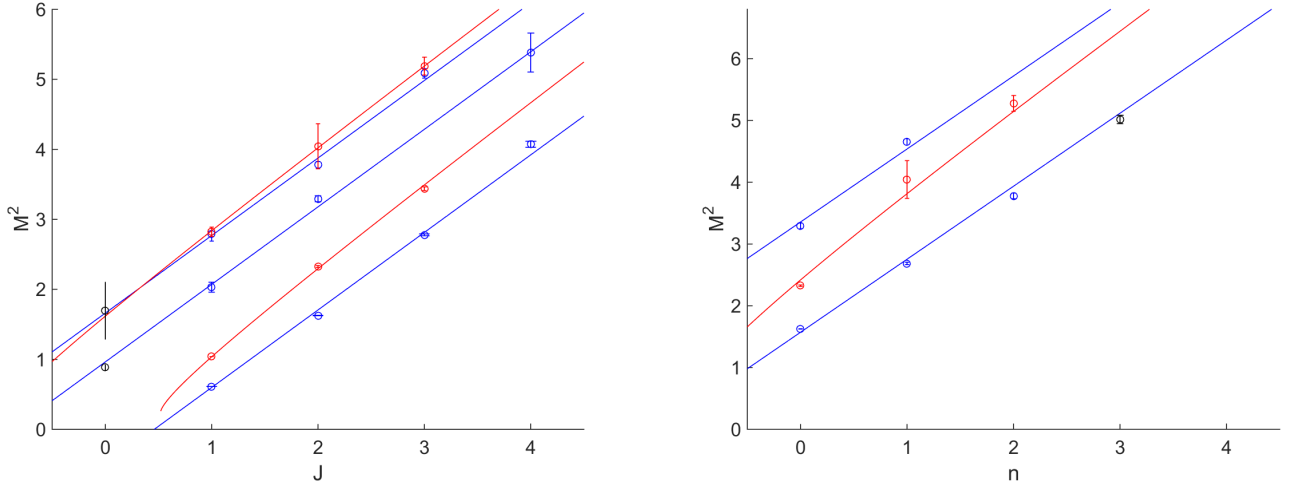


Figure 26: **Left:** The trajectory of the ω (blue) and ϕ (red) mesons in the (J, M^2) plane and their daughter trajectories. The fits have the common slope $\alpha' = 0.903 \text{ GeV}^{-2}$, and the $s\bar{s}$ trajectories are fitted using a mass of $m_s = 250 \text{ MeV}$ for the s quark. The states forming the trajectories are as follows: With $J^{PC} = 1^{--}$, $\omega(782)$, $\phi(1020)$, $\omega(1420)$, $\omega(1650)$, $\phi(1680)$. With $J^{PC} = 2^{++}$, $f_2(1270)$, $f_2'(1525)$, $f_2(1810)$, $f_2(1950)$, and $f_2(2010)$. With $J^{PC} = 3^{--}$, $\omega_3(1670)$, $\phi_3(1850)$, $*\omega_3(2255)$, and $\omega_3(2285)$. And with $J^{PC} = 4^{++}$, $f_4(2050)$ and $f_4(2300)$. We also plot at $J^{PC} = 0^{++}$ the $f_0(980)$ and $f_0(1370)$ which are found to lie near the trajectories fitted, but were not included themselves in the fits, as they are not theoretically expected to belong to them. **Right:** Some radial trajectories of the f_2 , with blue lines for light mesons and red for $s\bar{s}$. The fits have the common slope $\alpha' = 0.846 \text{ GeV}^{-2}$, and the $s\bar{s}$ trajectories are fitted using a mass of $m_s = 400 \text{ MeV}$ for the s quark. The states forming the trajectories are as follows: The first light meson trajectory with $f_2(1270)$, $f_2(1640)$, and $f_2(1950)$, and followed by the unconfirmed state $*f_2(2240)$ which was not used in the fit. The $s\bar{s}$ trajectory with $f_2'(1525)$, $f_2(2010)$, and $f_2(2300)$. And the second light meson trajectory with $f_2(1810)$ and $f_2(2150)$.

use the $f_J(2220)$ in place of the $*f_2(2240)$, but it seems an unnatural choice because of the widths of the states involved (the $f_J(2220)$ is much narrower than the others with $\Gamma = 23 \pm 8 \text{ MeV}$).

The projected trajectory of the $f_2'(1525)$, using the same slope as the $f_2(1270)$ trajectory and adding mass corrections for the s quark, includes the $f_2(2010)$ and the $f_2(2300)$.

This leaves out the states $f_2(1430)$, $f_2(1565)$, $f_2(1810)$, $f_2(1910)$, $f_J(2220)$, and $f_2(2340)$, as well as the five resonances classified as further states.

The next state we look at is $f_2(1810)$, classified as a light meson in the (J, M^2) fits of the previous section. It can be used as the head of another light meson trajectory, and the state that would follow it then is $f_2(2150)$. The next state could be $f_2(2340)$, except that it has been observed to decay to $\phi\phi$, making it very unlikely to be a light quark meson.

The state $f_2(1430)$ is intriguing, in part because of the very small width reported by most (but not all) experiments cited in the PDG, but also because it is located in mass between the two lightest mesons of $J^{PC} = 2^{++}$, that is between $f_2(1270)$ (light) and $f_2'(1525)$ ($s\bar{s}$). If we had to assign the $f_2(1430)$ to a Regge trajectory, then it is best placed preceding the $f_2(1810)$ and $f_2(2150)$ in the linear meson trajectory discussed in the last paragraph.

The $f_J(2200)$, previously known as $\xi(2230)$, is also a narrow state. It has been considered a candidate for the tensor glueball [79, 71]. It can be assigned to a linear meson trajectory, as already discussed, but it is clear already from its narrow width that it is not the best choice.

The $f_2(1565)$ is also left out, but it could be paired with $f_2(1910)$ to form another linear meson trajectory. To continue we need another state with a mass of around 2200 MeV.

To summarize, we may organize the f_2 resonances by picking first the resonances for the trajectories of the two known mesons,

$$\begin{aligned} \text{Light :} & \quad 1270, 1640, 1950 \\ s\bar{s}: & \quad 1525, 2010, 2300 \end{aligned}$$

then find the trajectories starting with the lightest states not yet included. This gives us another meson trajectory using the states

$$\text{Light :} \quad 1810, 2150$$

The trajectories formed by these eight states are drawn in figure 26.

To summarize, there are some simplifications in assigning the f_2 to radial trajectories compared to assigning the f_0 resonances. The reason is that we can look at both orbital and radial trajectories and it is easier to classify some states as mesons. The radial trajectories are consistent with the orbital trajectories: states classified as mesons in the latter are also classified as mesons in the former, and with the same quark contents.

The most interesting states after that remain the $f_2(1430)$ and $f_J(2220)$. While the latter has been considered a candidate for the glueball and has been the object of some research (see papers citing [79]), the former is rarely addressed, despite its curious placement in the spectrum between the lightest 2^{++} light and $s\bar{s}$ mesons. It seems a worthwhile experimental question to clarify its status - and its quantum numbers, as the most recent observation [80] can not confirm whether it is a 0^{++} or 2^{++} state, a fact which led to at least one suggestion [81] that the $f_2(1430)$ could be itself the scalar glueball.

6.4.4 Assignments with non-linear trajectories for the glueball

In this section we would like check the applicability of a glueball trajectory of the form

$$J = \alpha'_{gb} E^2 - 2\alpha'_{gb} m_0 E + a, \quad (142)$$

which is the general form we expect from a semi-classical calculation of the corrections to the trajectory in a curved background, and as put forward in section 6.4.4. The novelty here is a term linear in the mass E , which makes the Regge trajectory $\alpha(t)$ non-linear in $t = E^2$. The constant m_0 can be either negative or positive, depending on the specific holographic background, and a priori we have to examine both possibilities. It was also noted in section that there may be a correction to the slope, but we assume it is small compared to the uncertainty in the phenomenological value of the Regge slope, and we use

$$\alpha'_{gb} = \frac{1}{2} \alpha' \quad (143)$$

throughout this section. We also substitute $J \rightarrow J+n$ as usual to apply the formula to radial trajectories.

With the m_0 term we can write

$$\frac{\partial J}{\partial E^2} = \frac{\alpha'}{2} \left(1 - \frac{m_0}{E} \right). \quad (144)$$

We can look at this as an effective slope, and it is the easiest way to see that when m_0 is negative, the effective slope is higher than that of the linear trajectory, and vice versa.

Fits using the holographic formula Using the simple linear formula we could not, in most cases, find glueball trajectories among the observed f_0 and f_2 states. This is because the first excited state is expected to be too high in mass and outside the range of the states measured in experiment.

Adding an appropriate m_0 term can modify this behavior enough for us to find some pairs of states on what we would then call glueball trajectories, and by appropriate we mean a negative value that will make the effective slope of eq. 144 higher. The problem is then that we have only pairs of states,

Ground state	Excited state	α' [GeV ⁻²]	m_0 [GeV]	a
$f_0(980)$	$f_0(2200)$	0.79	-0.52	-0.78
$f_0(1370)$	$f_0(2020)$	0.87	-2.00	-3.21
$f_0(1500)$	$f_0(2200)$	0.87	-1.51	-2.97
$f_2(1430)$	$f_J(2220)$	0.81	-1.33	-2.42

Table 7: Values obtained for the parameters m_0 and a for some of the possible pairs of states on glueball trajectories. The states selected as the excited state of the glueball are those not included in the meson trajectories of the assignments of sections 6.4.2 and 6.4.3, and the slopes are selected based on the results of the meson fits presented in the same sections.

with two fitting parameters: m_0 and a (and α' which is fixed by the meson trajectory fits). We form these pairs by picking a state left out from the meson trajectories proposed in sections 6.4.2 and 6.4.3 and assigning it as the excited partner of the appropriate glueball candidate.

There is a solution for m_0 and a for any pair of states which we can take, and the question then becomes whether there is a reason to prefer some values of the two parameters over others. We list some other values obtained for m_0 and a in table 7.

Using the holographic formula with a constrained intercept [59] implies that a universal form of the first semi-classical correction of the Regge trajectory of the rotating folded string is

$$J + n = \frac{1}{2}\alpha' (E - m_0)^2, \quad (145)$$

up to further (model dependent) modifications of the slope, which in the cases calculated are small. In other words, the intercept obtained then from the semi-classical calculation is

$$a = \frac{1}{2}\alpha' m_0^2. \quad (146)$$

The intercept is always positive in this scenario. If we want to include the ground state with $J = n = 0$ the only way to do it is to take a positive m_0 , specifically we should take $m_0 = M_{gs}$, where M_{gs} is the mass of the ground state. There is no problem with the resulting expression theoretically, but it is not very useful in analyzing the observed spectrum. The trouble is that when using this expression the energy rises much too fast with J and we end up very quickly with masses outside the range of the glueball candidates. If we take, for instance, $f_0(980)$ as the ground state then the first excited state is expected to have a mass of around 2500 MeV, and the heavier candidates naturally predict even heavier masses for the excited states.

Another way to use eq. 142 is to begin the trajectory with a $J = 2$ state. Then m_0 can be either positive or negative. We can then proceed as usual: we pick the head of a trajectory and see if there are any matches for its predicted excited states. We can see, for example, that we can again pair $f_2(1430)$ with $f_J(2220)$. Constraining α' to be 0.90 GeV⁻², the best fit has $m_0 = -0.72$ GeV, and the masses calculated are 1390 and 2260 MeV for the experimental values of 1453 ± 4 and 2231 ± 4 MeV.

6.4.5 Glueball Regge trajectories in lattice QCD

The glueball spectrum has been studied extensively in lattice QCD. Some works have compared results with different stringy models, e.g. [82, 83, 84, 85]. However, the question whether or not the glueballs form linear Regge trajectories is not often addressed, due to the difficulty involved in computing highly excited states. When linear Regge trajectories are discussed, it is often when trying to identify the glueball with the pomeron and searching for states along the given pomeron trajectory,

$$\alpha(t) = \alpha' t + 1 + \epsilon \quad (147)$$

where the slope and the intercept are known from experiment to be $\alpha'_p = 0.25 \text{ GeV}^{-2}$ and $1 + \epsilon \approx 1.08$ [86].

The most extensive study of glueball Regge trajectories is that of Meyer and Teper [45, 46], where a relatively large number of higher mass states is computed, including both high spin states and some highly excited states at low spin. We present here fits to some trajectories with more than two states, based on the results in [46].

Results in lattice computations are for the dimensionless ratio between the mass of a state and the square root of the string tension: M/\sqrt{T} . To get the masses M in MeV one has to fix the scale by setting the value of T . This introduces an additional uncertainty in the obtained values. For the purpose of identifying Regge trajectories we can work directly with dimensionless quantities, avoiding this extra error. For the following, our fitting model will be

$$\frac{M^2}{T} = \frac{2\pi}{\eta}(N + a) \quad (148)$$

In this notation the ratio η , which is the primary fitting parameter (in addition to the intercept a), is expected to be 1 for open strings and $1/2$ for closed strings. It is referred to below as the “relative slope”. N will be either the spin J or the radial excitation number n .

Trajectories in the (J, M^2) plane: As mentioned above, [46] has the most high spin states. The analysis there observes that the first 2^{++} and 4^{++} states can be connected by a line with the relative slope

$$\eta = 0.28 \pm 0.02, \quad (149)$$

which, when taking a typical value of the string tension $\sqrt{T} = 430 \text{ MeV}$ ($\alpha' = 0.84 \text{ GeV}^{-2}$), gives a slope virtually identical to that expected for the pomeron, 0.25 GeV^{-2} . This trajectory can be continued with the calculated 6^{++} state. A fit to the three state trajectory gives the result

$$\eta = 0.29 \pm 0.15. \quad (150)$$

This trajectory leaves out the 0^{++} ground state. In [46] the lowest 0^{++} is paired with the second, excited, 2^{++} state, giving a trajectory with

$$\eta = 0.40 \pm 0.04. \quad (151)$$

A possibility not explored in [46] is that of continuing this trajectory, of the first 0^{++} and the excited 2^{++} , and with the 4^{++} and 6^{++} states following. Then we have the result

$$q = 0.43 \pm 0.03 \quad (152)$$

This second option not only includes more points, it is also a better fit in terms of χ^2 per degrees of freedom (0.37 instead of 1.24). The lowest 2^{++} state is then left out of a trajectory. There is also a $J = 3$ state in the $PC = ++$ sector that lies very close to the trajectory of the 0^{++} ground state. In the closed string model the $J = 3$ state is not expected to belong to the trajectory, so that state is also left out of the fit. The trajectories of the $PC = ++$ states are in the left side of figure 27.

Trajectories in the (n, M^2) plane: In trajectories in the (n, M^2) plane we assume n takes only even values, i.e. $n = 0, 2, 4, \dots$, as it does for the closed string. The results when taking $n = 0, 1, 2, \dots$ will be half those listed.

We again take the results from [46], as it offers calculations of several excited states with the same J^{PC} . Most notably we see there four states listed with $J^{PC} = 0^{++}$. We observe that those points are well fitted by a trajectory with the slope

$$q = 0.50 \pm 0.07, \quad (153)$$

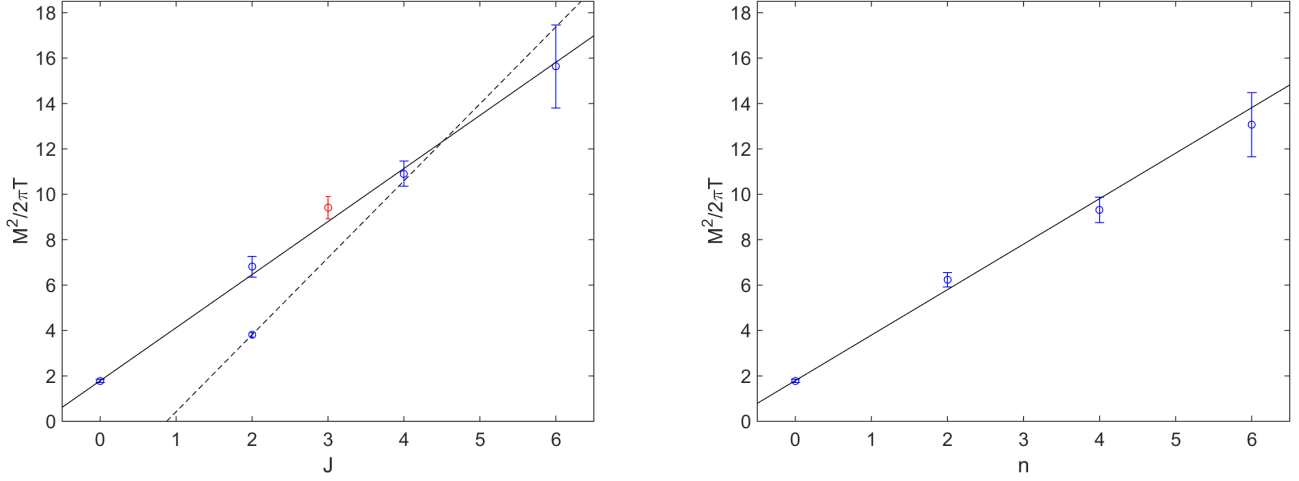


Figure 27: The trajectories of the $PC = ++$ glueball states found in lattice calculations in [46]. **Left:** Trajectories in the (J, M^2) plane. The full line is the fit to a proposed trajectory using four states with $J = 0, 2, 4, 6$, where the relative slope is 0.43 and the lightest tensor is excluded ($\chi^2 = 0.37$). The dotted line is the leading trajectory proposed in the analysis in [46], with a pomeron-like slope. It includes the $J = 2, 4$, and 6 states. ($\chi^2 = 1.24$). In this second option the scalar is excluded. Also plotted is the 3^{++} state, which was not used in the fit. **Right:** trajectory of four states with $J^{PC} = 0^{++}$. The relative slope is exactly 0.50 ($\chi^2 = 1.48$).

J^{PC}	0^{++}	2^{++}	4^{++}	0^{-+}	2^{-+}
Meyer [46]	0.50 ± 0.07	0.67 ± 0.10	0.30 ± 0.06	0.39 ± 0.07	0.56 ± 0.13
M&P [87]	0.51 ± 0.12	-	-	0.32 ± 0.02	0.38 ± 0.03

Table 8: Relative slopes q of trajectories in the (n, M^2) plane. The first result (Meyer/ 0^{++}) is that of a fit to the four point trajectory drawn in 27. The other results are obtained when calculating the slopes between pairs of states, where the lowest state is assumed to have $n = 0$, and the next calculated state is taken to be the first excited state with $n = 2$.

where $\chi^2 = 1.48$ for the fit. It is interesting to compare this with the trajectory that can be drawn from the 0^{++} ground state in the (J, M^2) plane. The (n, M^2) trajectory with $n = 0, 2, 4, 6$ is very similar to the trajectory beginning with the same state and continuing to $J = 2, 4$, and 6. This is what we see also for mesons and baryons in experiment: two analogous trajectories with similar slopes in the different planes.

Other than the trajectory of the four 0^{++} states (plotted in figure 27), we list the slopes calculated for pairs of states who share other quantum numbers. We also include there some results based on different lattice calculations. This is in table 8.

7 Summary and future directions

The model of holography inspired stringy hadrons (HISH) is still in its infant stage. The story is two folded. One side is the development of a fully consistent quantum theory from which one should be able to extract the spectra, decay and scattering processes and on the other side is the phenomenology of comparing the theoretical predictions to the actual data and to feedback from the data to the model. In the first part of the review we described the string configurations of certain holographic models that correspond to hadrons and we sketched the derivation of the HISH model. In the second part we

confronted the PDG hadronic spectrum with the model. A significant part of the spectra does fit nicely the model but there are also exceptional cases.

Not surprisingly there are still quite a lot of open questions and correspondingly directions for future investigation. Here we describe only few of them:

- Our model does not incorporate spin degrees of freedom. It is well known that the spin and the spin-orbit interaction play an important role in the spectra of mesons. Thus the simple rotating string models that we are using have to be improved by introducing spin degrees of freedom to the endpoints. One way to achieve it is by replacing the spinless relativistic particle with one that carries spin or in the holographic framework associating spin to the vertical segments of the holographic string.
- Our model assumes chargeless massive endpoint particles. The endpoint of a string on a flavor brane carries a charge associated with the symmetry group of the flavor branes. Thus it is natural to add an interaction, for instance Abelian interaction, between the two string endpoints. It is easy to check that this change will introduce a modification of the intercept.
- As was discussed in the introduction, the models we are using are not the outcome of a full quantization of the system. We have been either using a WKB approximation for the spectra in the (n, M^2) plane or using an ansatz of $J \rightarrow J + n - a$ for passing from the classical to the quantum model. In [8] the quantization of the rotating string without massive endpoints was determined. The quantum Regge trajectories associated with strings with massive endpoints require determining the contributions to the intercept to order J^0 from both the “Casimir” term and the Polchinski-Strominger term[61]. Once a determination of the intercept as a function of $\frac{m^2}{T}$ is made, an improved fit and a re-examination of the deviations from a universal model should be made.
- We have looked in the present work into only one feature of meson physics - the Regge trajectories of the spectra. One additional property that can be explored is the width of the decay of a meson into two mesons. The stringy holographic width was computed in [67]. A detailed comparison with decay width of mesons can provide an additional way to extract string endpoint masses that can be compared to the one deduced from the spectra.
- Eventually we have in mind to perform “precise comparisons” using holographic rotating string models instead of the model of rotating string with massive endpoints in flat space-time.
- As was emphasized in this note regarding the search for glueballs, one urgent issue is to gain additional data about flavorless hadrons. This calls for a further investigation of experiments that yield this kind of resonances and for proposing future experiments of potential glueball production, in particular in the range above 2.4 GeV. This can follow the predictions of the masses and width of the resonances as were listed in [5].
- Related to the exploration of experimental data is the investigation of efficient mechanisms of creating glueballs. This issue was not addressed in this paper. Among possible glueball formation one finds radiative J/ψ decays, pomeron pomeron collisions in hadron-hadron central production and in $p\bar{p}$ annihilation. Naturally, we would like to understand possible glueball formation in LHC experiments. It is known that we can find in the latter processes of gluon-gluon scattering and hence it may serve as a device for glueball creation.
- As was mentioned in section §5.2, the quantization of folded closed strings in D non-critical dimensions has not yet been deciphered. In [8] the expression derived for the intercept is singular in the case where is only one rotation plane - as it naturally is in $D = 4$. We mentioned a potential

avenue to resolve this issue by introducing massive particles on the folds, quantize the system as that of a string with massive endpoints [64], and then take the limit of zero mass.

- We have mentioned that the rotating closed strings are in fact rotating folded closed strings. However, we did not make any attempt in this note to explore the role of the folds. In fact it seems that very few research has been devoted to the understanding of folded strings [88]. It would be interesting to use the rotating closed string as a venue to the more general exploration of strings with folds which may be related to certain systems in nature.
- A mystery related to the closed string description of glueballs is the relation between the pomeron and the glueball. Supposedly both the glueball and the pomeron are described by a closed string. As we have emphasized in this note the slope of the closed string is half that of the open string and hence we advocated the search of trajectories with that slope. However, it was found from fitting the differential cross section of p - p collisions that the slope of the pomeron is $\alpha'_{\text{pomeron}} \approx 0.25 \text{ GeV}^{-2}$. That is, a slope which is closer to a quarter of that of the meson open string rather than half. Thus the stringy structure of the pomeron and its exact relation to the glueball is still an open question. The stringy holographic description of the pomeron physics was discussed in particular in [89].
- The closed string description of the glueball faces a very obvious question. In QCD one can form a glueball as a bound state of two, three, or in fact any number of gluons. The stringy picture seems to describe the composite of two gluons, and it is not clear how to realize those glueballs constructed in QCD from more than two gluons.
- Another prediction from holography is the presence of a baryonic vertex. Our fits exclude the presence of a baryonic vertex mass at the center of mass of the rotating baryon, but in the quark-diquark model which we prefer it is expected to be found at one of the string endpoints, with the diquark. If there is a baryonic vertex at an endpoint, there is no evidence to suggest it contributes greatly to the endpoint mass.
- We could also attempt enhancements of the model. Adding spin degrees of freedom to the endpoints would give us a much better chance of constructing a universal model that would describe the entire baryon spectrum. In [55] the distinction between spin zero and spin one diquarks played an important part in analyzing the spectrum, while we have only discussed the flavor structure of the diquark and ascribed its mass to the holographic string alone (with a possible small addition from the baryonic vertex). Spin interactions could also help explain the even-odd splitting observed in the light baryons - our simple classical model will not explain a phenomenon that distinguishes between symmetric and anti-symmetric states without some additional interaction.
- We should also strive to gain a better understanding of the intercept. While all previous sections discuss results for the slope and endpoint masses alone, the intercept, the results for which are listed in the summary tables of section §6.3.4, is an interesting parameter from a theoretical point of view, and understanding its behavior is an important goal in constructing a truly universal model of the baryon. Added interactions should contribute, in leading order, a correction to the intercept, which should also be affected by the endpoint masses, and understanding the intercept's behavior may also help us distinguish between different configurations of the baryon without requiring additional information from experiment.

Note added While the HISH models have been developed, an alternative way to describe the hadronic spectrum based on light-front holography was proposed ([146] and references therein). Though the two approaches are inspired by holography, they are different mainly since the latter is essentially a QFT description whereas the HISH is a stringy one .

Acknowledgments

I would like to thank all my collaborators in the various projects reviewed in this review paper: O. Aharony, A. Brandhuber, B. Burrington, O. Bergman, R. Casero, A. Dymarsky, E. Federovsky, G. Harpaz, N. Itzhaki V. Kaplunovsky, Y. Kinar, U. Kol M. Kruczenski, S. Kuperstein, D. Melnikov, O. Mintakevich, Pando Zayas, A. Paredes, K. Peeters, T. Sakai, E. Schreiber, S. Seki, D. Vaman, D. Weissman, S. Yankielowicz, M. Zamaklar. I would also like to thank D. Weissman for his help in preparing this review and O. Aharony for his remarks on manuscript. This work was supported in part by a centre of excellence supported by the Israel Science Foundation (grant number 1989/14), and by the US-Israel bi-national fund (BSF) grant number 2012383 and the Germany Israel bi-national fund GIF grant number I-244-303.7-2013

References

- [1] P. Collins, *An Introduction to Regge Theory and High Energy Physics*, Cambridge Univeristy Press (1977) 456.
- [2] J. Sonnenschein, “What does the string / gauge correspondence teach us about Wilson loops?,” hep-th/0003032.
- [3] J. Sonnenschein and D. Weissman, *Rotating strings confronting PDG mesons*, *JHEP* **1408** (2014) 013, [arXiv:1402.5603].
- [4] J. Sonnenschein and D. Weissman, *A rotating string model versus baryon spectra*, *JHEP* **1502** (2015) 147, [arXiv:1408.0763].
- [5] J. Sonnenschein and D. Weissman, “Glueballs as rotating folded closed strings *JHEP* **1512**, 011 (2015) doi:10.1007/JHEP12(2015)011 [arXiv:1507.01604 [hep-ph]].
- [6] M. Baker and R. Steinke, *Semiclassical quantization of effective string theory and Regge trajectories*, *Phys.Rev.* **D65** (2002) 094042, [hep-th/0201169].
- [7] E. Schreiber, *Excited mesons and quantization of string endpoints*, hep-th/0403226.
- [8] S. Hellerman and I. Swanson, *String Theory of the Regge Intercept*, arXiv:1312.0999.
- [9] J. Zahn, *The excitation spectrum of rotating strings with masses at the ends*, *JHEP* **1312** (2013) 047, [arXiv:1310.0253].
- [10] O. Aharony and Z. Komargodski, *The Effective Theory of Long Strings*, *JHEP* **1305** (2013) 118, [arXiv:1302.6257].
- [11] J. Erdmenger, N. Evans, I. Kirsch and E. Threlfall, “Mesons in Gauge/Gravity Duals - A Review,” *Eur. Phys. J. A* **35** (2008) 81 doi:10.1140/epja/i2007-10540-1 [arXiv:0711.4467 [hep-th]].
- [12] J. Polchinski and M. J. Strassler, “The String dual of a confining four-dimensional gauge theory,” hep-th/0003136.
- [13] O. Aharony, “The NonAdS / nonCFT correspondence, or three different paths to QCD,” hep-th/0212193.
- [14] J. M. Maldacena and C. Nunez, “Towards the large N limit of pure N=1 superYang-Mills,” *Phys. Rev. Lett.* **86**, 588 (2001) doi:10.1103/PhysRevLett.86.588 [hep-th/0008001].

- [15] E. Witten, *Anti-de Sitter space, thermal phase transition, and confinement in gauge theories*, *Adv.Theor.Math.Phys.* **2** (1998) 505–532, [[hep-th/9803131](#)].
- [16] I. R. Klebanov and M. J. Strassler, “Supergravity and a confining gauge theory: Duality cascades and chi SB resolution of naked singularities,” *JHEP* **0008**, 052 (2000) doi:10.1088/1126-6708/2000/08/052 [[hep-th/0007191](#)].
- [17] N. Itzhaki, J. M. Maldacena, J. Sonnenschein and S. Yankielowicz, “Supergravity and the large N limit of theories with sixteen supercharges,” *Phys. Rev. D* **58**, 046004 (1998) doi:10.1103/PhysRevD.58.046004 [[hep-th/9802042](#)].
- [18] S. Kuperstein and J. Sonnenschein, *Non-critical, near extremal AdS(6) background as a holographic laboratory of four dimensional YM theory*, *JHEP* **0411** (2004) 026, [[hep-th/0411009](#)].
- [19] J. Polchinski and M. J. Strassler, “Deep inelastic scattering and gauge / string duality,” *JHEP* **0305**, 012 (2003) doi:10.1088/1126-6708/2003/05/012 [[hep-th/0209211](#)].
- [20] A. Karch, E. Katz, D. T. Son, and M. A. Stephanov, *Linear confinement and AdS/QCD*, *Phys.Rev.* **D74** (2006) 015005, [[hep-ph/0602229](#)].
- [21] U. Gursoy and E. Kiritsis, “Exploring improved holographic theories for QCD: Part I,” *JHEP* **0802**, 032 (2008) doi:10.1088/1126-6708/2008/02/032 [[arXiv:0707.1324](#) [[hep-th](#)]].
- [22] A. Karch and E. Katz, “Adding flavor to AdS / CFT,” *JHEP* **0206**, 043 (2002) doi:10.1088/1126-6708/2002/06/043 [[hep-th/0205236](#)].
- [23] M. Kruczenski, D. Mateos, R. C. Myers and D. J. Winters, “Meson spectroscopy in AdS / CFT with flavor,” *JHEP* **0307** (2003) 049 doi:10.1088/1126-6708/2003/07/049 [[hep-th/0304032](#)].
- [24] B. A. Burrington, J. T. Liu, L. A. Pando Zayas and D. Vaman, “Holographic duals of flavored N=1 super Yang-mills: Beyond the probe approximation,” *JHEP* **0502**, 022 (2005) doi:10.1088/1126-6708/2005/02/022 [[hep-th/0406207](#)].
- [25] T. Sakai and J. Sonnenschein, “Probing flavored mesons of confining gauge theories by supergravity,” *JHEP* **0309**, 047 (2003) doi:10.1088/1126-6708/2003/09/047 [[hep-th/0305049](#)].
- [26] A. Dymarsky, S. Kuperstein, and J. Sonnenschein, *Chiral Symmetry Breaking with non-SUSY D7-branes in ISD backgrounds*, *JHEP* **0908** (2009) 005, [[arXiv:0904.0988](#)].
- [27] M. Jarvinen and E. Kiritsis, “Holographic Models for QCD in the Veneziano Limit,” *JHEP* **1203**, 002 (2012) doi:10.1007/JHEP03(2012)002 [[arXiv:1112.1261](#) [[hep-ph](#)]].
- [28] T. Sakai and S. Sugimoto, *Low energy hadron physics in holographic QCD*, *Prog.Theor.Phys.* **113** (2005) 843–882, [[hep-th/0412141](#)].
- [29] A. Brandhuber, N. Itzhaki, J. Sonnenschein and S. Yankielowicz, *Wilson loops, confinement, and phase transitions in large N gauge theories from supergravity*, *JHEP* **9806**, 001 (1998) doi:10.1088/1126-6708/1998/06/001 [[hep-th/9803263](#)].
- [30] Y. Kinar, E. Schreiber, and J. Sonnenschein, *Q anti-Q potential from strings in curved space-time: Classical results*, *Nucl.Phys.* **B566** (2000) 103–125, [[hep-th/9811192](#)].
- [31] O. Aharony, J. Sonnenschein and S. Yankielowicz, *Annals Phys.* **322**, 1420 (2007) doi:10.1016/j.aop.2006.11.002 [[hep-th/0604161](#)].

- [32] V. Kaplunovsky and J. Sonnenschein, *Searching for an Attractive Force in Holographic Nuclear Physics*, *JHEP* **1105** (2011) 058, [[arXiv:1003.2621](#)].
- [33] O. Bergman, S. Seki and J. Sonnenschein, *JHEP* **0712**, 037 (2007) doi:10.1088/1126-6708/2007/12/037 [[arXiv:0708.2839](#) [[hep-th](#)]].
- [34] R. Casero, E. Kiritsis and A. Paredes, “Chiral symmetry breaking as open string tachyon condensation,” *Nucl. Phys. B* **787**, 98 (2007) doi:10.1016/j.nuclphysb.2007.07.009 [[hep-th/0702155](#) [[HEP-TH](#)]].
- [35] A. Dhar and P. Nag, “Sakai-Sugimoto model, Tachyon Condensation and Chiral symmetry Breaking,” *JHEP* **0801**, 055 (2008) doi:10.1088/1126-6708/2008/01/055 [[arXiv:0708.3233](#) [[hep-th](#)]].
- [36] O. Aharony and D. Kutasov, “Holographic Duals of Long Open Strings,” *Phys. Rev. D* **78**, 026005 (2008) doi:10.1103/PhysRevD.78.026005 [[arXiv:0803.3547](#) [[hep-th](#)]].
- [37] B. A. Burrington, V. S. Kaplunovsky and J. Sonnenschein, “Localized Backreacted Flavor Branes in Holographic QCD,” *JHEP* **0802**, 001 (2008) doi:10.1088/1126-6708/2008/02/001 [[arXiv:0708.1234](#) [[hep-th](#)]].
- [38] J. M. Maldacena, “Wilson loops in large N field theories,” *Phys. Rev. Lett.* **80**, 4859 (1998) doi:10.1103/PhysRevLett.80.4859 [[hep-th/9803002](#)].
- [39] U. Kol and J. Sonnenschein, *JHEP* **1105**, 111 (2011) doi:10.1007/JHEP05(2011)111 [[arXiv:1012.5974](#) [[hep-th](#)]].
- [40] E. Witten, *Baryons and branes in anti-de Sitter space*, *JHEP* **9807** (1998) 006, [[hep-th/9805112](#)].
- [41] A. Dymarsky, D. Melnikov, and J. Sonnenschein, *Attractive Holographic Baryons*, *JHEP* **1106** (2011) 145, [[arXiv:1012.1616](#)].
- [42] S. Seki and J. Sonnenschein, *Comments on Baryons in Holographic QCD*, *JHEP* **0901** (2009) 053, [[arXiv:0810.1633](#)].
- [43] G. S. Bali, *Casimir scaling of SU(3) static potentials*, *Phys.Rev.* **D62** (2000) 114503, [[hep-lat/0006022](#)].
- [44] N. Isgur and J. E. Paton, *A Flux Tube Model for Hadrons in QCD*, *Phys.Rev.* **D31** (1985) 2910.
- [45] H. B. Meyer and M. J. Teper, *Glueball Regge trajectories and the pomeron: A Lattice study*, *Phys.Lett.* **B605** (2005) 344–354, [[hep-ph/0409183](#)].
- [46] H. B. Meyer, *Glueball regge trajectories*, [hep-lat/0508002](#).
- [47] C. Burden and L. Tassie, *Rotating Strings, Glueballs and Exotic Mesons*, *Austral.J.Phys.* **35** (1982) 223–233.
- [48] L. A. Pando Zayas, J. Sonnenschein, and D. Vaman, *Regge trajectories revisited in the gauge / string correspondence*, *Nucl.Phys.* **B682** (2004) 3–44, [[hep-th/0311190](#)].
- [49] M. Kruczenski, L. A. Pando Zayas, J. Sonnenschein, and D. Vaman, *Regge trajectories for mesons in the holographic dual of large-N(c) QCD*, *JHEP* **0506** (2005) 046, [[hep-th/0410035](#)].

- [50] G. 't Hooft, *Minimal strings for baryons*, hep-th/0408148.
- [51] G. Sharov, *Quasirotational motions and stability problem in dynamics of string hadron models*, *Phys.Rev.* **D62** (2000) 094015, [hep-ph/0004003].
- [52] E. Federovsky, *Stringy baryons and scattering amplitudes*, Master's thesis, Tel Aviv University, August, 2010.
- [53] G. Harpaz, *Simulating stringy baryons*, Master's thesis, Tel Aviv University, June, 2008.
- [54] G. Sharov, *String Models, Stability and Regge Trajectories for Hadron States*, arXiv:1305.3985.
- [55] A. Selem and F. Wilczek, *Hadron systematics and emergent diquarks*, hep-ph/0602128.
- [56] S. Dubovsky and V. Gorbenko, "Towards a Theory of the QCD String," arXiv:1511.01908 [hep-th].
- [57] J. Arvis, *The Exact $q\bar{q}$ Potential in Nambu String Theory*, *Phys.Lett.* **B127** (1983) 106.
- [58] O. Aharony and E. Karzbrun, *On the effective action of confining strings*, *JHEP* **0906** (2009) 012, [arXiv:0903.1927].
- [59] F. Bigazzi, A. Cotrone, L. Martucci, and L. Pando Zayas, *Wilson loop, Regge trajectory and hadron masses in a Yang-Mills theory from semiclassical strings*, *Phys.Rev.* **D71** (2005) 066002, [hep-th/0409205].
- [60] S. Frolov and A. A. Tseytlin, "Semiclassical quantization of rotating superstring in $AdS(5) \times S^{**5}$," *JHEP* **0206**, 007 (2002) doi:10.1088/1126-6708/2002/06/007 [hep-th/0204226].
- [61] J. Polchinski and A. Strominger, *Effective string theory*, *Phys.Rev.Lett.* **67** (1991) 1681–1684.
- [62] S. Hellerman, S. Maeda, J. Maltz and I. Swanson, "Effective String Theory Simplified," *JHEP* **1409**, 183 (2014) doi:10.1007/JHEP09(2014)183 [arXiv:1405.6197 [hep-th]].
- [63] G. Lambiase and V. V. Nesterenko, "Quark mass correction to the string potential," *Phys. Rev. D* **54**, 6387 (1996) doi:10.1103/PhysRevD.54.6387 [hep-th/9510221].
- [64] O. Aharony, J. Sonnenschein, and S. Yankielowicz, *On the quantization of rotating open strings with massive endpoints [In preparation]*, .
- [65] Y. Kinar, E. Schreiber, J. Sonnenschein, and N. Weiss, *Quantum fluctuations of Wilson loops from string models*, *Nucl.Phys.* **B583** (2000) 76–104, [hep-th/9911123].
- [66] G. Sharov, *String baryon model 'triangle': Hypocycloidal solutions*, *Phys.Rev.* **D58** (1998) 114009, [hep-th/9808099].
- [67] K. Peeters, J. Sonnenschein, and M. Zamaklar, *Holographic decays of large-spin mesons*, *JHEP* **0602** (2006) 009, [hep-th/0511044].
- [68] **Particle Data Group** Collaboration, K. Olive et al., *Review of Particle Physics*, *Chin.Phys.* **C38** (2014) 090001.
- [69] E. Klempt and A. Zaitsev, *Glueballs, Hybrids, Multiquarks. Experimental facts versus QCD inspired concepts*, *Phys.Rept.* **454** (2007) 1–202, [arXiv:0708.4016].

- [70] V. Mathieu, N. Kochelev, and V. Vento, *The Physics of Glueballs*, *Int.J.Mod.Phys.* **E18** (2009) 1–49, [[arXiv:0810.4453](#)].
- [71] V. Crede and C. Meyer, *The Experimental Status of Glueballs*, *Prog.Part.Nucl.Phys.* **63** (2009) 74–116, [[arXiv:0812.0600](#)].
- [72] W. Ochs, *The Status of Glueballs*, *J.Phys.* **G40** (2013) 043001, [[arXiv:1301.5183](#)].
- [73] J. Nebreda, J. Pelaez, and G. Rios, *Enhanced non-quark-antiquark and non-glueball N_c behavior of light scalar mesons*, *Phys.Rev.* **D84** (2011) 074003, [[arXiv:1107.4200](#)].
- [74] A. Anisovich, V. Anisovich, and A. Sarantsev, *Systematics of q anti- q states in the (n, M^{**2}) and (J, M^{**2}) planes*, *Phys.Rev.* **D62** (2000) 051502, [[hep-ph/0003113](#)].
- [75] V. Anisovich, *Systematics of quark anti-quark states and scalar exotic mesons*, *Phys.Usp.* **47** (2004) 45–67, [[hep-ph/0208123](#)].
- [76] P. Masjuan, E. Ruiz Arriola, and W. Broniowski, *Systematics of radial and angular-momentum Regge trajectories of light non-strange $q\bar{q}$ -states*, *Phys.Rev.* **D85** (2012) 094006, [[arXiv:1203.4782](#)].
- [77] D. Bugg, *Comment on Systematics of radial and angular-momentum Regge trajectories of light nonstrange $q\bar{q}$ -states*, *Phys.Rev.* **D87** (2013), no. 11 118501, [[arXiv:1209.3481](#)].
- [78] **BESIII** Collaboration, M. Ablikim et al., *Study of the near-threshold $\chi\chi$ mass enhancement in doubly OZI-suppressed J/ψ decays*, *Phys.Rev.* **D87** (2013), no. 3 032008, [[arXiv:1211.5668](#)].
- [79] **BES Collaboration** Collaboration, J. Bai et al., *Studies of χ (2230) in J/ψ radiative decays*, *Phys.Rev.Lett.* **76** (1996) 3502–3505.
- [80] V. Vladimirovsky, V. Grigorev, O. Erofeeva, Y. Katinov, V. Lisin, et al., *Resonance maximum in the system of two $K(S)$ mesons at 1450-MeV*, *Phys.Atom.Nucl.* **64** (2001) 1895–1897.
- [81] J. Vijande, F. Fernandez, and A. Valcarce, *Constituent quark model study of the meson spectra*, *J.Phys.* **G31** (2005) 481, [[hep-ph/0411299](#)].
- [82] A. Athenodorou, B. Bringoltz, and M. Teper, *Closed flux tubes and their string description in $D=3+1$ $SU(N)$ gauge theories*, *JHEP* **02** (2011) 030, [[arXiv:1007.4720](#)].
- [83] M. Bochicchio, *Yang-Mills mass gap, Floer homology, glueball spectrum, and conformal window in large- N QCD*, [arXiv:1312.1350](#).
- [84] M. Bochicchio, *Glueball and meson spectrum in large- N massless QCD*, [arXiv:1308.2925](#).
- [85] M. Caselle, A. Nada, and M. Panero, *Hagedorn spectrum and thermodynamics of $SU(2)$ and $SU(3)$ Yang-Mills theories*, [arXiv:1505.0110](#).
- [86] A. Donnachie and P. Landshoff, *Elastic Scattering and Diffraction Dissociation*, *Nucl.Phys.* **B244** (1984) 322.
- [87] C. J. Morningstar and M. J. Peardon, *The Glueball spectrum from an anisotropic lattice study*, *Phys.Rev.* **D60** (1999) 034509, [[hep-lat/9901004](#)].
- [88] O. Ganor, J. Sonnenschein, and S. Yankielowicz, *Folds in 2-D string theories*, *Nucl.Phys.* **B427** (1994) 203–244, [[hep-th/9404149](#)].

- [89] E. Shuryak and I. Zahed, “New regimes of the stringy (holographic) Pomeron and high-multiplicity pp and pA collisions,” *Phys. Rev. D* **89**, no. 9, 094001 (2014) doi:10.1103/PhysRevD.89.094001 [arXiv:1311.0836 [hep-ph]].
- [90] R. Casero, A. Paredes, and J. Sonnenschein, *Fundamental matter, meson spectroscopy and non-critical string/gauge duality*, *JHEP* **0601** (2006) 127, [hep-th/0510110].
- [91] O. Mintakevich and J. Sonnenschein, *On the spectra of scalar mesons from HQCD models*, *JHEP* **0808** (2008) 082, [arXiv:0806.0152].
- [92] K. Peeters, J. Sonnenschein, and M. Zamaklar, *Holographic melting and related properties of mesons in a quark gluon plasma*, *Phys.Rev.* **D74** (2006) 106008, [hep-th/0606195].
- [93] T. Imoto, T. Sakai, and S. Sugimoto, *Mesons as Open Strings in a Holographic Dual of QCD*, *Prog.Theor.Phys.* **124** (2010) 263–284, [arXiv:1005.0655].
- [94] J. Sonnenschein, *Holographic stingy hadrons, Talks delivered in September IPMU, October NBI and November NS/WAS 2013*.
- [95] A. Chodos and C. B. Thorn, *Making the Massless String Massive*, *Nucl.Phys.* **B72** (1974) 509.
- [96] **Particle Data Group** Collaboration, J. Beringer et al., *Review of Particle Physics (RPP)*, *Phys.Rev.* **D86** (2012) 010001.
- [97] E. Eichten, S. Godfrey, H. Mahlke, and J. L. Rosner, *Quarkonia and their transitions*, *Rev.Mod.Phys.* **80** (2008) 1161–1193, [hep-ph/0701208].
- [98] N. Brambilla, S. Eidelman, B. Heltsley, R. Vogt, G. Bodwin, et al., *Heavy quarkonium: progress, puzzles, and opportunities*, *Eur.Phys.J.* **C71** (2011) 1534, [arXiv:1010.5827].
- [99] S. Gershtein, A. Likhoded, and A. a. Luchinsky, *Systematics of heavy quarkonia from Regge trajectories on (n, M^{**2}) and (M^{**2}, J) planes*, *Phys.Rev.* **D74** (2006) 016002, [hep-ph/0602048].
- [100] D. Ebert, R. Faustov, and V. Galkin, *Mass spectra and Regge trajectories of light mesons in the relativistic quark model*, *Phys.Rev.* **D79** (2009) 114029, [arXiv:0903.5183].
- [101] D. Ebert, R. Faustov, and V. Galkin, *Heavy-light meson spectroscopy and Regge trajectories in the relativistic quark model*, *Eur.Phys.J.* **C66** (2010) 197–206, [arXiv:0910.5612].
- [102] D. Ebert, R. Faustov, and V. Galkin, *Spectroscopy and Regge trajectories of heavy quarkonia and B_c mesons*, *Eur.Phys.J.* **C71** (2011) 1825, [arXiv:1111.0454].
- [103] **LHCb** Collaboration, R. Aaij et al., *Study of D_J meson decays to $D^+\pi^-$, $D^0\pi^+$ and $D^{*+}\pi^-$ final states in pp collision*, *JHEP* **1309** (2013) 145, [arXiv:1307.4556].
- [104] Z.-G. Wang, *Analysis of strong decays of the charmed mesons $D_J(2580)$, $D_J^*(2650)$, $D_J(2740)$, $D_J^*(2760)$, $D_J(3000)$, $D_J^*(3000)$* , *Phys.Rev.* **D88** (2013) 114003, [arXiv:1308.0533].
- [105] A. Inopin and G. Sharov, *Hadronic Regge trajectories: Problems and approaches*, *Phys.Rev.* **D63** (2001) 054023, [hep-ph/9905499].
- [106] A. Tang and J. W. Norbury, *Properties of Regge trajectories*, *Phys.Rev.* **D62** (2000) 016006, [hep-ph/0004078].

- [107] E. Klempt and J.-M. Richard, *Baryon spectroscopy*, *Rev.Mod.Phys.* **82** (2010) 1095–1153, [arXiv:0901.2055].
- [108] H. Hata, T. Sakai, S. Sugimoto, and S. Yamato, *Baryons from instantons in holographic QCD*, *Prog.Theor.Phys.* **117** (2007) 1157, [hep-th/0701280].
- [109] V. Kaplunovsky, D. Melnikov, and J. Sonnenschein, *Baryonic Popcorn*, *JHEP* **1211** (2012) 047, [arXiv:1201.1331].
- [110] V. Kaplunovsky and J. Sonnenschein, *Dimension Changing Phase Transitions in Instanton Crystals*, *JHEP* **1404** (2014) 022, [arXiv:1304.7540].
- [111] A. Brandhuber, N. Itzhaki, J. Sonnenschein, and S. Yankielowicz, *Baryons from supergravity*, *JHEP* **9807** (1998) 020, [hep-th/9806158].
- [112] J. Callan, Curtis G., A. Guijosa, K. G. Savvidy, and O. Tafjord, *Baryons and flux tubes in confining gauge theories from brane actions*, *Nucl.Phys.* **B555** (1999) 183–200, [hep-th/9902197].
- [113] T. Friedmann, *QCD vs. the Centrifugal Barrier: a New QCD Effect*, *EPJ Web Conf.* **70** (2014) 00027.
- [114] J. Sonnenschein and D. Weissman, *On decays of stringy hadrons [work in progress]*, .
- [115] C. Csaki, H. Ooguri, Y. Oz, and J. Terning, *Glueball mass spectrum from supergravity*, *JHEP* **9901** (1999) 017, [hep-th/9806021].
- [116] R. C. Brower, S. D. Mathur, and C.-I. Tan, *Glueball spectrum for QCD from AdS supergravity duality*, *Nucl. Phys.* **B587** (2000) 249–276, [hep-th/0003115].
- [117] D. Elander, A. F. Faedo, C. Hoyos, D. Mateos, and M. Piai, *Multiscale confining dynamics from holographic RG flows*, *JHEP* **05** (2014) 003, [arXiv:1312.7160].
- [118] G. Bhanot and C. Rebbi, *SU(2) String Tension, Glueball Mass and Interquark Potential by Monte Carlo Computations*, *Nucl.Phys.* **B180** (1981) 469.
- [119] A. J. Niemi, *Are glueballs knotted closed strings?*, hep-th/0312133.
- [120] G. Sharov, *Closed String with Masses in Models of Baryons and Glueballs*, arXiv:0712.4052.
- [121] L. Solovev, *Glueballs in the string quark model*, *Theor.Math.Phys.* **126** (2001) 203–211, [hep-ph/0006010].
- [122] S. Talalov, *The Glueball Regge trajectory from the string inspired theory*, hep-ph/0101028.
- [123] F. J. Llanes-Estrada, S. R. Cotanch, P. J. de A. Bicudo, J. E. F. Ribeiro, and A. P. Szczepaniak, *QCD glueball Regge trajectories and the Pomeron*, *Nucl.Phys.* **A710** (2002) 45–54, [hep-ph/0008212].
- [124] A. P. Szczepaniak and E. S. Swanson, *The Low lying glueball spectrum*, *Phys.Lett.* **B577** (2003) 61–66, [hep-ph/0308268].
- [125] J. Pons, J. Russo, and P. Talavera, *Semiclassical string spectrum in a string model dual to large N QCD*, *Nucl.Phys.* **B700** (2004) 71–88, [hep-th/0406266].

- [126] E. Abreu and P. Bicudo, *Glueball and hybrid mass and decay with string tension below Casimir scaling*, *J.Phys.* **G34** (2007) 195207, [[hep-ph/0508281](#)].
- [127] F. Brau and C. Semay, *Semirelativistic potential model for glueball states*, *Phys.Rev.* **D70** (2004) 014017, [[hep-ph/0412173](#)].
- [128] V. Mathieu, C. Semay, and F. Brau, *Casimir scaling, glueballs and hybrid gluelumps*, *Eur.Phys.J.* **A27** (2006) 225–230, [[hep-ph/0511210](#)].
- [129] Y. Simonov, *Glueballs, gluerings and gluestars in the $d=2+1$ $SU(N)$ gauge theory*, *Phys.Atom.Nucl.* **70** (2007) 44–52, [[hep-ph/0603148](#)].
- [130] V. Mathieu, C. Semay, and B. Silvestre-Brac, *Semirelativistic potential model for low-lying three-gluon glueballs*, *Phys.Rev.* **D74** (2006) 054002, [[hep-ph/0605205](#)].
- [131] H. Boschi-Filho and N. R. Braga, *Gauge / string duality and scalar glueball mass ratios*, *JHEP* **0305** (2003) 009, [[hep-th/0212207](#)].
- [132] J. Polchinski, *String theory. Vol. 1: An introduction to the bosonic string*, .
- [133] A. Armoni and B. Lucini, *Universality of k -string tensions from holography and the lattice*, *JHEP* **06** (2006) 036, [[hep-th/0604055](#)].
- [134] A. L. Cotrone, L. Martucci, and W. Troost, *String splitting and strong coupling meson decay*, *Phys. Rev. Lett.* **96** (2006) 141601, [[hep-th/0511045](#)].
- [135] F. Bigazzi and A. L. Cotrone, *New predictions on meson decays from string splitting*, *JHEP* **11** (2006) 066, [[hep-th/0606059](#)].
- [136] K. Hashimoto, C.-I. Tan, and S. Terashima, *Glueball decay in holographic QCD*, *Phys. Rev.* **D77** (2008) 086001, [[arXiv:0709.2208](#)].
- [137] F. Br  nner, D. Parganlija, and A. Rebhan, *Glueball Decay Rates in the Witten-Sakai-Sugimoto Model*, *Phys. Rev.* **D91** (2015), no. 10 106002, [[arXiv:1501.0790](#)].
- [138] F. Br  nner and A. Rebhan, *Nonchiral enhancement of scalar glueball decay in the Witten-Sakai-Sugimoto model*, [arXiv:1504.0581](#).
- [139] **CLEO** Collaboration, K. Benslama et al., *Anti-search for the glueball candidate $f(J)(2220)$ in two -photon interactions*, *Phys.Rev.* **D66** (2002) 077101, [[hep-ex/0204019](#)].
- [140] E. Gregory, A. Irving, B. Lucini, C. McNeile, A. Rago, et al., *Towards the glueball spectrum from unquenched lattice QCD*, *JHEP* **1210** (2012) 170, [[arXiv:1208.1858](#)].
- [141] **APE** Collaboration, M. Albanese et al., *Glueball Masses and String Tension in Lattice QCD*, *Phys.Lett.* **B192** (1987) 163–169.
- [142] Y. Chen, A. Alexandru, S. Dong, T. Draper, I. Horvath, et al., *Glueball spectrum and matrix elements on anisotropic lattices*, *Phys.Rev.* **D73** (2006) 014516, [[hep-lat/0510074](#)].
- [143] **UKQCD Collaboration** Collaboration, G. Bali et al., *A Comprehensive lattice study of $SU(3)$ glueballs*, *Phys.Lett.* **B309** (1993) 378–384, [[hep-lat/9304012](#)].
- [144] B. Lucini, *Glueballs from the Lattice*, *PoS QCD-TNT-III* (2013) 023, [[arXiv:1401.1494](#)].

- [145] B. Lucini, M. Teper, and U. Wenger, *Glueballs and k-strings in $SU(N)$ gauge theories: Calculations with improved operators*, *JHEP* **0406** (2004) 012, [[hep-lat/0404008](#)].
- [146]
- [146] S. J. Brodsky, A. Deur, G. F. de Tramond and H. G. Dosch, “Light-Front Holography and Superconformal Quantum Mechanics: A New Approach to Hadron Structure and Color Confinement,” *Int. J. Mod. Phys. Conf. Ser.* **39** (2015) 1560081 doi:10.1142/S2010194515600812 [[arXiv:1510.01011 \[hep-ph\]](#)].